Miniaturization Methodology Applied to Deep Space Microspacecraft

by
Lilac Muller

S.B., Massachusetts Institute of Technology (1993)

SUBMITTED TO THE DEPARTMENT OF
AERONAUTICS AND ASTRONAUTICS IN PARTIAL
FULFILLMENT OF THE REQUIREMENTS
FOR THE DEGREE OF

MASTER OF SCIENCE
in Aeronautics and Astronautics

at the

MASSACHUSETTS INSTITUTE OF TECHNOLOGY

May 1994

Signature of Author _____
Department of Aeronautics and Astronautics
May 6, 1994

Certified by _____
Professor Stanley Weiss
Thesis Supervisor, Department of Aeronautics and Astronautics

Certified by _____
Ross M. Jones
Thesis Supervisor, Jet Propulsion Laboratory

Accepted by _____
Professor Harold Y. Wachman
Chairman, Department Graduate Committee

Miniaturization Methodology Applied to Deep Space Microspacecraft

by

Lilac Muller

Submitted to the Department of Aeronautics and Astronautics
on May 6, 1994 in partial fulfillment of the requirements for the
degree of Master of Science in Aeronautics and Astronautics

Abstract

Due to the shrinking NASA budget, future scientific spacecraft programs will be driven by their "life-cycle" cost. This cost figure, which includes development, integration, launch, and operation, can be reduced by making spacecraft smaller and more autonomous. Such miniature spacecraft allow the launch of several on a single launch vehicle or the launch of a single craft as a "piggyback ride" to a primary payload. Although each of these small spacecraft will not be capable of performing the diversified science that is accomplished by such spacecraft as Voyager and Magellan, a group of microspacecraft can conduct a composite of many different kinds of useful science as well as enhance overall mission reliability.

Over the past four years, the Jet Propulsion Laboratory (JPL) has been developing concepts for asteroid flyby microspacecraft. The research presented in this thesis develops an approach to miniaturization for deep-space scientific spacecraft and applies it to the latest JPL asteroid flyby concept. This miniaturization process involves reduction in size of specific components or systems by focusing efforts on such parameters as power consumption and volume, as well as modification of the system's functional and physical architecture so that it can better support this class of spacecraft. These techniques, applied to JPL's "Second Generation Microspacecraft," resulted in two concepts: the first employs an RF communication system and yields a 44% reduction in mass; and the second uses an optical communication system providing a 50% reduction in mass. These two options were developed in parallel because of the immaturity of the optical communication relative to the RF, however, they were applied to the same physical architecture. The approaches developed in this study, though specifically directed towards the miniaturization of a vehicle designed for a scientific investigation of an asteroid, may be applied to various deep space microspacecraft.

Thesis Supervisor: Stanley I. Weiss
Title: Prof. of Aeronautics and Astronautics, MIT
Thesis Supervisor: Ross M. Jones
Title: Group Supervisor, Advanced Spacecraft Systems Studies
and Engineering Technology Group, JPL

Acknowledgments

My appreciation goes to:

Prof. Stan Weiss, Ross Jones, and Dave Collins for all your help over the past year (special thanks to Ross for hiring me in the summer of 1991 and giving me the opportunity to be a part of his group and a member of the microspacecraft team).

The many people at JPL who took the time to help me in my quest for the spacecraft of the future (or the imaginary spacecraft, as some may say): Division 33: Marty Herman, Jack Meeker, Hamid Hemmati, and John Huang; Section 342: Richard Bennett; Section 343: Randy Bartman and Pat Waddell; Section 347: Leon Alkalaj; Section 352: Kim Aaron and Josh Powlesson; Section 353: Dave Stevens; Section 355: Lynn Lowry; and Section 382: Tom Chrien and Cesar Sepulveda. Thanks for all your time, help, and patience.

My mother, Rachel, for teaching me the value of knowledge and education. This thesis belongs to you just as much as it belongs to me.

My father, Joe, for instilling the engineer in me.

My brother and sister, Sean and Rikky, for having to live in the same house with me for most of your lives.

Matt W. for my sanity and many hours of proofreading (thanks for correcting my many grammatically-challenged sentences), and Rob C. for the late night/early morning company and the many interesting hours we spent at the Coffee House and Tosci's discussing the oddest things. Wouldn't have made it without you.

Shally and Eileen for all your support over the past 3 years.

And finally, the Miracle of Science, Adam (our usual waiter), Sam (our favorite patriot), and especially Alex for the great company.

Table of Contents

List of Figures

List of Tables

List of Acronyms

ADC	Analog-to-Digital Converter
AIM	Asteroid Invetigation with Microspacecraft
ASIC	Application Specific Integrated Circuit
AU	Astronomical Unit
CMOS	Complementary Metal-Oxide Semiconductor
CTE	Coefficient of Thermal Expansion
DRAM	Dynamic Random Access Memory
DSN	Deep Space Network
EIRP	Effective Isotropic Radiated Power
EMI	Electromagnetic Interaction
FOV	Field of View
IC	Integrated Circuit
IOM	Interoffice Memorandum
IMU	Inertial Measurement Unit
IRU	Inertial Reference Unit
JPL	Jet Propulsion Laboratory
KGD	Known Good Die
LOS	Line of Sight
LV	Launch Vehicle
MCM	Multi-Chip Module
MEMS	Microelectromechanical Systems
MESUR	Mars Environmental Surevey
MIPS	Million of Instructions per Second
MLI	Multi-Layer Insulation
MSTI	Miniature Seeker and Technology I??
MUX	Engineering Multiplexer
NEA	Near Earth Asteroids
NEO	Near Earth Objects
NGM	Next Generation Microspacecraft
PCB	Printed Circuit Board
PDU	Power Distribution Unit
PNEAF	Pegasus-launched Near Earth Asteroid Flyby
PPT	Peak Power Tracker
RCS	Reaction Control System
RF	Radio Frequency
ROM	Read Only Memory
S/A	Solar Array

S/C	Spacecraft
SEU	Single Event Upset
SGM	Second Generation Microspacecraft
SRAM	Static Random Access Memory
SRM	Solid Rocket Motor
SSPA	Solid-State Power Amplifier
SWG	Science Working Group
TCM	Trajectory Correction Manuever
TMU	Telemetry Modulation Unit
UHDI	Ultra High Density Integration
VD	Valve Drivers
VLSI	Very Large Scale Integration

Chapter 1

Introduction

1.1 The Microspacecraft Vision

Today's planetary spacecraft (Cassini, Mars Observer, Galileo, Voyager) carry many instruments on board and conduct many scientific experiments at their destination. Because of this, they are viewed as being heavy, power-demanding, and complex. Qualification tests for their parts and subsystems are long and expensive, adding to the already long development time and high costs. The recent loss of the Mars Observer brought to attention (yet again) the risk of placing large resources into a single, complex vehicle. This unfortunate setback has increased the support for smaller, more focused missions.

The idea of microspacecraft was conceptualized in 1981 by Jim Burke of the Jet Propulsion Laboratory (JPL) [1]. Burke's study concluded that "while the laws of physics do impose some fundamental size constraints, they do not forbid the building of deep-space craft significantly smaller than our present ones." He also identified a need to:

> "examine more demanding deep-space applications that are impractical or impossible without miniature spacecraft: multi-point measurements in space, multiple high-g landings on planets, small tethered and solar-sailing devices, and high-speed missions such as Mercury orbiters, close solar orbiters, and the upper stages of sample-returners."

In 1987, Ross Jones (also of JPL) revived Burke's microspacecraft vision in his discussion of electromagnetic (EM) launchers [2]:

> "Instead of one large, expensive spacecraft launched every few years, projects could launch many, perhaps 10-50 identical, small, relatively inexpensive spacecraft per year. Whereas failure of current planetary spacecraft would be catastrophic, failure of small EM-launched spacecraft would not be critical to the mission due to the redundancy provided by multiple spacecraft."

With the shrinking NASA budget, scientists and engineers are looking at ways of conducting valuable planetary science for less. Smaller spacecraft are envisioned to do just that. The vision is that of micro scale vehicles that will weigh orders of magnitude less than current spacecraft, consume far less power, evolve from concept to launch in less time and for less money, and still support focused world-class science investigation.

1.2 Rationale for Miniaturization

The main rationale for designing and building smaller spacecraft is the need to lower total project costs. Smaller spacecraft can be launched on smaller launch vehicles (LVs) which cost much less than heavy ones. Even smaller vehicles can be launched as "piggy-back" riders on other missions when mass margins are available, or they can be launched as multiple spacecraft on a single LV, thus reaching more than a single target or conducting science than can only be accomplished by multiple views of a single object. In addition, small spacecraft allow for a greater upper stage within a given launch vehicle envelope, thus enabling shorter cruise phases for long distances.

There are several other factors that may make smaller spacecraft less expensive. Compact spacecraft require smaller integration and test facilities. Smaller spacecraft generally support simpler missions and simpler system architectures which lead to lower operations costs. On the other hand, these vehicles require advanced technologies which incur high development costs. Many would require more expensive manufacturing and qualification techniques. However, as the use of and demand for these technologies increase, these costs will can be amortized over multiple uses.

The reasons for making spacecraft smaller, as outlined above, are very attractive; however, it is clear that miniaturization beyond a certain point will require an investment in technology development that may be more expensive than the cost savings attained through reduction in size. This crossover point, however, has not yet been identified. This is one of the primary reasons for developing concepts for smaller, more application-specific spacecraft. Small spacecraft (100-1000kg) are quite common, and minispacecraft (10-100kg) are emerging. Microspacecraft (1-10kg) concepts are now being developed, while nanospacecraft (<1kg) concepts are still to come. Only by producing concepts that push to reduce spacecraft size will we be able to identify, using assumptions about technology readiness, the point at which miniaturization does not provide further benefits.

Developing concepts that push the limit of technology in order to miniaturize has additional benefits. This type of research identifies the physical limits of miniaturization and those which are independent of engineering capabilities. In addition, it identifies the technologies which need to be developed in order to build mini- and microspacecraft in the future. This process can encourage R&D funding to be directed appropriately. Finally, these concepts might encourage the development of a new class of launch vehicles with lower performance and much lower costs.

1.3 Prior Work

In the late 1980s, the Pegasus launch vehicle was introduced. Although it did not fly until 1990, it brought about an interest in smaller spacecraft that could be launched for less cost. In 1990, a Pegasus-launched Near Earth Asteroid Flyby (PNEAF) study [3] introduced the design of a spacecraft that

could conduct deep space science after launch from a small and cheap launch vehicle. Near earth asteroids (NEAs) were chosen since the ΔV required to reach them is rather modest, yet their exploration provides significant scientific contributions to the study of the solar system:

> "Individual NEAs are transient bodies on the geologic (and astronomical) timescale,..many are samples of mainbelt asteroids which are, in turn, mostly likely the debris left over when a planet failed to form in the region between Mars and Jupiter." And, "...the environmental stress resulting from NEA impacts has been a fundamental factor in biological evolution. It would obviously be useful to clarify the precise nature of the NEA threat...[4]"

The PNEAF concept is a spinning spacecraft weighing 77.5 kg wet (upper stage weighs an additional 240.4kg). Taking the NEA exploration a step further, the Asteroid Investigation with Microspacecraft (AIM), a study conducted in 1991, explored the concept of flying three spacecraft on a single Pegasus, each headed towards a different asteroid [5,6]. Each of the three spacecraft weighs 35.7kg wet (upper stage for each weighs an additional 108.6kg). An additional effort to miniaturize took place in the summer of 1993 [7]. This "second generation" microspacecraft (SGM) for asteroid flybys weighs 5.5kg wet (upper stage issues are still unresolved). Figure 1-1 shows the progress in miniaturization for NEAs flyby missions.

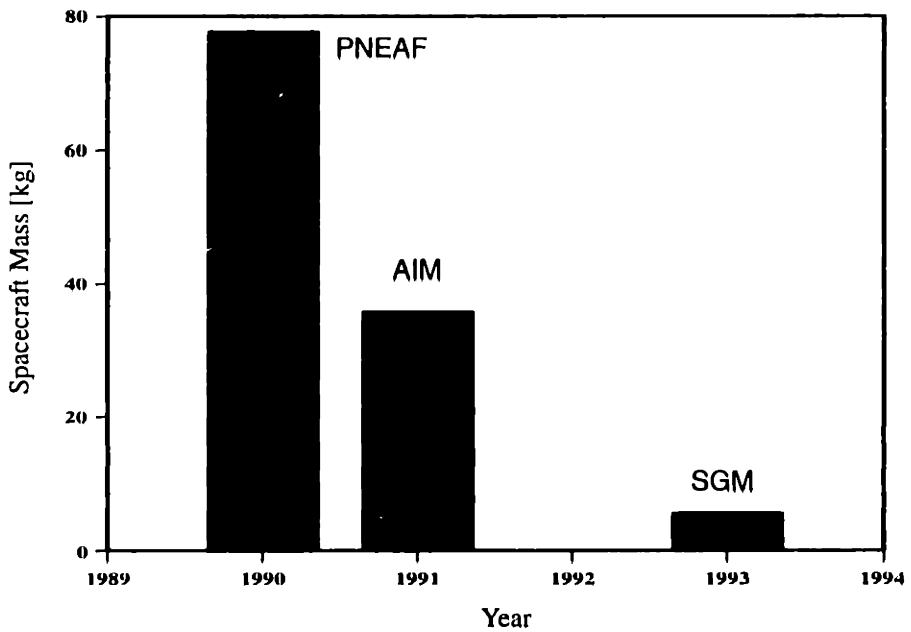

Figure 1-1: Trend in miniaturization for proposed near-earth asteroid flyby missions.

It is important to note that mass is not the only factor that determines cost effectiveness. As discussed above, miniaturization has the potential of reducing mission cost; the science return, however, must also be considered. Table 1-1 shows that the miniaturization of spacecraft does not necessarily

mean reduction in science quality and data return. The quality of the scientific instrument and on-board data handling, much like the rest of the spacecraft, can benefit from advanced technologies. Therefore, although PNEAF, AIM, and SGM return considerably less data than traditional interplanetary spacecraft as Magellan and Galileo, the miniaturization process within the asteroid flyby class of spacecraft shows that science quality and data return does not necessarily deteriorate with reduced spacecraft mass.

Table 1-1: Science Data Return for Proposed Near Earth Asteroid Flyby Missions

MISSION	INSTRUMENT	RESOLUTION	RETURN
PNEAF	Visible Imager	30 m/pixel	22 1-color images 15 color images
AIM	IR/Visible Spectral Imager Radio Doppler	8 m/pixel	B&W images[a] color images[a]
SGM	NIR/Visible Camera with Push-Broom Spectrometer	2-24 m/pixel	14 B&W images 10 color images

a. Number of acquired images is unavailable.

1.4 System Design Goals and Objectives

Based on the reasons outlined in Section 1.2, there is an interest in developing a concept for an asteroid flyby spacecraft that is even smaller than the second generation microspacecraft. This thesis aims to develop an approach to the miniaturization of microspacecraft and to use that methodology to develop a concept for a vehicle weighing less than 5kg. This design uses the second generation concept as a building block. In addition, this study intends to identify and implement advanced architectures and technologies wherever they may provide an advantage. The process used for this design evolution is shown in Figure 1-2.

1.5 Study Support

Work was conducted at the Jet Propulsion Laboratory in Pasadena, Calif. as part of the Engineering Internship Program at MIT. Funding was provided by the System Analysis RTOP under NASA's Office of Advanced Concepts and Technology (Code C). Technical support on lab was provided by Ross Jones and David Collins (Spacecraft Systems Engineering Section) and various advanced technology experts at JPL. Their contributions are referenced in the text. Technical review and guidance at MIT was provided by Dr. Stanley Weiss, visiting professor of Aeronautics and Astronautics.

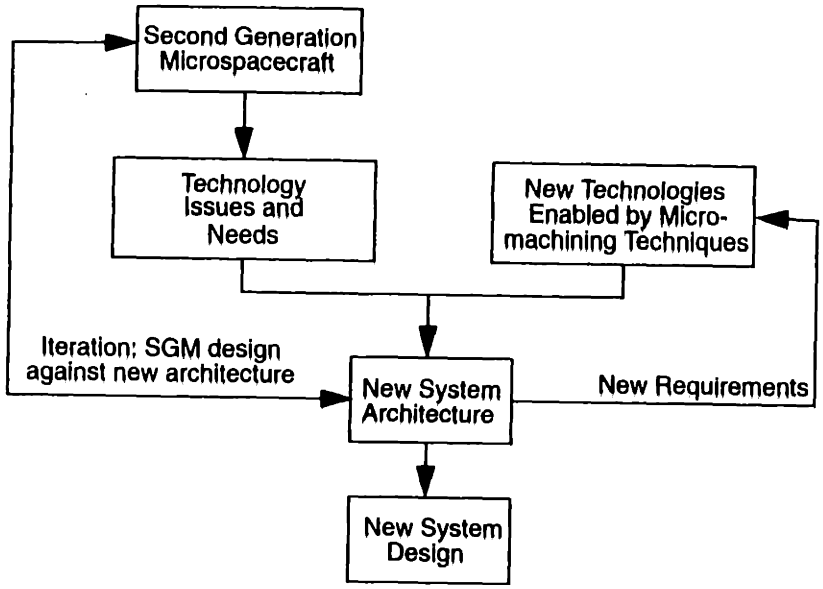

Figure 1-2: Evolutionary design development used in this thesis project.

1.6 Thesis Outline

Much of the design work is based on the Second Generation Microspacecraft, but it is also important to understand the preceeding concepts in order to appreciate the progress in miniaturization. Chapter 2 describes the mission design which is common to all missions discussed in this thesis, while Chapter 3 gives a brief overview of the three corresponding concepts: PNEAF, AIM, and SGM. Chapter 4 traces the process that was used in the miniaturization of the spacecraft designed in this study. The final system design is shown in Chapter 5. Chapter 6 summarizes the advanced technologies that are necessary to turn the concept into reality. Finally, Chapter 7 describes the achievements of this study and briefly discusses the issues of reliability, cost, applicability to other missions, and future outlook.

Chapter 2

The Mission

2.1 Mission Concept

Near earth asteroid flyby is a relatively simple mission requiring a relatively small on-board ΔV capability; a Hohmann transfer using an upper stage can be used. This modest mission does not place great constraints on the design and allows the system engineer to focus more on the miniaturization and architecture modification processes. Nonetheless, near earth asteroid science investigation is a valuable aspect of the solar system exploration as outlined in the introduction.

The first of this series of asteroid flyby studies, PNEAF, developed a specific mission and flight trajectory based on predetermined earth range, sun range, and mission duration constraints. The AIM study that followed, used those same constraints to develop a mission plan for a later launch date [8]. The 1996-97 time frame used in the AIM mission design was too early for the technology readiness levels that were assumed for the second generation design. For SGM, launch dates of 2003-4 were more appropriate. This study uses the SGM mission designs The following mission boundary conditions apply to all asteroid flyby missions mentioned above:

- Injection energy (C_3) of less than $4km^2/sec^2$ (injection ΔV = 3400m/sec)
- Asteroid-sun range in the range of 0.8 - 1.2AU
- Asteroid-Earth range no greater than 1.6AU

2.2 Scientific Objectives

The importance of near earth objects (NEO) study within the solar system exploration program was outlined in the Report of the Discovery Science Working Group (SWG) [9]:

1. "...NEOs may preserve clues to the nature of planetesimals from which terrestrial planets formed. They certainly are the source of most meteorites that strike the Earth. They are a very diverse class of objects, including primitive and evolved bodies."
2. "NEOs represent the primary source population of relatively large objects that strike the Earth, and which have influenced the evolution of the Earth's atmosphere and biosphere."
3. "NEOs may represent the potential source of raw materials for the future utilization and exploitation of space."
4. "Their low gravity, combined with the possibility of abundant H_2O, make them realistic candidates for future sites to develop the techniques of human deep space exploration."

The SWG also outlined the primary scientific objectives of an asteroid mission as gross physical properties (size, shape, configuration, volume, mass, density, and spin rate), surface composition, and surface morphology. A payload of a visual imager, an infrared spectrometer/mapper, a gamma-ray spectrometer, and radio science accomplish all primary objectives. Although the SWG determined that a rendezvous is appropriate to accomplish all asteroid study scientific objectives, a flyby mission is considerably simpler and requires less propellant. Valvuable science can still be conducted during a flyby. Imaging during a flyby will be constrained to shorter exposure durations and fewer images will be taken; resolution, however, will be unaffected.

The PNEAF concept includes a visible camera (with six color filters). The AIM spacecraft carries an imaging camera (with three color filters) and uses its on-board telecommunication system for radio science, while the SGM uses its integrated optics system as imaging camera/spectrometer during encounter. None of these concepts satisfy all the scientific objectives outlined by the SWG for a rendezvous mission, however, they still accomplish valuable scientific investigation for a flyby. The NGM will utilize the same instrument capabilities and mission design as SGM and thus will accomplish the same quality of scientific investigation.

2.3 Target Selection and Trajectory Design

Of the many asteroids that can be targeted during a 2003-2006 launch window, six were chosen as examples. They were chosen because they did not violate any of the specified mission constraints. Most require far less injection energy than the $4km^2/sec^2$ limit set for this class of missions and are much closer to earth than 1.6AU. Table 2-1 shows a list of flyby opportunities, asteroid characteristics, and basic mission parameters for cruise and flyby phases for six asteroids [7]. These are just a few of many asteroid encounter opportunities that exist in the 2003-6 launch period [8].

Table 2-1: Near-Earth Asteroid Flyby Launch Opportunities and Mission Parameters

Asteroid (number)	Diam. [km]	Launch Date	Flight Time [days]	C_3 [km^2/s^2]	V_∞ [km/s]	Max Earth Dist. [AU]	Sun Range [AU]
Betulia (1580)	7.4	1/4/2002	149	1.13	27.25	0.57	1 - 1.17
Ra-Shalom (2100)	2.4	4/5/2003	181	1.70	8.60	0.72	1 - 1.2
Toutatis (4179)	5.4	4/26/2004	153	0.63	10.81	0.19	0.96 - 1
1980 PA (3908)	1.2	7/20/2004	115	1.17	6.77	0.35	1 - 1.06
Orpheus (3361)	0.8	6/18/2005	139	2.07	10.75	0.72	1 - 1.17
1977 VA (N/A)	0.4	7/12/2005	116	2.89	5.99	0.84	1 - 1.23

To establish guidelines for a configuration, a sample mission was chosen. The Ra-Shalom (2100) target asteroid with a 2003 launch date was used in the SGM study and will also be used here. Figure 2-1 shows the mission trajectory. Figures 2-2 and 2-3 show relative distances and angles (respectively) during the mission which includes the 181 day cruise phase, encounter, and a two months post-encounter downlink phase. The relative distances were used to size the power and telecommunication systems and the relative angles were used to determine the proper solar array configuration relative to the rest of the vehicle so that maximum solar power is utilized. The relative angles convey the following information:

- Sun-Asteroid-Spacecraft: shows how close the sun appears within the telescope's FOV. Ideally, this angle should be 0^{o} at encounter (sun is right behind the spacecraft) so that the asteroid is fully lit. However, to avoid viewing the sun an angle of 90^{o} is sufficient;
- Sun-Spacecraft-Asteroid: shows the sun angle during target tracking and encounter phases;
- Sun-Spacecraft-Earth: shows the sun angle during the data transmission phase.

The last curve (sun-spacecraft-earth angle versus time) determines the deployed solar array position relative to the spacecraft bus, or more precisely to the antenna. Since the data transmission requires the highest levels of power consumption, this position allows for maximum utilization of solar power during the data transmission phase. Therefore, since post-encounter sun angles are between 55^{o} and 58^{o}, the solar array panel is angled at about 55^{o} relative to the nearest bus edge (for a pictorial explanation of this configuration, refer to Figure 5-22 on page 97).

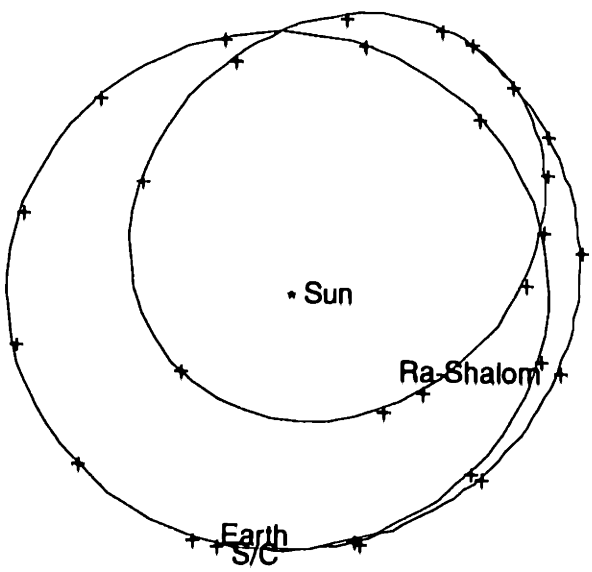

Figure 2-1: Trajectory for encounter with the asteroid Ra-Shalom (2100).

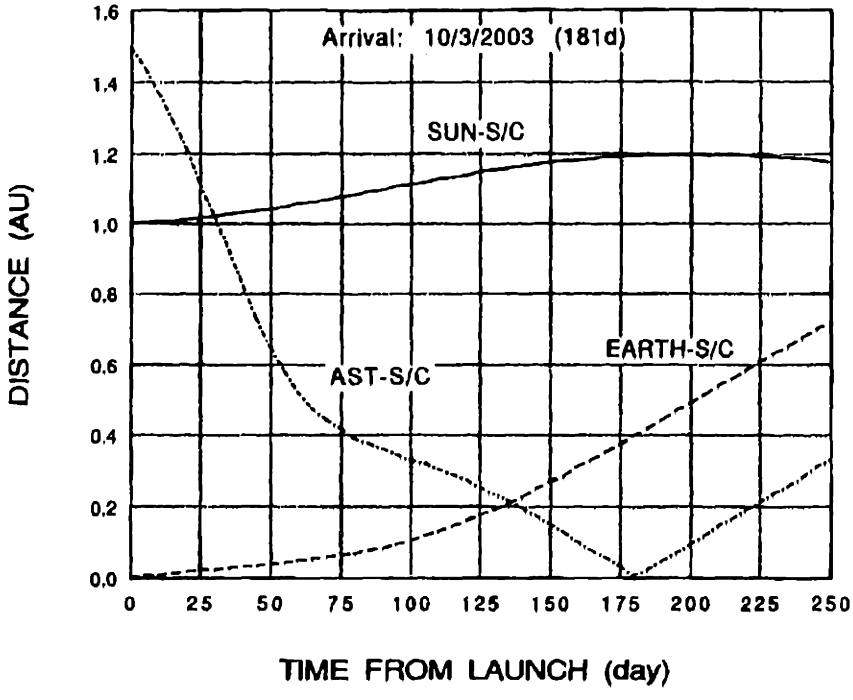

Figure 2-2: Relative distances of sun, earth, asteroid, and spacecraft for a 2003 encounter with 2100 Ra-Shalom.

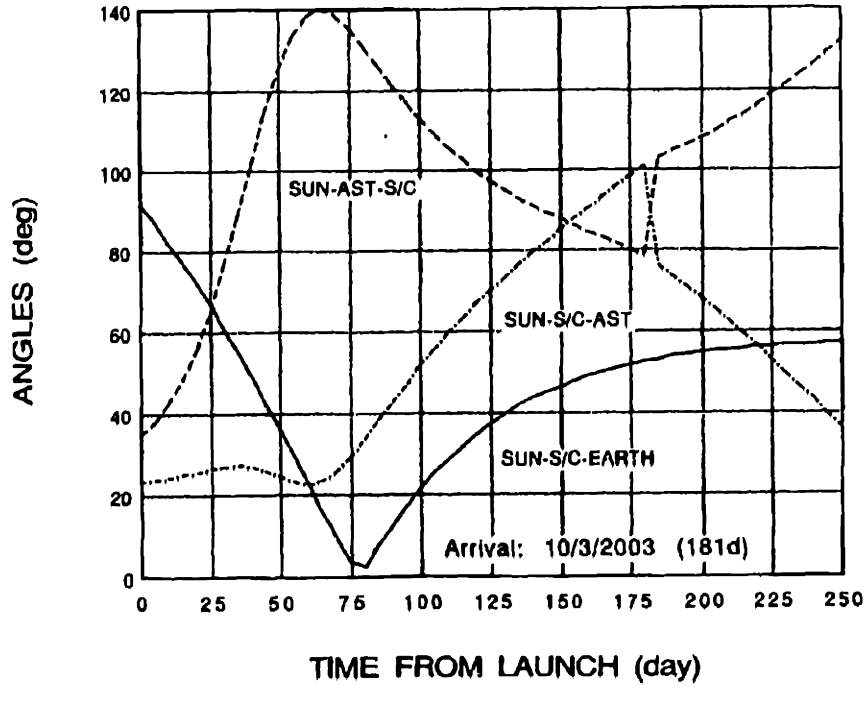

Figure 2-3: Relative angles of sun, earth, asteroid, and spacecraft for a 2003 encounter with 2100 Ra-Shalom.

Chapter 3

Background Work

The following three sections give a short, system-level description of the PNEAF, AIM, and SGM spacecraft. Requirements, science, system, and subsystem summaries are provided, as well as configurations and functional block diagrams. Mass and power lists for each are given in Appendix A. The purpose of this information is to show the progression from a conventional spacecraft design using conventional architecture (PNEAF) to produce a highly integrated architecture that was developed for SGM and the microspacecraft proposed in this study.

3.1 Pegasus-launched Near Earth Asteroid Flyby (PNEAF)

The Pegasus-launched Near Earth Asteroid Flyby (PNEAF) is a JPL concept for a single spin-stabilized spacecraft to be launched on the (then) newly-introduced Pegasus launch vehicle. This system concept was developed by David Collins for Ross Jones and was completed in October 1990 [3].

3.1.1 Requirements

The requirements established at JPL for this spacecraft are as follows:

- Fit within the Pegasus shroud and mass constraints
- High resolution imaging (30m/pixel)
- Provide large ΔV (3.3km/sec) for injection plus 130 m/sec for trajectory corrections
- Optical navigation
- Low cost ($70M for development, launch, and upper stage)

3.1.2 Science

The scientific payload is a visible-light camera which shares electronics with the Canopus/earth scanner used for attitude control. It has a one meter focal length (f/10), and six-color filters. The detector is a 1024x1024 exposed array of 12μm pixels (12x12mrad FOV). Imaging is conducted over ten hours, starting five hours prior to encounter. 64 equivalent full-frame images are taken during this time and are stored in memory.

3.1.3 System Description

Functionally, the PNEAF spacecraft has a traditional architecture. The functional block diagram shown in Figure 3-1 clearly shows the telecommunication, power, attitude control, propulsion, and the centralized computing. However, the initial step toward integration was taken with the integration of

the imaging electronics. The spacecraft bus is cylindrical and occupies the full diameter of the Pegasus. The length, including upper stage, is still shorter than the Pegasus shroud. The PNEAF configuration is shown in Figure 3-2.

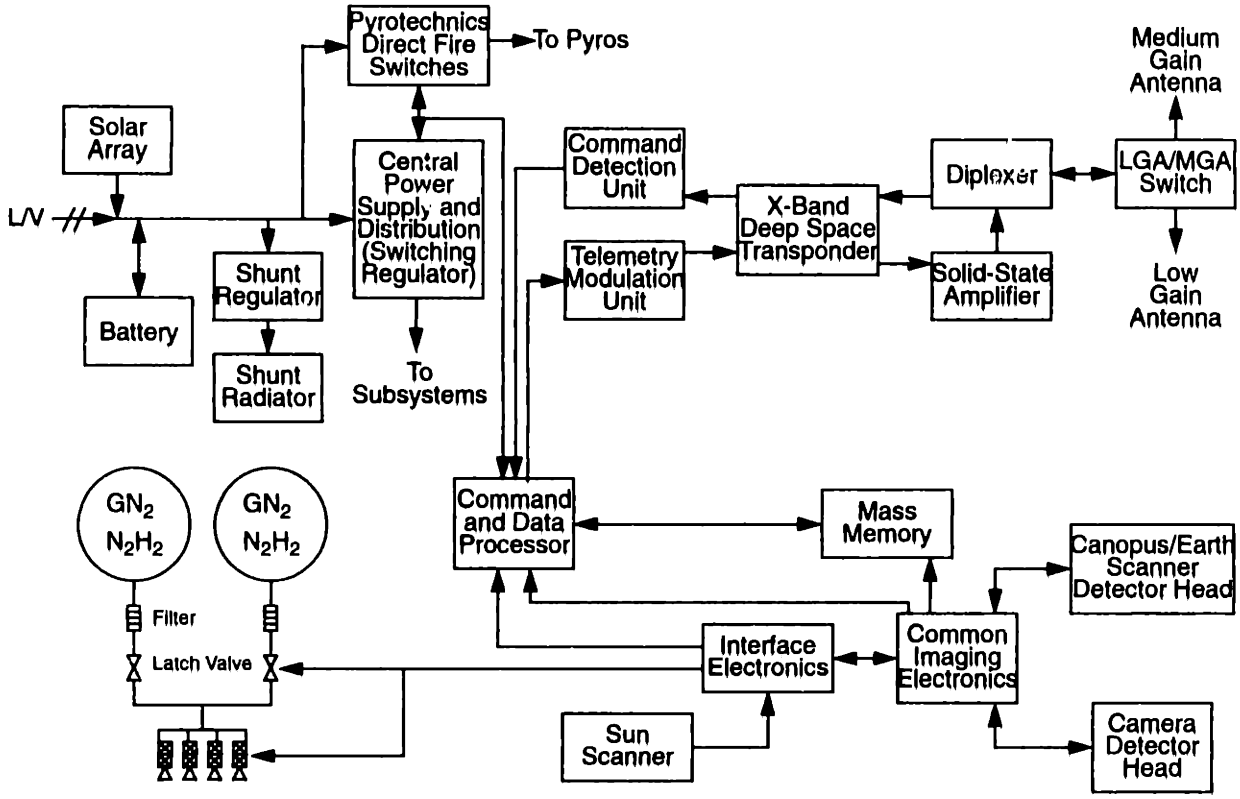

Figure 3-1: PNEAF functional block diagram.

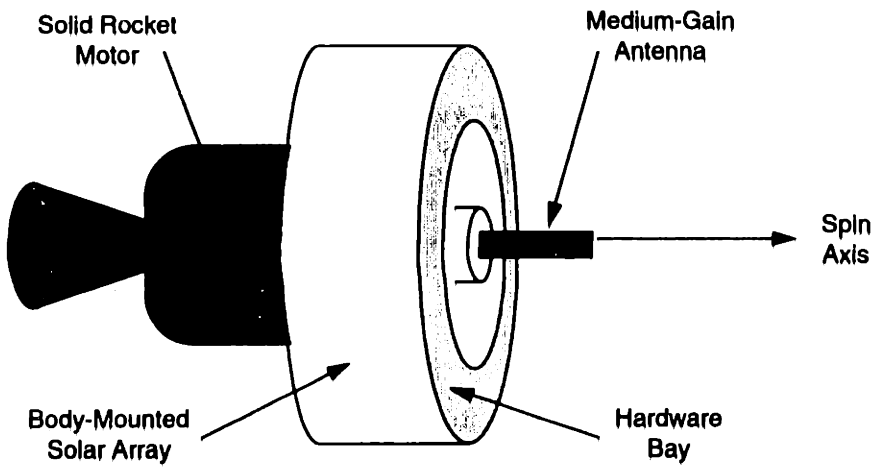

Figure 3-2: (a) PNEAF spacecraft configuration, and (b) PNEAF launch configuration.

3.1.4 Subsystem Overview

Telecommunication. Communication is accomplished using an all X-band system that transmits up to 99bps through the 70m Deep Space Network (DSN) antenna.

Electrical Power. Solar power is captured using body-mounted Si solar cells which provide 66W at encounter. A one Ampere-Hour NiCd secondary battery is used during short transients above solar array capacity and a centralized power supply system provides regulated voltages to all subsystems.

Attitude Determination and Control. The spacecraft is spin-stabilized with passive nutation damping. A sun scanner provides sun cone angle with respect to spin axis, rotation rate, and phase. A canopus/earth scanner provides clock angle with respect to sun line.

Computation and Memory. A 1750A microprocessor with more than 1MIPS computation throughput provides processing for all subsystems. 0.5Gbit solid-state memory is used.

Structure. A central aluminum cylinder is used as primary structure and radial honeycomb plates provide secondary support.

Thermal Control. A solid insulation ring minimizes conductive heat transfer from SRM to spacecraft. Electrical heaters are used to warm valves, propellant lines, and catalyst beds when necessary.

Propulsion (post-injection). Four 0.2lb_f hydrazine thrusters are used for spin-up/spin-down control, each controlled by redundant valves. Hydrazine is stored in two 9.4in diameter tanks and pressurized with gaseous nitrogen.

3.2 Asteroid Investigation with Microspacecraft (AIM)

The Asteroid Investigation with Microspacecraft (AIM), now one of the Asteroid, Comet, Moon Exploration (ACME) series, is another JPL concept for an asteroid flyby using first generation microspacecraft technology. Three of these 3-axis stabilized vehicles can be launched on a single Pegasus (mated using a single adapter), each using its own upper stage. This system concept was developed by Christopher Salvo, for and with the guidance of Ross Jones, and was completed in October 1991 [5,6].

3.2.1 Requirements

The requirements established at JPL for this spacecraft are as follows:

- Launch three spacecraft on a single Pegasus
- Trajectory constraints: C_3 (injection energy) < $4km^2/sec^2$, solar range of 0.9 - 1.2AU, and earth range of no more than 1.6AU
- Post-injection ΔV < 200m/sec
- Visible imaging with 10-20m/pixel resolution
- Use of advanced technologies which have been demonstrated in the lab

3.2.2 Science

The payload is an integrated telescope that obtains visible and infrared spectral images. It is used for science as well as for optical navigation during cruise. The highest achieved resolution is 8m/pixel-pair. Full face images of the asteroid fill the camera frame. In addition, radio doppler using the telecommunication system on board is used for mass determination to within 10%.

3.2.3 System Description

The primary achievement of the AIM design is its size. Its system functionality is quite similar to that of the PNEAF (functional block diagram shown in Figure 3-3) yet it weighs less than half. Compact primary structure and more advanced miniature technologies (such as advanced millimeter wave devices for the transponder, high efficiency solar cells, and micro IMU) are responsible for this reduction in mass. This configuration is shown in Figure 3-4.

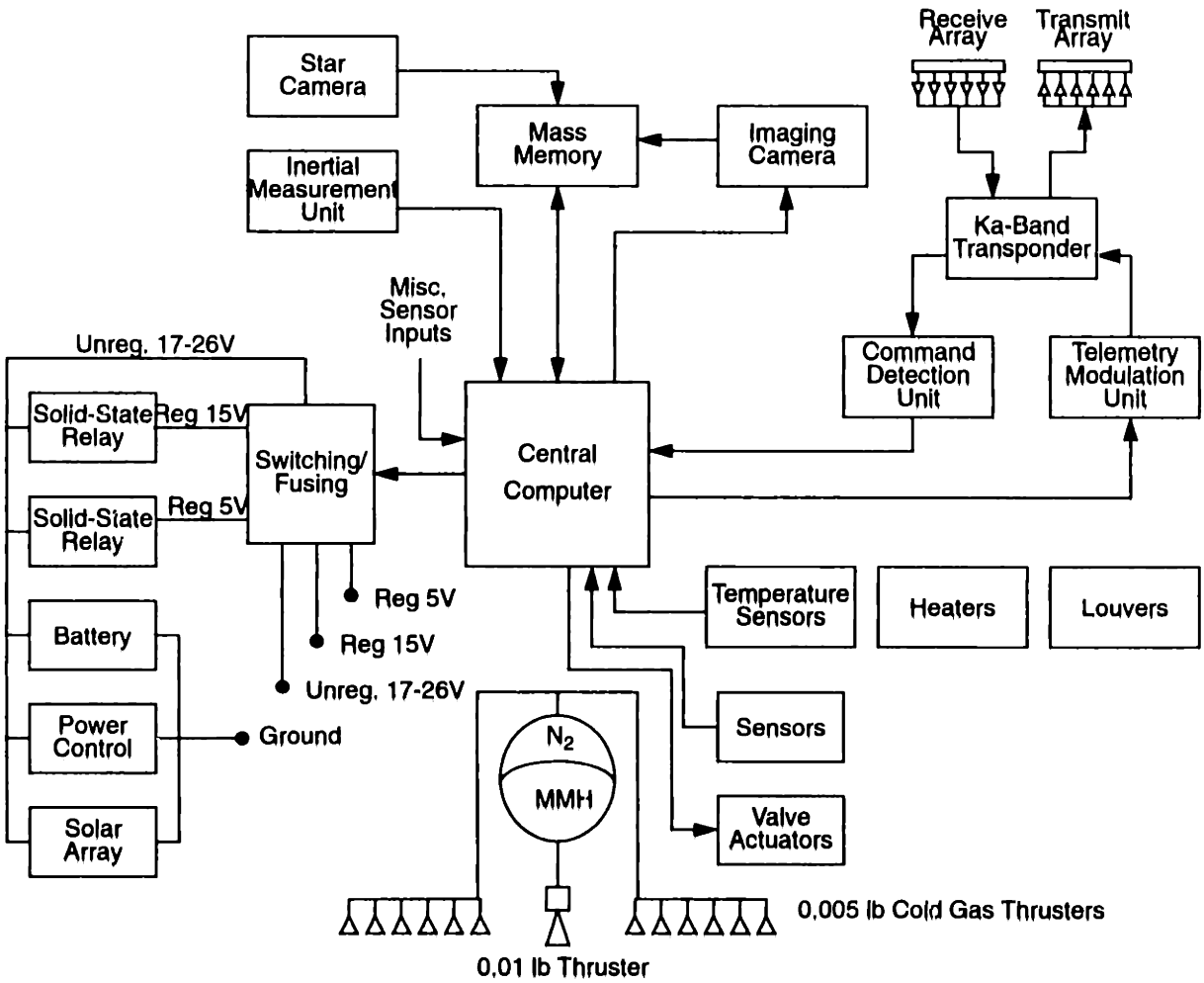

Figure 3-3: AIM functional block diagram.

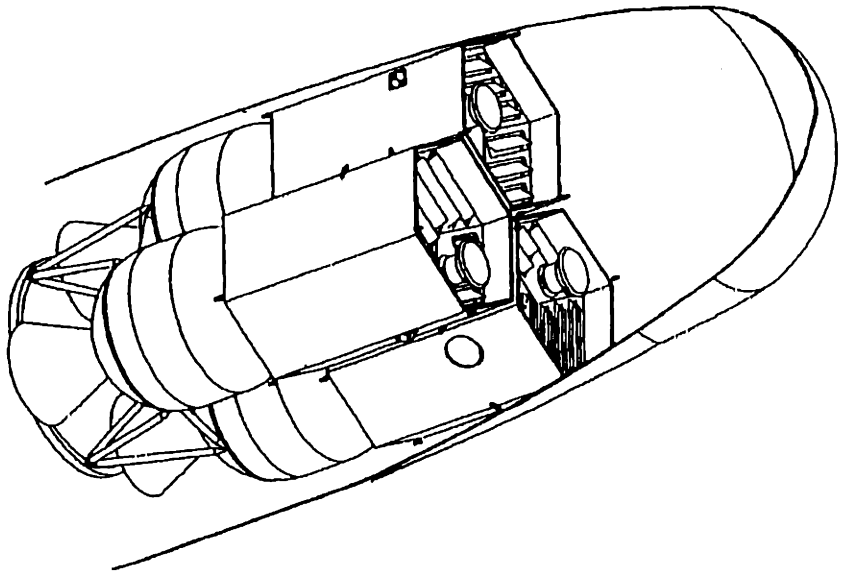

Figure 3-4: AIM spacecraft configuration in the Pegasus payload shroud.

3.2.4 Subsystem Overview

Telecommunication. Communication is accomplished using an all Ka-band system that transmits 100 bits per second at 1.6AU using the 34m DSN antenna. The subsystem uses a 1W solid-state power amplifier and interleaved antenna area that utilizes a single aperture for transmitting and receiving and requires neither diplexing nor beam scanning.

Electrical Power. Solar power is captured using body-mounted (6 panels) GaAs solar cells which provide 37-96W depending on distance from the sun and spacecraft orientation. A 2A-Hr $LiTiS_2$ secondary battery is used during transients above solar array capacity. Unregulated as well as regulated power and centralized switching is provided to all subsystems.

Attitude Determination and Control. 12 cold gas thrusters provide full 3-axis control. A star camera provides 0.01° accuracy, wide FOV sun sensors provide coarse attitude, and solid-state rate transducers (gyros) provide spin data along each of the three axes.

Computation and Memory. A VLSI 1750 microprocessor with application specific integrated circuits (ASICs) provides processing for all subsystems. Memory chips with 1Gbit storage capability are 3-D packaged.

Structure. The primary structure is hexagonal, allowing three vehicles to fit into a cylindrical shroud. The interior is divided into three vertical bays, which allow easier thermal management.

Thermal Control. The primary structure thermally isolates the interior from deep space. Louvered radiators and heaters are used to isothermalize the spacecraft. Heat pipes are used in the solar panels as thermal equalizers for outer walls.

Propulsion (post-injection). The primary propulsion system uses hydrazine. There is no redundancy in this design. The cold gas thrusters for attitude control use nitrogen and are partially redundant. The nitrogen is used as both cold gas and pressurant for the hydrazine.

3.3 Second Generation Microspacecraft (SGM)

This concept is an example of a second generation microspacecraft that is designed to greatly reduce life-cycle costs. The vision for this class of spacecraft, first developed by Ross Jones, is of a small, highly integrated, highly autonomous vehicle. David Collins created the first SGM design and presented it in October 1993 [7]. There are two key attributes to this concept. First, it has an integrated optics system; a single aperture is used for all on-board optical functions. Second, it has no uplink; navigation is optical and completely autonomous. This second attribute greatly reduces post-launch ground operations costs.

3.3.1 Requirements

The requirements established at JPL for this spacecraft are as follows:

- Same mission plan as AIM (see Chapter 4)
- Spacecraft total mass (not including upper stage) should be ~5kg
- Use aggressive advanced technologies with technology readiness later than the year 2000

3.3.2 Science

Science is conducted through a camera shared by several subsystems on board. During encounter, this instrument takes black and white images using an unfiltered 2048x2048 Si detector as well as colored pictures using a linear variable filter on top of two narrow Indium Galium Arsenide (InGaAs) detectors used in "push-broom" mode. Depending on the distance of closest approach, the resolution can be better than 10m/pixel.

3.3.3 System Description

The functional block diagram of the SGM (shown in Figure 3-5) shows a slightly new functional architecture. Although the telecommunication, power, and propulsion subsystems are still clearly identified, the distributed optical apertures on-board PNEAF and AIM were combined into a single optics subsystem. Another architectural design change from the prior two systems occurred in the physical architecture. Instead of housing each subsystem in its own bay, all electronics were integrated into two bays (one for DC which also hold the optics, and the other for RF). This made the system much more compact and less massive. The configuration is shown in Figure 3-6.

3.3.4 Subsystem Overview

Telecommunication. Downlink of compressed data at a rate of 68bps (into a 34m DSN station) is accomplished using X-band. No uplink is accommodated. A patch antenna is utilized.

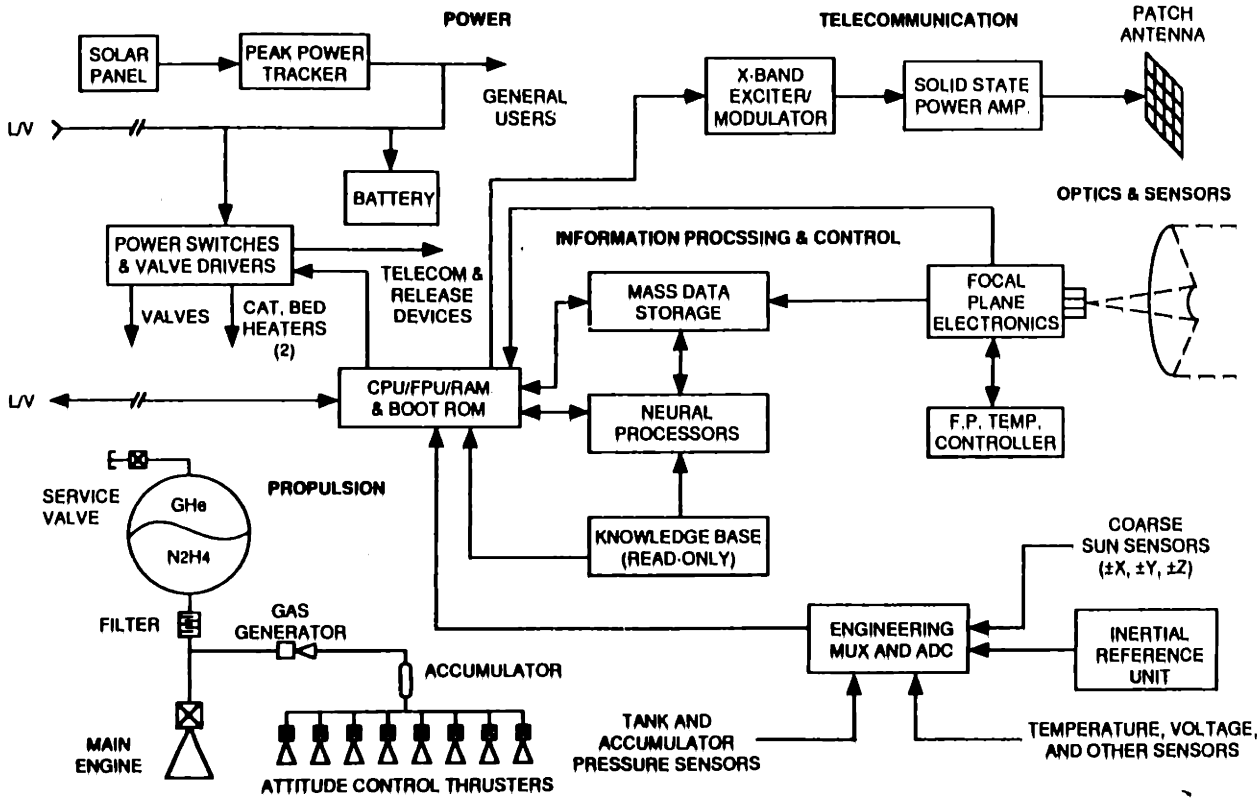

Figure 3-5: SGM functional block diagram.

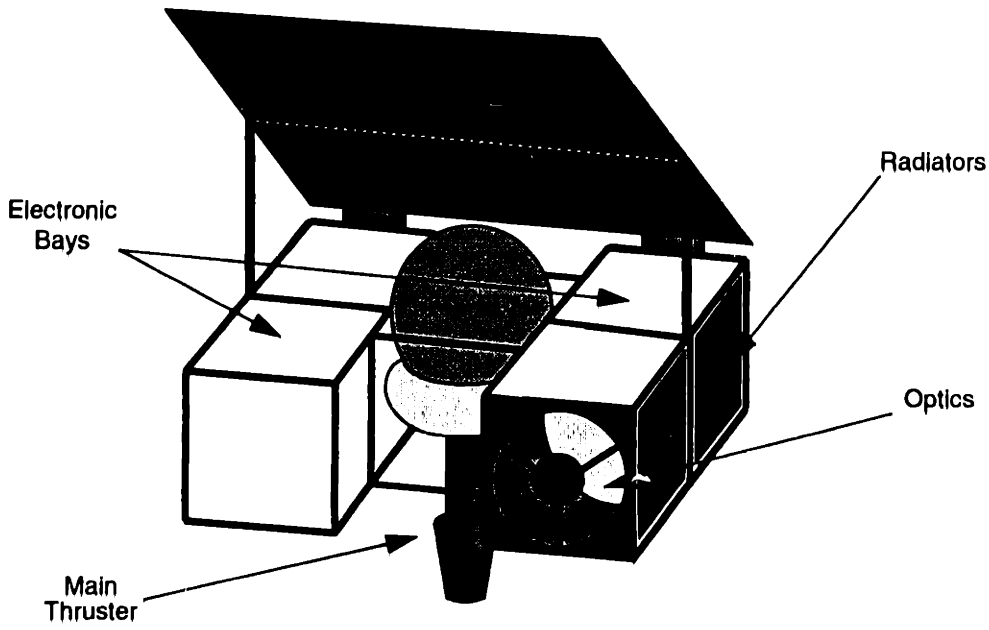

Figure 3-6: SGM cruise configuration.

Electrical Power. A thin-film CdTe solar array provides a maximum of 13W. A peak power tracker optimizes power over a wide range of array temperatures. Eight $LiTiS_2$ "AA" batteries provide energy storage and limit bus voltage swings. Continuous and switched power are provided to all subsystems over a 4V bus.

Attitude Determination. An integrated optics system is used as a star tracker during cruise and as a target tracker during encounter. A micromachined inertial reference unit (IRU) is used as a nominal attitude reference and low resolution sun sensors are used to track the sun.

Attitude Control. Eight attitude control thrusters provide 3-axis control in couples.

Computation and Memory. Three types of processors are used: logic/fuzzy logic processor for resource management, math processor for attitude determination and navigation analyses, and neural processor for star/planet/target identification. On-board memory capability includes 4Gbit of knowledge base (star maps and navigation algorithms) and 1Gbit of mass data storage.

Structure. An H-shaped primary frame supports the propulsion module and high density electronic packages. Most cabling is replaced by interconnections on multi-chip module packages.

Thermal Control. The propellant tank and main engine valve are thermally coupled radiatively/conductively to the electronics. Sun-free radiators reject excess heat and the solar panel is cooled by radiation on both its sides.

Propulsion (post-injection). The main engine is a 0.9N hydrazine thruster. The attitude control thrusters use hydrazine gas generated from the liquid hydrazine used in the main system. All valves are single string.

Chapter 4

Miniaturization Concepts

This chapter describes the miniaturization concepts that were used in the specific design of an asteroid flyby mission. The elements of the process used can be applied to other missions or even other systems; the specific conclusions discussed, however, result from the specific constraints and guidelines for this particular mission.

4.1 Elements of Miniaturization

There are many ways to make a device smaller. This is apparent from the designs that were presented in the background chapter which showed how the two designers of the AIM and SGM applied different methodologies and thus, achieved different levels of miniaturization. Needless to say, the "success" of the two methodologies cannot really be compared, since the SGM design built on the achievements of AIM, taking them a step further. It is the objective of this study to consider all possible aspects of the miniaturization process, which can also be used in other missions, and apply them to a design that represents the next step; a next generation microspacecraft (NGM)[1].

The term miniaturization applies to the downsizing of those key properties of the spacecraft that have direct bearing on its overall mass and size. The most obvious property is the mass of each individual component. Other properties to which the miniaturization can be applied are power, volume, number and size of apertures, and number of individual components. Each of these has an impact on the overall mass and size of the system. Lower power requirements reduce the size and mass of the energy storage hardware as well as individual component size. Smaller volumes and smaller apertures (such as antennas, solar arrays, and optics) require less support structure. Finally, a smaller number of components, each with a higher level of functionality, weigh less. In addition, the reduction in the number of apertures reduces the need for surface area on the outside of the spacecraft, which affects its volume and hence its mass. The effect of these elements on each other and on the entire system in this miniaturization process is more clearly expressed on a block diagram chart (see Figure 4-1). This figure provides a view of how one can approach the miniaturization process. By reducing, lowering or eliminating all or part of any of the four elements, the system mass and size can be reduced.

1. "Third generation" is not used here because the extent of generational change has not yet been established.

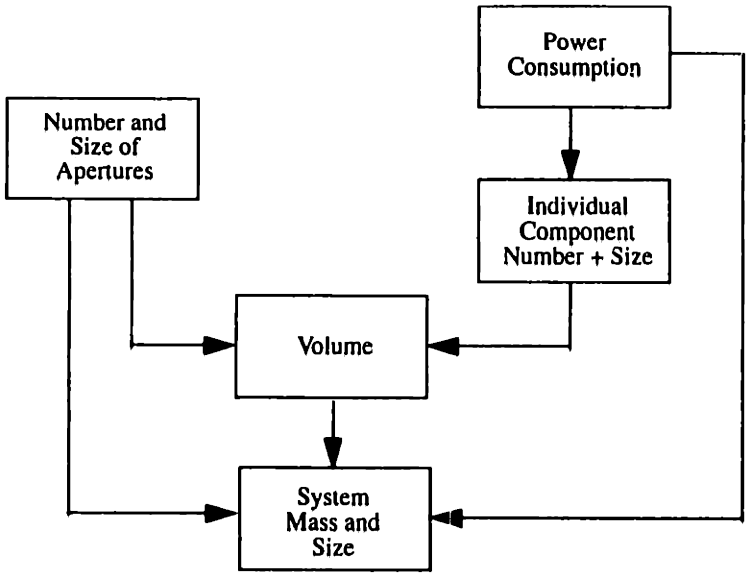

Figure 4-1: Relationship of key properties which affect the size and mass of the system.

Embedded in the four aspects of the miniaturization process mentioned above is the issue of functionality, or rather functional integration. Too often the architecture of a flight system is dictated by a long-standing organizational structure. Many functionally similar processes, components, or events that take place on-board exist in parallel to support the needs of each individual subsystem, which is traditionally looked upon as a stand-alone "box." This creates a certain level of unnecessary redundancy in the overall system. The elimination of this redundancy can greatly miniaturize the system.

In addition to functional redundancy, traditional space systems include hardware redundancy. For example, redundancy in the support structure is a result of each subsystem group claiming "ownership" to each piece of hardware for which it is responsible. The system integrators then take these pieces of hardware and incorporate them into a box (support frame) which is in turn supported by the spacecraft bus. Elimination of the middle structure (the boxes) can greatly reduce mass. The following sections will discuss the specific methods used in the design of the asteroid flyby mission as they relate to functional integration, hardware integration (including apertures), volume reduction, and power reduction.

4.2 Re-examining Functionality

On the system level, a spacecraft needs to perform a set of well-defined functions. In the past, these were grouped into subsystems, which are now deeply rooted into company and laboratory structures. However, as the architecture of spacecraft changes and designs become more integrated, some functions that should be performed on the system level and at a central node end up being performed at several locations on-board. Identifying all functions that need to be performed, independent of who will build the hardware to support them, might allow for a higher level of integration. Although the

corporate and research structures necessary to support the program for such a spacecraft might be different than the structures we have today, this issue was not considered a constraint on the design. Those differences will be resolved as the level of integration gradually increases and programs change to accommodate them.

4.2.1 Design Through Functionality

In this research project, the design was started by defining the primary and secondary functions. A primary function defines an operating characteristics of the spacecraft, such as acquire data; this does not indicate how the function will be performed, but rather what will be accomplished. A secondary function is an activity which is required to implement the primary function, such as convert energy to electrical signals. Each primary and secondary function was then examined as to its real need. Then, instead of defining interfaces, overlap properties were identified to determine if they could be integrated. Only then were requirements developed and interfaces and hardware units defined. The list of primary and secondary functions for this mission is shown in Table 4-1.

4.2.2 Elimination of Specific Functions

The list presented in the prior section provides a set of functions that must be fulfilled by any spacecraft regardless of mission requirements. The goal of reducing mass, power, volume, and cost calls for the evaluation of the absolute need for each. Two functions have been eliminated as a result. The first is the uplink function, primarily used for navigation, external vehicle control, and anomaly correction. If the vehicle is designed to be completely autonomous, this function is unnecessary, and its elimination greatly reduces the mission operations segment. The second function eliminated from the NGM design is the structural support. Because of advances in electronic packaging technologies, the need to box certain elements man be eliminated. The responsibility of the structure is reduced to structural integration as opposed to hardware housing.

Elimination of Uplink

As spacecraft autonomy increases the need for uplink as a day-to-day operations tool decreases. Accordingly, the reduced ground operations as a result of the elimination of ground sequencing, lowers project costs. According to a JPL analysis performed for the SGM study [7], the elimination of the uplink function is estimated to reduce mission operations cost by over 60%. Of course, the design must incorporate on-board most of the functions traditionally handled from the ground.

Navigation has traditionally been accomplished using a combination of on-board and ground-based capabilities: star camera images are compared to star maps stored in memory in addition to radio frequency (RF) techniques that track the spacecraft from the ground. The autonomous navigation process baselined for the SGM design is accomplished independently by triangulation algorithms (see

Table 4-1: Primary and Secondary Functions Performed On-Board an Asteroid Flyby Spacecraft

Primary Function	Secondary Function	Primary Function	Secondary Function
Scientific Data Acquisition	Energy Collection	Telecom-munication	Signal Reception
	Energy to Signal Conversion		Demultiplex/Demodulation
Propulsion	Thrust Generation		Frequency Generation (necessary for no uplink)
	Propellant Containment/Feed		Code
	Fluid Flow Control		Modulation/Multiplexing
Attitude Determination	Acceleration/Axial Forces		Amplification
	Angular Rates/Torques		Transmission
	Sun Reference	Power Management	Power Generation
	Horizon Reference		Energy Storage
Navigation	Position Determination		Power Regulation
	Tracking		Distribute Power
	Relative Distance Determin.		Power Switching
Attitude Control	Axis Spin Rate Control	Anomaly Detection	Temperature
	Articulation		Pressure
Thermal Control	Heat Transfer		Voltage
	Heat Expulsion/Cooling		Current
	Heating	Data Storage	Random Access Memory
	Insulation		Read Only Memory
Structural and Mechanical Support	Support Loads	Data Processing and Management	Data Distribution
	Packaging		Math Processing
	Cabling		Logic Processing
	Mechanisms		Neural Processing

discussion in Section 5.5 on page 63). Once the target is in the FOV, target tracking techniques are used to guide it in its path. In addition to guidance, the ground controls the vehicle in case of an anomaly. The decreased number of elements on-board, as well as the increased computing and memory capabilities, however, allow the spacecraft to activate pre-programed contingency plans. Of course, such an extensive assembly of contingency plans involves higher costs for the software development and testing aspect of the program. Finally, the absence of an uplink function cannot accommodate any changes to the mission profile which might be requested by scientists (or other end users) and program managers. The elimination of the ground intervention for navigation and anomaly correction provides an additional level of risk that is assumed to be allowed in this type of vehicle.

Elimination of Structural Boxes

As mentioned earlier, traditional spacecraft designs include three layers of structure: *elements*, such as sensors, chips, optical devices, detectors etc.; *boxes*, which hold elements together as a subsystem; and *a bus*, which integrates the boxes into a single structure that can withstand loads and provides mechanical interfaces. The SGM design eliminated the use of boxes. All electronics (in the form of Multi-Chip Modules, see Section 4.4.1), optics, and other elements are housed in a single structural unit. This H-shaped frame provides the mechanical integration of the spacecraft.

In the NGM design, the need for a dedicated frame for structural integration is eliminated. This is primarily achieved by using more aggressive multi-chip module (MCM) technologies. All hardware elements were designed so that they could be integrated on such a module. Not only do silicon dies and other circuitry elements reside on MCMs, but other elements, such as microwave electronics, attitude control, and power hardware, are integrated there as well. Since the size of the MCMs is uniform and rather small, they are simply placed "around" the optical cavity, and some of them even provide part of that structure. These units are held together by fibers drawn from the composite tank. Thus, the need for a dedicated structure was eliminated by directly mounting elements to each other and to the propellant tank, which can provide structural support as well as integration.

4.2.3 Integration of Overlapping Functions

There are certain on-board resources that are used by many of the elements. Computing resources are necessary to control the attitude control functions, navigation, anomaly detection and correction, data acquisition and processing, and others. In addition, all these functions require a certain memory allocation. The computing and memory functions, to a certain degree, have been distributed throughout the spacecraft. Another shared resource, discussed in the previous section, is the structural support. Functions such as science acquisition, attitude determination, and navigation use optical elements. Although these elements have different properties, a compromising design that satisfies as many of the requirements as possible can build these functions around a single set of optics, as was done in the SGM design.

4.3 Hardware Integration

The hardware that supports the functions described above is a prime focus for the miniaturization process. If the number of functions can be reduced by either elimination or combination, the number of hardware units may be reduced as well. Each hardware unit occupies a certain volume and is supported by a structure, most use power-consuming electronic devices for their operation, and several require access to the environment outside the spacecraft. As discussed above, each of these three elements

contributes to the mass and size of the overall system. Thus, if several functions can be performed using a common set, a considerable amount of mass and volume may be eliminated.

Figure 4-2 traces the steps taken to integrate the three parameters mentioned above: apertures ('a'), electronics ('e'), and structures ('s'). The column on the left shows the traditional subsystem breakdown and its needs for any of these three resources. In each of the subsequent columns a major step is taken in order to integrate the system. The first step shows the level of integration achieved by the SGM, which set the precedence for the following two. This step primarily involved the integration of all electronics and optical functions. The next step involved the integration of electronics with the structure, which is accomplished by allowing the electronic packages to provide the primary structure of the system. The final step in this integration process results in a single unit that provides a primary structure which supports the optics and other miscellaneous hardware using the electronics packages and is fully integrated with the propellant tank (the main element in the propulsion structure). Thus the chart shows all 'e' and 's' elements in a single box plus six independent access apertures. The NGM concept achieves the second integration process and most of the third. Because the electronics hardware was miniaturized so drastically, it was impossible for it to provide full structural support for the optics. This will be further discussed in the next Chapter. This remains of this section attempt to explain Figure 4-2 by examining the integration within each of these elements as well as the integration among them.

4.3.1 Apertures

An aperture is defined here as an access interface between an internal piece of hardware and the external environment. Such an interface is referred to here as an external interaction vector. There are five types of primary external interaction vectors on board a spacecraft[2]:

1. Optical line-of-sight (LOS)
2. Communications link (antenna)
3. Thrust (main)
4. Solar energy collection (vector perpendicular to solar array)
5. Energy radiation (vector perpendicular to radiators)

The attitude control thrusters are not listed here because they require vectors that are pointed in several directions. However, special emphasis was placed on reducing the total number of these external interaction vectors. To provide a full 3-axis control twelve thrusters are required (four for each of the three axes). This can be reduced to an eight-thruster configuration which is described in further detail in Section 5.6.2 on page 65. This control architecture covers only four out the six possible "faces" on the spacecraft, yet it still provides 3-axis control in couples.

2. Assuming an optical payload.

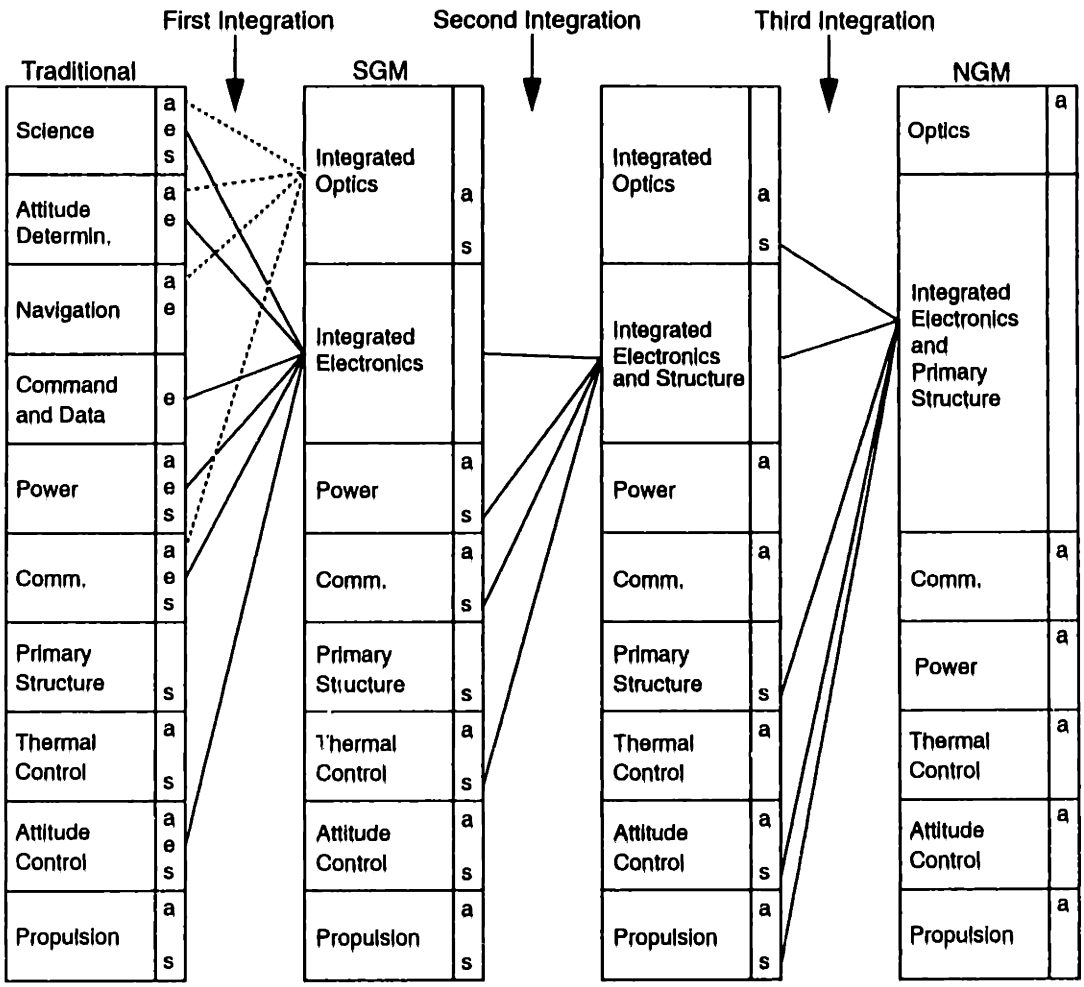

Figure 4-2: Integration of access apertures ('a'), electronics ('e'), and structure ('s') among the hardware used to perform primary functions on board.

Traditionally, there are several optical line-of-sight vectors on board. Optical scientific payloads require a LOS to their targets, star trackers require a LOS to a portion of the sky, sun sensors require a LOS to the sun, etc. In addition, the new type of communication link that uses lasers requires a LOS to Earth. Although each of these requires a LOS to a different target and uses a different set of optical parameters, the design team for the SGM developed an optical apparatus that satisfies the need of all of the above functions. This is shown in Figure 4-2 as the merging of the science, attitude control, and navigation "apertures" ('a') into the single aperture of the integrated optics. This design allows for a single optical external interaction vector.

The communication link vector represents the RF beam used to carry data to and from the ground. The thrust vector indicates the orientation of the main thruster in the direction in which thrust is applied. The solar energy collection vector is parallel to incoming sun rays, which optimally hit the

solar array panel at a normal angle. Finally, the energy radiation vector traces the direction in which excess heat is radiated from the spacecraft to deep space.

Mission requirements govern the orientation of the vectors. The requirements for the asteroid flyby mission are shown in Table 4-2. These constraints, defined prior to the SGM design but used in the NGM design, are both the basis of the spacecraft configuration as well as the limitation on the spacecraft volume. A schematic of the vector orientation used in the SGM design is shown in Figure 4-3. In this case, each of the six sides of the cube supports an "aperture". The antenna, solar array, optical LOS, and thrust vectors are in the plane of the ecliptic while the radiation vectors point out of plane ensuring that this vector will never be parallel to incoming sunlight.

Table 4-2: Constraints on External Interaction Vectors

	Aperture	Must Point	Cannot Point
1.	Optical Line of Sight	At Target At star background	At Sun
2.	Antenna	At Earth (post-encounter primarily)	
3.	Thrust	90° orientation to LOS†	
4.	Solar Array	At Sun	
5.	Radiators	Out of Solar plane	At Sun

†. Since the LOS is along the velocity vector (in order to navigate) and the thrust will be used primarily to correct trajectory, burns will be required to be perpendicular to the velocity vector and thus to the LOS.

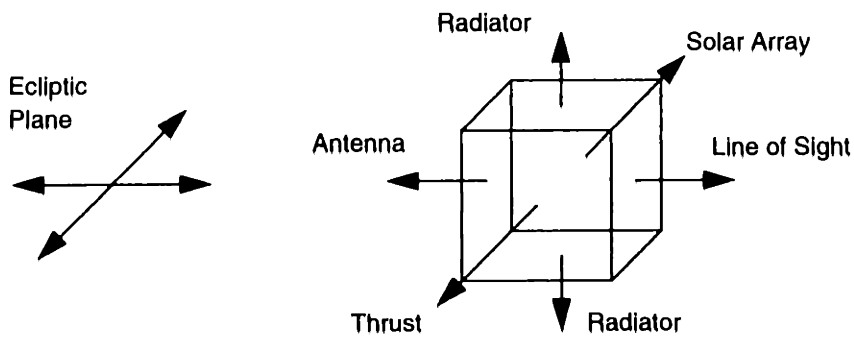

Figure 4-3: External interaction vector orientation on the SGM.

The combination of any of the vectors could potentially free one or more of the six faces. The resulting advantage is the flexibility in the sizing of that side. The designer may choose its dimensions in such way that the total volume of the box-shaped bus is reduced. Note that in the case of the two

heat rejection vectors, combining the two into one gives no benefit since a certain area is required to radiate the heat generated on board. As a matter of fact, an opposing radiator configuration presents a more efficient use of volume since the required total area is halved.

In trying to combine two or more of the external interaction vectors, the designer must ensure that the alignment does not contradict any of the mission-imposed requirements stated in Table 4-2. There are ten possible combinations of pairs (1 and 2, 1 and 3, etc.) and nine possible combinations of triples in a set of five vectors. Most of these can easily be eliminated because they present a direct contradiction of the requirements. For example, the combination of the energy collection vector (#4) with the energy radiation vector (#5) can be eliminated since one must view the sun and the other must avoid it. Of the 19 possible combinations, four are plausible:

- *Optical LOS and communication (1 and 2)* - optical communication (using lasers) can be integrated so that it can use the existing set of optics used by the science payload, attitude control, and navigation. Although each function needs to view a different object or objects, the mission can be designed such that each function is performed at a different time.
- *Optical LOS and energy radiation vector (1 and 5)* - neither can view the sun during any phase of the mission.
- *Optical LOS, communications, and radiation vectors (1, 2, and 5)* - a combination of the two previous options. This multi-purpose aperture leads to a totally different type of architecture -- a thin satellite [10] -- which is basically a thin sheet where most external interaction vectors point out the top or the bottom.
- *Energy collection and communications vector (2 and 4)* - patch antennas (see next chapter) which use small, equally-spaced radiating patches, can be integrated with solar cells. The cells can be placed on the substrate around the radiating patches.

These options for integrating the external interface vectors will be considered in Chapter 5 in developing the overall system architecture and configuration.

4.3.2 Electronics

Most components on board a spacecraft are active components. That is, there are some logical or mechanical functions that they perform with the guidance of electronic components. These components are guided by a dedicated set of electronics composed of logic circuitry (generally, Application Specific Integrated Circuits, or ASICs), memory, and various other electrical elements. Although the complete integration of these computational functions might not provide an optimum architecture (a distributed architecture has many advantages), integration of the computational hardware will certainly reduce mass.

The co-location of electronics becomes more natural as spacecraft and electronic components become smaller. Since electronic components require a certain level of environmental control they need to be provided with adequate packaging. It is that packaging that consumes most of the mass. The optimum solution then would be to place all electronics in the same place and to provide a single set of

housing. One of the problems associated with such an architecture is the complexity of cabling that is necessary to extend from the electronics "box" to the rest of the components on the spacecraft. However, a clever architecture, which places the instruments close to, or even as a part of the electronic packages, in combination with the smaller bus resulting in much shorter distances between individual components, can make this problem seem insignificant.

The SGM design integrated the electronics into two bays. Instead of merging seven sets of electronics into one, as shown in the first integration step in Figure 4-2, the seven sets merged into two. However, there are no redundant functions being performed, which is why the SGM design has achieved that first level of integration. The first bay contained the optics as well as the electronics to support them: mass memory, inputs/outputs, and the focal plane temperature control. It also included all computation circuitry and the knowledge base (read-only memory, or ROM). The second bay contained the power-integrated circuitry (including power switches and valve drivers), an inertial reference unit, an engineering multiplexer, and the telecommunication hardware. The separation of the radio frequency (RF) circuitry from the rest of the electronics is essential since the magnetic fields generated by the microwave electronics can damage the other components. Therefore, a package that contains all electronics on a spacecraft which uses RF communication must include an electromagnetic interference (EMI) shield which adds mass.

The next level of integration took place in the NGM design. The electronics packages (this time in a single package) were designed to also withstand loads. This made these packages the bus of the vehicle and in a way provided an integration of the electronics and the primary structure as shown in the second integration step in Figure 4-2. In the initial stages of the design, it was intended that the multi-chip modules (see Section 4.4.1), which are the electronic packages, would provide the optical bench as well. That is, the optics would be embedded in and supported by the MCMs, which could be configured into various shapes to accommodate this new function and thus achieve the third step of integration. However, as the design progressed, it was evident that the level of miniaturization possible with the electronics would not have a sufficient amount of packaging to provide the entire optical bench. Therefore, the third integration step was not necessary. It is possible that more complicated missions with a greater system functionality would require more electronics hardware that could provide enough packages to be fully integrated with the optics.

4.3.3 Structure and Thermal Control

As the levels of integration increase, more requirements are being placed on the packages that house electronics. Not only are they designed to provide the necessary electrical properties, but as part of the structure, they are designed to support structural loads. Additionally, since these packages are very dense and electronics produce heat, they also need to be thermally conductive enough to transfer

the heat generated on them to their edges, where it can be radiated away. In the second integration level shown in Figure 4-2 the structure housing all the electronics is integrated with the additional hardware of power and communication (which it logically supports), as well as the primary structure and the thermal control. These versatile structures have to be made using advanced materials and advanced micromachining techniques.

In the third integration step, the electronic packages are integrated with the propulsion and attitude control hardware. The integration with propulsion involves "meshing" the propellant tank with the packages. This can be done by "drawing" fibers from the composite-wrapped tank and extending them so that they can attach to the edges of the electronic packages [11]. These fibers not only structurally support the electronic packages but also allow unidirectional heat transfer from the electronics to the propellant in the tank which needs to be kept warm. The integration with the attitude control hardware refers to the mounting of the reaction control thrusters directly onto the edges of an electronics module, occupying the space between one module to the next. These thrusters are very small, thus they do not interfere with the module configuration of the electronic packages. In addition, since the packages are now the bus (virtually the entire spacecraft), the placement of the thrusters, as described above, is easily matched with attitude control needs.

4.4 Volume Reduction

As evident in nature, smaller things are inherently stronger. For example, bones in small animals are much more slender than in large animals. This is so because the reduction in size of structures is an elastic scaling problem. In geometric scaling, mass is proportional to the cube of the length, or the volume. However, structural downscaling preserves constant resistance to buckling and bending as well as reduces stress levels under equal loads. This causes the structural mass to decrease more proportionally to l^4, as opposed to l^3 [12]. Thus it is important to also try and minimize the volume which the system occupies so that the structural support mass can be reduced.

4.4.1 Electronic Packaging

Advanced electronic packaging is the technology currently sweeping the portable electronics industry. This method of packaging bare die saves a considerable amount of support structure, which is the greatest consumer of volume and mass in electronic hardware. This new technique is a result of the integrated circuit (IC) revolution that took place during the 1980s. It opened the door for a new level of hardware integration where several types of components, such as electrical, mechanical, and energy storage, can exist on a single module that performs many functions yet is very compact. With the many advantages of miniaturization there are also many new issues to be addressed. The density of such modules and their high level of integration make them difficult to test or repair in the event of a fault.

Also, thermal issues become more severe. On the other hand, many people are interested in solving these problems for the consumer markets, which is why it is safe to assume that rapid advances are still to come in this field.

From PCBs to MCMs

The traditional way of packaging electronic devices involves embedding a silicon die inside a chip. This plastic package is then placed on a dedicated interface notch on a printed circuit board (PCB). The interconnection between the circuitry on the board and the bare die is accomplished through wires that come out from the sides of the chip and fit right into "holes" in the interface unit on the PCB. This, of course, allows the testing of each individual chip before it is integrated into the circuit. The new packaging technique eliminates the middle structure of the chip. Bare IC dies are deposited, using microelectronics micromachining technology, directly on the Multi-Chip Module (MCM) as part of the many integrated circuits it carries. Since the active material (silicon) requires less than 10% of the chip mass, the new packaging technique greatly reduces the mass of the entire package. In addition, this technique improves IC system performance; higher speeds, reduced time delays, and reduced system power are possible [13]. A schematic of a sample surface layout of an MCM is shown in Figure 4-4.

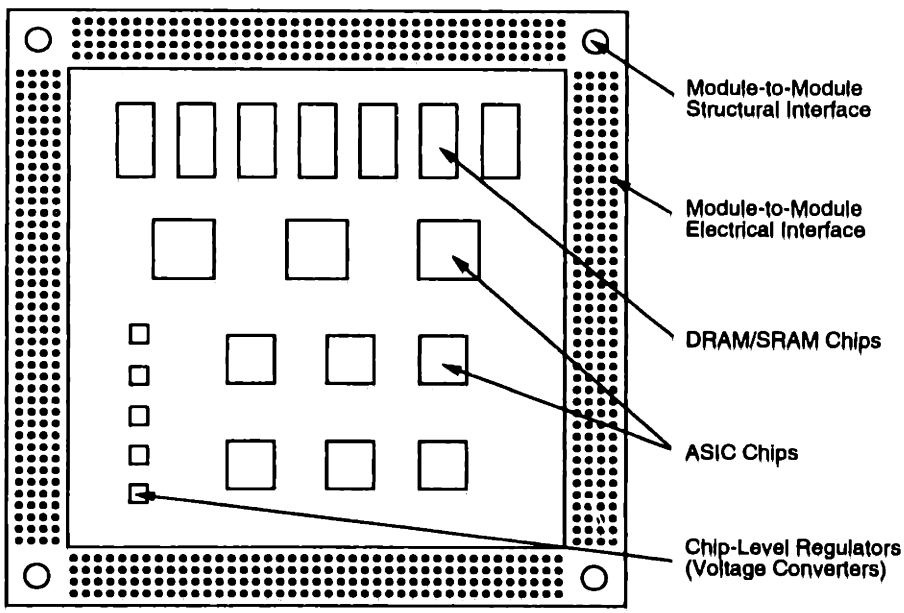

Figure 4-4: Schematic of sample Multi-Chip Module (MCM) surface layout.

The need to reduce volume even further resulted in various ways of stacking bare dies on an MCM. Figure 4-5 shows three chip-stacking techniques in addition to the basic (unstacked) MCM in which each bare die is deposited directly onto the support substrate. Schematics (b) and (c) show two

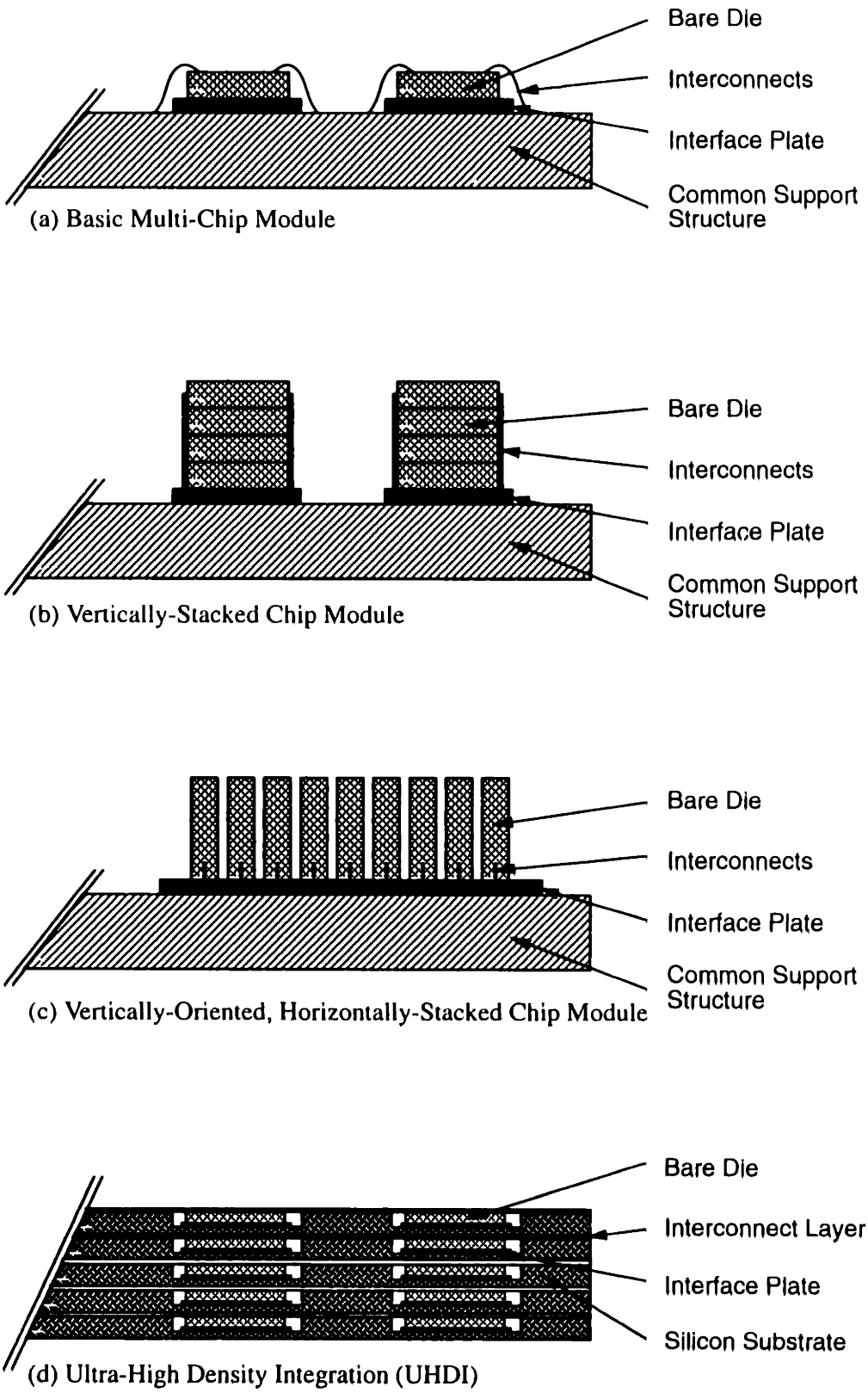

Figure 4-5: Overview of various packaging techniques for MCMs.

orientations of stacked chips. The vertically-stacked chip module provides greater challenges in fault detection and isolation. In addition, it sets a requirement on the separation between one module and the next, which increases the "dead" volume on the spacecraft. A higher level of compactness is possible with the Ultra High Density Integration (UHDI) shown in schematic (d). In this configuration, chips which perform similar functions, such as SRAM and DRAM, and thus have the same dimensions, can be embedded in a silicon substrate and "capped" by a laminated layer that provides the interconnectivity. In this manner, minute substrates can be stacked one on top of the other. The latest laboratory demonstration of this technology included five such layers with a thickness of about 10 mils, or about 250 microns [14]. In all these configurations thermal issues are of prime concern. These will be addressed in Section 5.12.2, "Heat Dissipation in Electronic Packages."

The Greater Functionality of MCMs

The microelectronics revolution began due to the ability to fabricate structures and materials down to the micron scale. This new micromachining revolution spawned several other new technologies, allowing MCMs to carry much more than electronic circuitry. Microelectromechanical systems (MEMS) are micron-scale mechanical devices consisting of mechanical components, sensors, and electronics (see Section 4.6). Inertial reference units, inertial measurement units, and fine microactuators of that small size can be integrated directly onto the MCM, thus reducing the additional support structure that would be necessary to support them elsewhere. In addition, various power technologies allow energy storage and voltage regulation directly on the chip. Thin film batteries [15] could be laid on portions of the MCM (or as a thin layer right on top) and would provide that MCM with all its energy needs. Chip-level regulators could provide the module with the exact voltages the MCM needs. Again, this reduces the number of "free" components on-board that would need mechanical interface to the bus and reduces the amount of cabling necessary. If all elements could be integrated on MCMs, they could be used as the spacecraft structure.

Advanced Substrate Materials

Current MCM designs, such as the ones proposed for the MESUR Network mission [16], are not strong enough to support launch loads. The MESUR study placed the MCMs in a box to provide structural support. In addition, as the density (cm^2 of silicon per cm^2 of surface area) of MCMs increases, the heat generated per module increases. Advanced substrate materials could allow MCMs to be strong enough to withstand mechanical loads as well as conductive enough to direct the heat to the edges where it could be radiated into space.

The ideal substrate would have a very high thermal conductivity, very low coefficient of thermal expansion, high elastic modulus and flexural strength, low density, and high melting point. This way,

any thermal or mechanical loads would have the smallest effect on its configuration, which affects the electronics it carries. It is clear from Table 4-3 that synthetic diamonds have all the desired qualities for a substrate material. Studies on the use of diamond substrates for implementing MCMs were conducted [17] and their performance, not surprisingly, was better than other materials used as substrates. Since the process for synthesizing synthetic diamonds is still expensive and only small quantities can be produced, however, other materials should be considered. Current MCM substrates use Alumina (96% Al_2O_3) or Aluminum Nitrate. These are relatively cheap materials with relatively good performance. Silicon is being considered as a possibility, especially for the UHDI packaging. In that case, the silicon can be micromachined, layer by layer, to include almost all elements, substrate and chips alike.

Table 4-3: Thermal and Mechanical Properties of Various MCM Substrate Materials [18]

Substrate Material	Thermal Conductivity [W/cm°K]	Coef. of Thermal Expansion [μm/°K]	Elastic Modulus [10^{11}N/m^2]	Density [g/cm^3]	Flexural Strength [MPa]	Melting Temp. [°K]
96% Al_2O_3	0.3	6.2	3.0	3.72	400	†
AlN	2.2	4.0	3.5	3.26	300	2473
Si	1.5	2.6	1.7	2.32	†	1683
SiC	2.7	3.7	3.2	4.14	450	2970
Syn. Diamond	15.0	1.0	10.5	3.51	†	2823

†. Values are unavailable.

Of special interest to this design effort is Silicon Carbide (SiC). One of the unique features of the optics package is that it are constructed from a single material. When it goes through thermal cycles, the whole unit expands or contracts, thus affecting the optical characteristics as little as possible. The SGM used SiC for the optics. If the MCMs could be made from SiC as well, the whole spacecraft could be a monolithic unit that reacts uniformly to temperature variations. In addition, forming the MCM substrate from the same material would allow its use as the optical bench as well.

Testing and Reliability

The reliability of MCMs is a serious concern, since they are highly integrated boards whose total operability is dependent on the operability of each of its components. Moreover, this chip-level integration makes it quite difficult to locate, isolate, and replace a faulty component. Thus, it would be cost efficient for the MCM to be tested as a single unit instead of testing each individual die. It is essential that each of the dies is of the highest quality, to ensure the total quality of the module. Although testing

on the chip level raises the cost of individual chips, it reduces the overall cost of the MCM. This testing methodology is known as Known Good Die (KGD) and it implies that each chip is tested either on a "dummy" substrate, packaged in an epoxy tack, or on a fixture [13]. In addition, the MCM as a unit is scanned, chip by chip, to test internal chip vectors and package interconnects.

4.4.2 Compact Optics

The majority of the volume occupied by the optical bench is empty. This is because the distances between the optical elements are fixed by the optical performance required and by the laws of physics. This "dead" volume can be reduced only by changing the telescope configuration, a design change that can require additional components. If the volume reduction is significant, however, the mass of support structure saved can be greater than the mass required for the additional components.

The SGM design baselined a Cassegrain telescope. This configuration was primarily chosen for its simplicity, although it places the focal plane far behind the primary mirror. In addition to the space between the primary and secondary (and that required for baffling), there is the extra space between the primary mirror and the focal plane. Another problem with this configuration is that it is quite long. This constrains the overall spacecraft configuration; there are only few ways in which it can be oriented relative to other components without making the spacecraft bulky or requiring additional structure.

In the design presented in this thesis, the telescope was changed to a Schmidt configuration. In this new configuration an additional mirror is placed in the center of the primary, where a hole exists to allow the light to reach the focal plane, at an angle which deflects the light to one of the sides along the tube holding the primary mirror. This way, the light reflected from the tertiary mirror is repeating part of the path it took to reach the primary. Figure 4-6 shows a schematic of the two configurations. The total distance between the secondary mirror and the focal plane is the same in both cases; however, in the second case that path is "folded" on itself. This does not affect the optical performance, yet it allows the telescope to be much more compact. Although the second configuration requires an additional mirror, the volume reduction it achieves also reduces the amount of support structure required to support the optical bench. In addition, it makes the telescope much more compact and symmetric, and allows for greater flexibility in the development of the configuration of the spacecraft.

4.5 Power Reduction

Reducing the power consumption of various components on-board affects the mass and size of the spacecraft both directly and indirectly. Fewer power-consuming components produce less heat, which in turn require less structure mass to transfer it to where it can be radiated. Indirectly, high power requirements put a greater demand on the power-supply resources of the spacecraft. Whether bigger

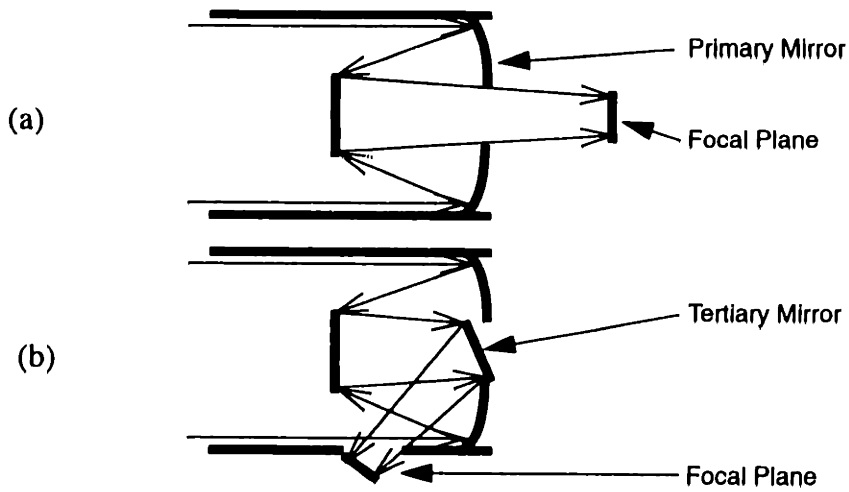

Figure 4-6: Reduction in optical bench volume by using a different telescope configuration: (a) schematic of a Cassegrain telescope, (b) schematic of a Schmidt telescope.

batteries or a greater area of solar array are needed, the higher power requirement increases both the mass and size of the power subsystem.

The portable electronics industry produced many new technologies in recent years that reduce power consumption in electrical devices. These advances can be used in space applications, though the higher radiation environment in space requires that additional care be taken. There are two primary methods to reduce power consumption. The first is to increase the efficiency of the device, thus reducing the amount of energy being wasted, and the second it to reduce the voltage applied to ICs. While these methods are being applied today to such products as cellular phones and computer laptops, the specific technologies have yet to be space-qualified. Even though the space industry lags the state-of-the-art technology in this field by several years, it is safe to assume that these technologies will eventually be qualified to be used in space applications.

4.5.1 Higher Efficiency Instruments

The effective design of logic and memory devices, as well as of the electrical systems they compose, can considerably increase efficiency, thus reducing the amount of power that turns into heat as well as reducing overall power consumption. There are several ways to increase this efficiency. The first is to use static components where possible. A static CMOS chip consumes very little or no power at all when not in use. If dynamic devices such as dynamic random access memory (DRAM) are necessary, there are still ways to make the "refresh" process less power-taxing. Advances in processes such as staggered or slow-refreshing will soon approach SRAM power consumption levels [19].

Another method to increase the efficiency of electrical components is to actively control the frequency with which they are operated. This can be applied at both the device and the system levels.

Since power scales linearly with clock frequency rates, the ability to control the frequency could allow the system to prioritize and vary the speed in which it performs its various tasks. For computations or functions that are not very time-critical, a slower clock rate can reduce the power necessary to drive the device. Active power management, which varies processing speed according to needed response rate can, over time, reduce power consumption.

4.5.2 Low Voltage Technology

Since power scales as voltage squared, another effective way to reduce power consumption is to reduce the operating voltage. Table 4-4 shows the percentage reduction in power as the operating voltage is reduced ($P \propto V^2$). These figures are relative to the 5V standard currently being used in space designs (but is being replaced by 3.3V in commercial applications). It is projected that logic voltage will decrease to 2.5V by 1996 and 1.5V by the year 2000 [20]. While these have been demonstrated, the 0.3V logic is still in the research stage [14].

Table 4-4: Effects of Voltage Reduction on Power Consumption

Operating Voltage [V]	Reduction in power relative to a 5V Operating Voltage
3.3	56.4%
2.5	75.0%
1.5	91.0%
0.3	99.6%

4.5.3 Reliability Issues

A decrease in power consumption via the two methods described above has two reliability ramifications which work against each other. Because low-voltage devices are much more susceptible to single event upsets (SEUs), the radiation environments in space might cause a reduction in the reliability of the system. There are many fault detection, isolation, and correction methods implemented via software, that can considerably reduce this risk. On the other hand, the low power consumption, due to the low voltage, generates less heat. Because heat generated is proportional to the square of the voltage, low power consumption allows electronics to run cooler, enhancing their reliability. The issue of reliability, as well as the tough space qualification process which it commands, will surely be solved as these technologies migrate from commercial to space applications.

4.6 Miniature Components: Microelectromechanical Systems (MEMS)

All of the techniques mentioned above affect the size and mass of the overall system. The more obvious method to achieve this effect is the miniaturization of the individual elements, such as sensors and mechanisms, that make up the subsystems. The micromachining manufacturing technique that catalyzed the integrated circuit revolution is now expanding into other fields. Using this technique, researchers can now build entire sensors and instruments, including mechanics and electronics, the size of a silicon chip [21, 22, 23]. These devices are called MicroElectroMechanical Systems (MEMS) and they hold a great potential for miniaturizing many bulky components on board as well as allow for integration directly onto MCMs.

Many instruments and devices can be built using the MEMS technology. Devices such as microvalves, micropumps, microactuators, microtransducers, microdeformable structures, micro-optical elements, and micro-IRUs and IMUs have been built and tested in laboratory settings. The applications for such instruments vary from biomedical products to portable electronics. With sufficient effort to space-qualify these technologies, they can revolutionize the way spacecraft are built. The advantages of MEMS go beyond their miniature size, mass, and power consumption. This class of devices offers robust performance with solid-state reliability. In addition, their tiny size enables the arraying of many identical devices, which allows for VLSI fault tolerant and distributed architectures. Currently, maturity is the biggest problem with this technology.

Chapter 5

Flight System Design

This chapter describes the design process as well as the final point design that resulted from the miniaturization process described in Chapter 4. That process, applied to the Second Generation Microspacecraft (SGM) design, is the reason why many of the elements in the current design are similar to those in the SGM. This thesis focuses on the changes from the prior design; thus it is necessary at times to describe the analysis and design produced for SGM. These aspects will be described below and referenced as such.

5.1 Constraints and Goals

To meet the design objectives of a miniature spacecraft weighing less than 5kg required the use of unique advanced technologies. These technologies are not only used to replace SGM technologies, but are also used to modify the architecture of the system (as described in Chapter 4). This microspacecraft design is constrained by two elements: it must perform the same mission as the SGM, and it must have an equivalent or greater functionality and performance than were provided by the SGM.

The vision for this "Next Generation" Microspacecraft (NGM) is that of an all, or near all, solid-state spacecraft in which the electronics packages make up the spacecraft bus, and significant power reduction is achieved using low-voltage logic. This vision led to the development of two parallel concepts, one with an RF communication system and the other with an optical communication system. The sections below describe the development of these two concepts, which share many common elements.

5.2 Vehicle Functionality

One of the top-level requirements for the NGM design is that it maintains the functionality of the SGM although it is allowed to perform additional functions. These functions define the subsystem requirements. As part of the miniaturization process, all primary functions needed for an asteroid flyby mission were assembled (refer to Table 4-1 on page 38). Table 5-1 presents a modified list of functions, showing only those that are being performed on the SGM (and NGM). In addition, the table presents specific requirements (pertinent to functionality) associated with these functions as derived from the SGM.

Table 5-1: Primary Functions and Supporting Characteristics for the NGM

Function	Characteristics	Req't	Function	Characteristics	Req't
Scientific Data Acquisition	Energy Collection	40μr/pxl	Communication	Frequency Generation	
	Energy to Signal Conv.			Modulation/Multiplex	
Propulsion	Thrust Generation (ΔV)	200m/s		Amplification	1.6AU range
	Fluid Containment			Transmission	68 b/s
Attitude Determination	Accel./Axial Forces		Power Management	Power Generation	at 1.2AU
	Sun Reference			Energy Storage	
	Horizon Reference			Power Regulation	
Navigation	Position Determination			Power Distribution	1.5VDC
	Relative Distance		Anomaly Detection	Temperature	
Attitude Control	Low Thrust Generation			Pressure	
Thermal Control	Heat Transfer			Voltage	
	Heat Expulsion			Current	
	Insulation		Data Storage	Random Access Mem.	1 Gbit
Structural and Mechanical Support	Load Supports			Read Only Memory	4 Gbit
	Packaging		Data Processing and Management	Data Distribution	
	Cabling			Math Processing	
	Deployment Mechanisms			Logic Processing	
				Neural Processing	

5.3 Spacecraft Concepts

The various functional and physical architectures that were traded resulted in two concepts. The first uses an RF communication system and weighs 3.0kg (including a 30% contingency) and the second uses an optical communication system and weighs 2.7kg (including a 30% contingency). These two options were carried in parallel since the optically-based system allowed for a lighter vehicle yet it presents problems which are beyond the scope of this study such as the effects of weather on transmission, the narrow beamwidth that requires an extremely tight pointing control, and the lack of support infrastructure in the form of receiving stations. Nonetheless, this architecture shows great promise for increasing datarates and providing a more integrated and compact architecture.

5.3.1 Functional Architecture

Though the functional architecture of the NGM (shown in Figure 5-1) was derived from that of the SGM (refer to Figure 3-5 on page 33), there are several key differences between the two. The most apparent difference is the organization; the block diagram for the NGM reflects more of its physical architecture. Dotted lines separate functional as well as physical layers; optics and optical communica-

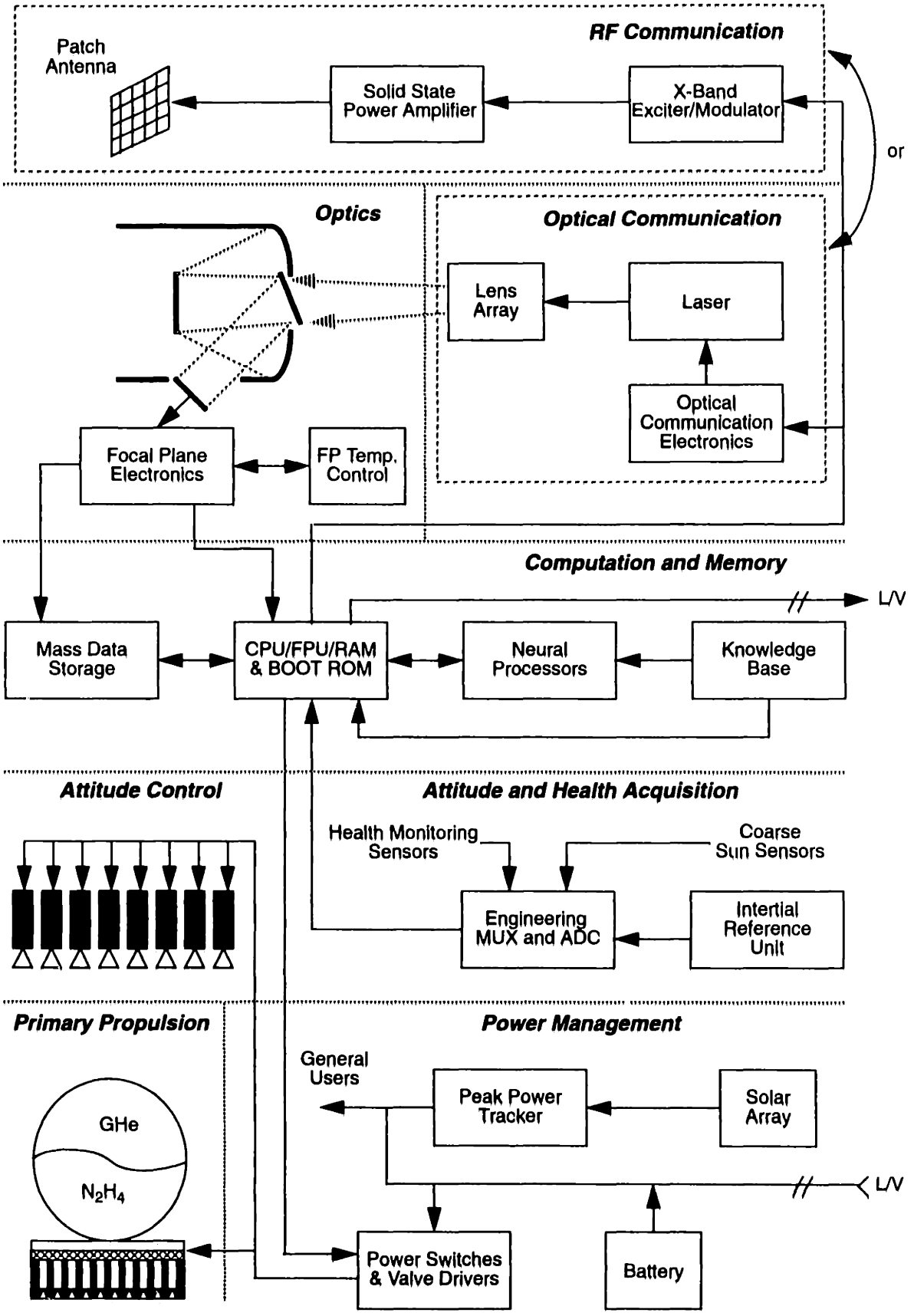

Figure 5-1: Functional block diagram of the NGM system showing both comm. options.

tion on top, computation and data handling next, followed by attitude management, and power and propulsion on the bottom. Specific functional differences are evident; in the communication architecture where both RF and optical communication systems are shown; in the propulsion architecture, where a thruster array replaces a single primary thruster and the attitude control thrusters are isolated from the primary propellant system; and in the power system, where a primary battery replaces a secondary.

5.3.2 Physical Architectures

The primary building blocks of this physical architecture are the optics, the electronics, and the propulsion. These three systems can be simply put together as well as be integrated in several ways. In either case, the configuration is driven by the required vector orientation (discussed in Chapter 4, refer to Figure 4-3 on page 42). Based on this information several configurations were developed. Figure 5-2 shows these in the order in which they were conceived.

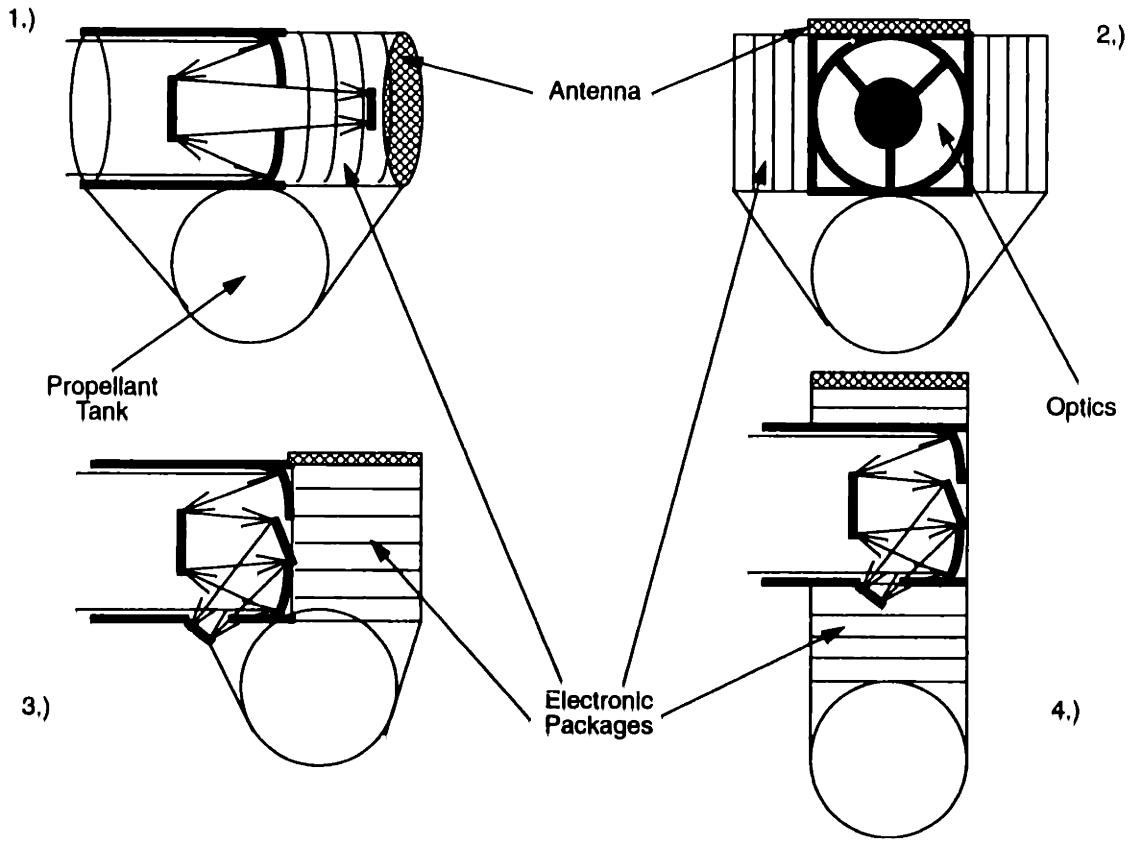

Figure 5-2: Schematics of physical architectures considered for the NGM.

Another driver of the configuration is the issue of compactness. The trend towards a more compact system is evident from the evolution of the configurations shown in Figure 5-2. The final concept required a change in the configuration of the optics (from the SGM baseline). This change

allowed the spacecraft to be relatively symmetric along all three axes making the integration of many such spacecraft on a single launch vehicle an easier job.

The chosen configuration was further developed for each of the two communication options. Cross-sectional schematics of the derived physical architecture for both the RF and optical communication options are shown in Figures 5-3 and 5-4, respectively. The specific differences between these two options dimensions derivations will be discussed throughout this chapter.

5.4 Optics

The optical performance of the telescope is critical for successful operations of the spacecraft, since this single optical aperture is used to perform several critical functions on board. Scientific data acquisition, navigation, and attitude control are expected to utilize this system, yet each has different specific optical requirements. For example, fuzzy images are preferred for navigation purposes (it is easier to identify the center point of a planet when it is as close to a uniform circle as possible) while crisp images are clearly preferred by the science community. To satisfy the needs of each of these functions, a group of experts at JPL came up with a set of optical parameters that satisfies as many of the requirements as possible. This effort was conducted as part of the SGM study [24] and its results were also used in this design. These optical parameters are as follows:

- 8.3cm aperture
- 250mm focal length
- f/3.0 (with an effective f/3.7)
- A single corrector with the following spot sizes: 8μm on axis, 10μm @5mm, and 21μm @10mm

5.4.1 Focal Plane

In addition to conforming to optical parameters, the focal plane was designed such that the detector space was used in the most efficient way. The focal plane is divided into three detector areas. The first is a square pixel array capable of detecting in the visible and near infrared wavelengths. This is an unfiltered detector used for taking black and white pictures. Two filtered line detectors are located to the right of the square detector. These provide "color" images in the higher wavelengths and are used as spectrometers. The right edge of the square detector is also used as a spectrometer. The configuration of the focal plane is shown in Figure 5-5. This SGM focal plane configuration was used (as is) for the NGM design.

5.4.2 Optical Configuration

The SGM optical design is that of a Cassegrain telescope located in one of the two bays. Two factors led to the reexamination of this configuration. The first was the need to reduce overall volume as was discussed in Section 4.4.2 (page 50). The other was the need to reduce the overall length of the

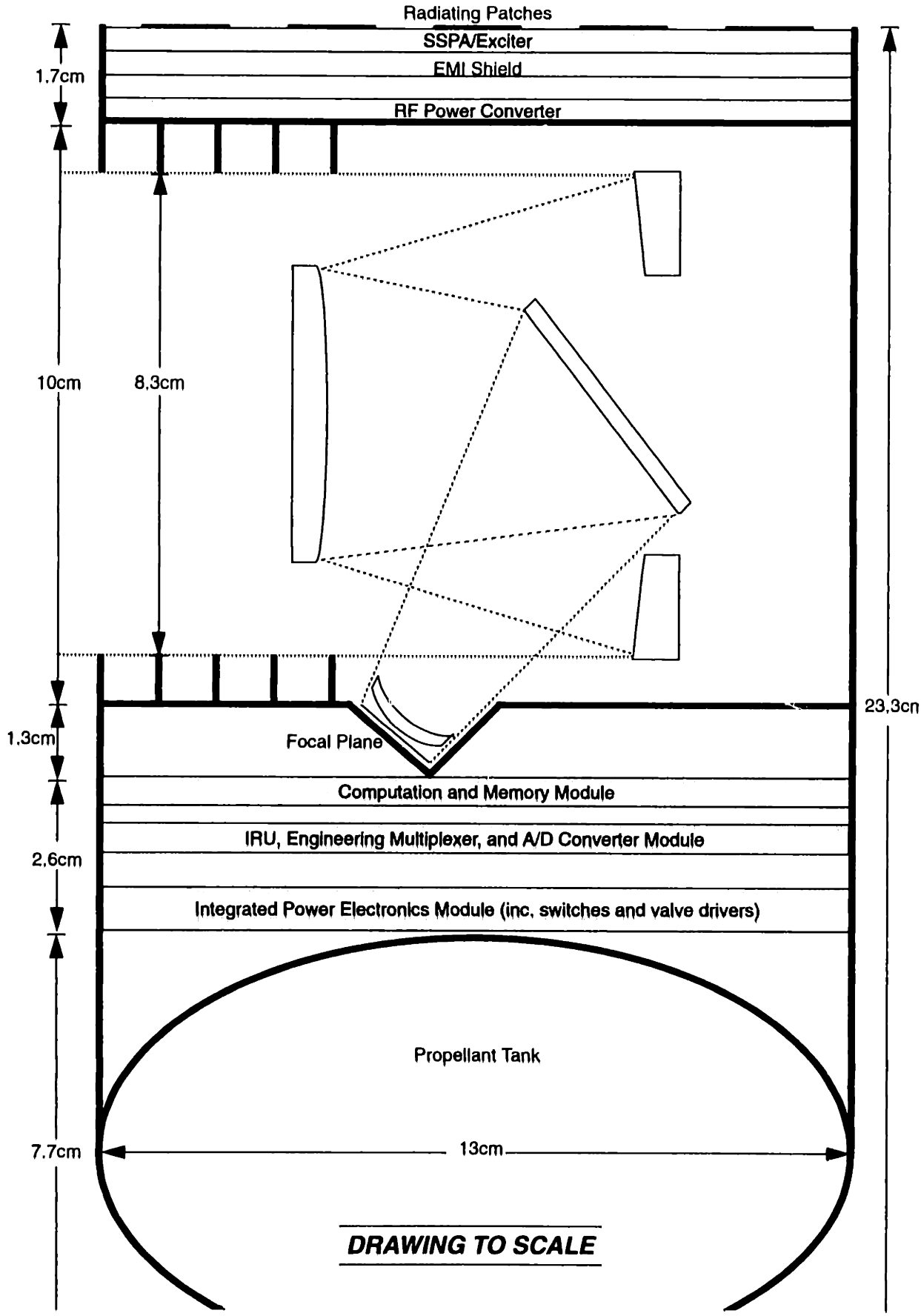

Figure 5-3: NGM physical architecture, assuming an RF communication system.

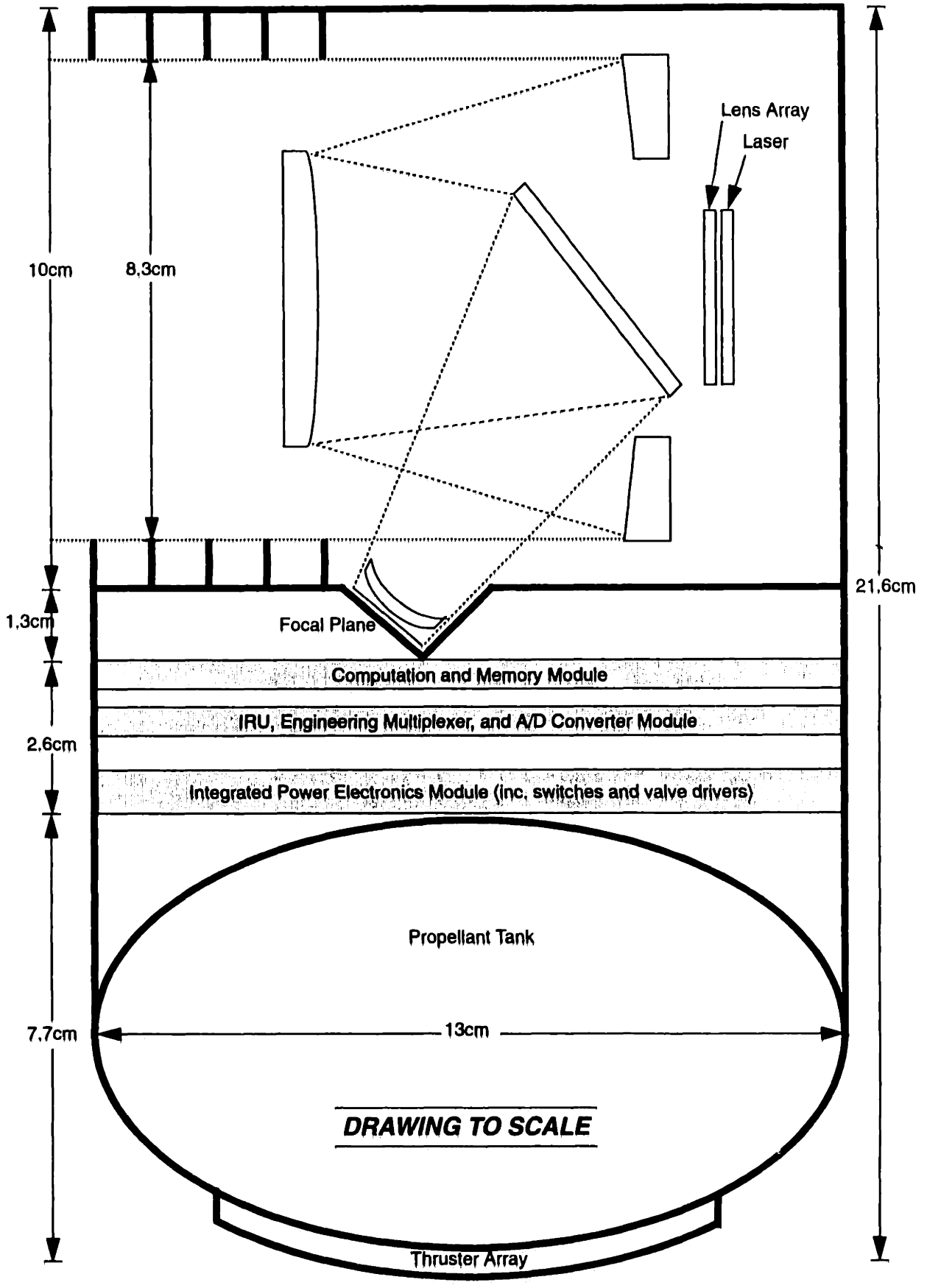

Figure 5-4: NGM physical architecture, assuming an optical communication system.

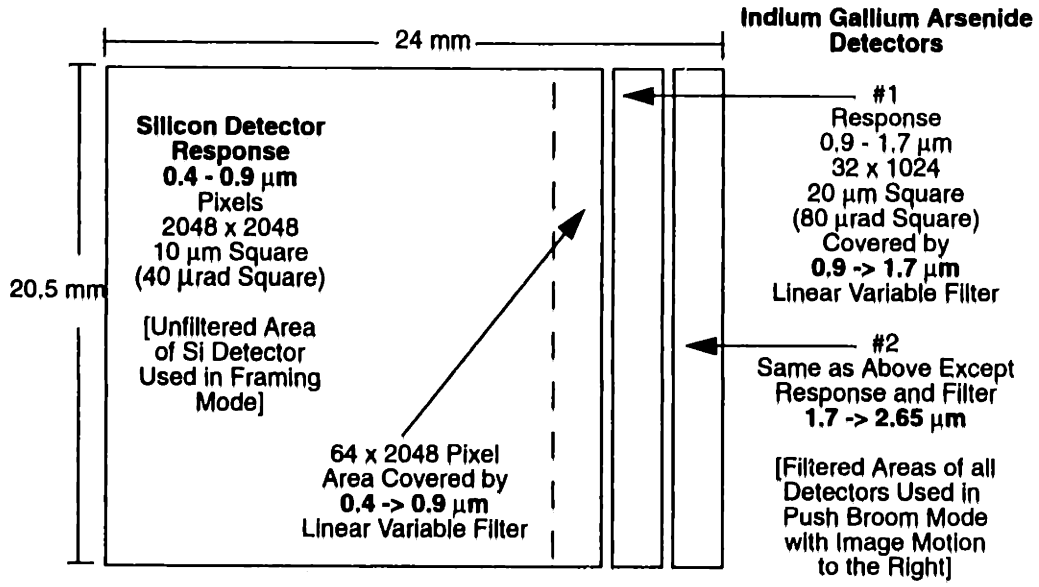

Figure 5-5: Focal plane configuration [7]

optics without compromising the length of the optical path. Both factors resulted from the effort to reduce the spacecraft to a single bay configuration. A single bay spacecraft would require that both the electronics and optics be placed directly on top of the propellant tank, to produce a compact design. It is also necessary to maintain the 90^0 requirement between the FOV and the thrust vector, which is dictated by the mission (see Section 4.3.1, page 40).

The optical path can be divided into three major sections: baffling (telescope entry to primary), optics (primary to secondary), and back end (secondary to focal plane). In a Cassegrain configuration these paths are lined up (the optical path is on top of part of the baffling path). It is possible to bend the back end path, however, so that it repeats part of the baffling path. This places the focal plane to the side of the telescope as opposed to right behind the primary. The two configurations are shown in Figure 4-6 on page 51. Although the latter configuration, the Schmidt, is more complex than the Cassegrain and requires an additional reflective element, the telescope is much more compact; the back-end volume required beyond the baffling section is reduced from 62.5 to $5.5cm^3$, and the overall length of the system is reduced from 17 to 10cm, which is the diameter of the propellant tank. Optical performance is unaffected by this change [25].

5.4.3 Optical Bench

The optical elements are supported by a primary tube and a set of spiders (a spider is a group of struts, usually three, that extend from the edge of the supported element to a primary support structure). While the primary and secondary mirrors are spidered to this tube, the tertiary is spidered directly to the primary. All optical components, with the exception of the corrector, are manufactured

from a single material. This is so that thermal fluctuations have a uniform affect on the entire system and thus minimize the degradation in the quality of the images. Several materials were considered [26]. Table 5-2 shows key properties for aluminum (Al), beryllium (Be), and two types of silicon carbide (SiC). The chemical vapor deposition (CVD) SiC was chosen because of its strength, low coefficient of thermal expansion and high thermal conductivity. These are the same reasons why this material was also considered as a possible MCM substrate material (see Section 4.4.1). Should the MCMs be made from SiC, it would be possible to make the whole spacecraft an athermal unit.

Table 5-2: Properties of Various Materials Used for Optical Components

Property	Al	Be	SiC (reaction bonded)	SiC (CVD)
Density, ρ, [g/cm^3]	2.78	1.85	2.92	3.22
Elastic Modulus, *E*, [GPa]	69	303	311	466
Specific Stiffness, *E*/ρ, [Gm^2/sec^2]	.025	.164	.107	.145
CTE [ppm/K @ 300K]	25.0	11.4	2.6	2.4
Thermal Conductivity [W/m·K]	237	216	156	250

In addition to the tube that structurally supports the optics, a different structure is necessary to integrate the optics with the spacecraft bus. Traditionally, a box is provided. In the case of the SGM, the tube was placed inside one of the two bays and was supported by the main frame (primary structure). In this design, the compactness of the system eliminates the need for a dedicated structure. Because there are MCMs above and below the optics tube, the substrates of those which border the optics are used as two of the four "walls" necessary to make up the optical bench. The other two are provided by the back of the radiators. The back side of the substrates and radiators are painted black for additional optical isolation. If further isolation is needed, thin films (such as aluminum foils) can be added with an insignificant mass penalty. A component mass list for the optics subsystem is shown in Table 5-3.

5.5 Navigation

The navigation function on spacecraft such as SGM and NGM is more complicated than in past and present spacecraft due to the absence of an uplink. Autonomous navigation to an asteroid has two fundamental difficulties. One is that earth doppler ranging cannot be used, and the other is that target tracking cannot be used until much later in the mission because of the small size of the target. Navigation therefore has to be accomplished using geometrical comparisons of bright objects to the positions in which they are supposed to be at a given time.

Table 5-3: Component Mass List for the Optical Subsystem

Element	Mass [g]
Optical Elements	
Primary Mirror	20.0
Secondary Mirror	3.5
Tertiary Mirror	1.5
Corrector	9.0
Focal Plane	50.0
Support Structure	
Main Support Tube	23.5
Focal Plane Tube	1.0
Spiders (primary, secondary, tertiary)	1.0
Secondary Alignment	15.0
Baffling	30.0
Optical Insulators	10.0
Total:	164.5

Using triangulation to determine a spacecraft's position in space involves sighting close planets and well-known bright asteroids and comets and comparing each reference against the observed star background [7]. Any two such angularly separate references are sufficient to determine the location of the spacecraft. Repeating this triangulation process multiple times throughout the cruise phase establishes the spacecraft's trajectory. Trajectory correction maneuvers (TCMs) are calculated based on comparison of this derived trajectory with the planned one. As soon as the target is sighted, the vehicle "locks on" to it, much in the same manner as heat-seeking guided missiles do. Aside from the requirements it imposes on the optical system, the navigation function is primarily addressed through software, and thus has no direct bearing on the spacecraft size or mass.

5.6 Attitude Determination and Control

Attitude maintenance on-board the NGM is relatively similar to that of the SGM. The attitude determination is unchanged, while the attitude control is changed only in respect to the implementation. The NGM reaction control system is comprised of a set of independent thrusters, as opposed to a set of thrusters tied to the primary propulsion system, as is the case on the SGM.

5.6.1 Attitude Determination

The precision of the on-board attitude determination is mission-critical for several reasons. Since no uplink is provided, trajectory corrections will have to be made using spacecraft-acquired attitude

knowledge. The precision of this system will therefore determine the quality of the navigation. A poor attitude determination system will require more trajectory corrections, and thus a greater amount of fuel to perform them. In addition, a certain amount of pointing accuracy is necessary for the communications link. The amount of transmitted data is reduced in response to any degradation in the quality of the attitude maintenance. This is of greater concern in the case of optical communication, where the beamwidth is very narrow and even small reductions in attitude quality can greatly reduce the quality as well as the quantity of data. An attitude knowledge of four milliradians (0.23^{o}) is assumed for the SGM and therefore will be used here as well.

Spacecraft attitude is acquired on-board both inertially and optically. A miniature inertial reference unit (IRU) detects rotational motion along each of the three controlled axes and the telescope captures images of the sky in the direction of the field of view (which is also the direction of motion), comparing those to a knowledge base of star maps. Advanced micromachining techniques enable the construction of a complete IRU the size of a silicon chip. This micro-IRU can be integrated, with its electronics, directly on an MCM. Should the need for velocity determination arise, an inertial measurement unit (a 6-DOF gyro plus accelerometers) can be manufactured and integrated in the same manner [27]. The associated drift rates can be compensated for using the adaptive spacecraft modelling routine which would be used constantly to evaluate the status of the vehicle. Adaptive modelling will be discussed further in the context of anomaly management in Section 5.10. The star tracker utilizes the optical system already on-board. At any given time during the mission, the camera's field of view can be compared to a large database of star maps stored in the knowledge base. Neural networks are used for efficient search-and-compare techniques in this large pool of memory.

Coarse knowledge of sun angle is acquired using seven sun sensors distributed on all sides of the vehicle. This knowledge is used primarily to help maintain the solar array face as close as possible to perpendicular to incoming sun rays. These sun sensors are basically a single fiber optic line with a microlens at the end. Their mass is negligible and they are passive devices that do not consume power.

The mass of the attitude determination hardware is embedded in the masses of other systems on-board. The "star tracker" is the telescope and the IRU is integrated on the same MCM as is the engineering multiplexer and the analog-to-digital converter. The sun sensors are included in the spacecraft cabling mass.

5.6.2 Attitude Control

The 3-axis attitude control is accomplished using an eight-thruster configuration similar to that used on the SGM. This configuration (shown in Figure 5-6) is the minimum coupled-thruster configuration for an all-axis control. In the SGM these thrusters are warm gas thrusters using decomposed

hydrazine as a propellant. The hydrazine is drawn from the main propellant tank, passed through a gas generator (a catalyst bed), and then through plumbing to the thrusters distributed throughout the craft. Specific impulse (I_{sp}) for these engines is in the upper 60 second range. The NGM design disconnects the attitude control from the primary propulsion for two reasons. The first is the elimination of plumbing; the other is the tendency toward solid state.

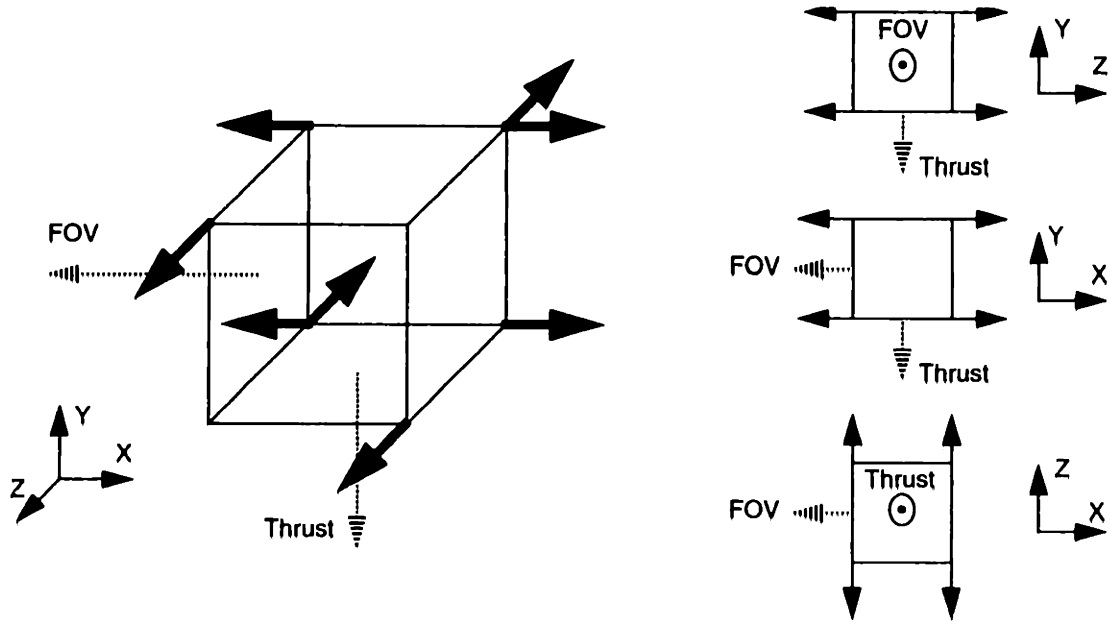

Figure 5-6: Attitude control thruster configuration.

Performance of solid-state thrusters is similar to that of gas thrusters. These thrusters offer solid-state reliability and lightweight tankage (due to low operating pressures), and nearly eliminate the issue of propellant leakage. These type of thrusters have not been exploited since they produce very low levels of thrust (≤0.001lbf/4.45mN) -- too low for use on conventional-size spacecraft but ideal for microspacecraft. On the down side, since the system is distributed instead of centralized, more contingency fuel is needed. This ensures that no single thruster will run out of fuel during the spacecraft's life; however, should that happen, attitude can still be controlled using the remaining thrusters, although more complex algorithms would be needed and performance might degrade. Two types of solid-state thrusters were considered: laser-driven [28] and sublimated propellants [29]. Although laser-driven thrusters promise a much higher I_{sp}, sublimated thrusters were chosen because of their simplicity.

The basic operation of the sublimated thrusters requires heating the propellant whenever a pulse is needed. The heater consists basically of a wire wrapped around the propellant. When a current flows through the wire, the propellant is heated enough to sublimate. Since the flow of propellant through the narrow section directly upstream of the nozzle gets plugged by solidified propellant whenever no heat

is supplied, these thrusters require no cumbersome valves. A configuration of such a thruster is shown in Figure 5-7. The most effective propellants are salts of ammonia, which can have theoretical I_{sp} up to 90 seconds. Ammonium Hydrosulfide (NH_4HS) has a delivered I_{sp} of 65 seconds at 25°C, and was chosen for its performance and non-toxicity.

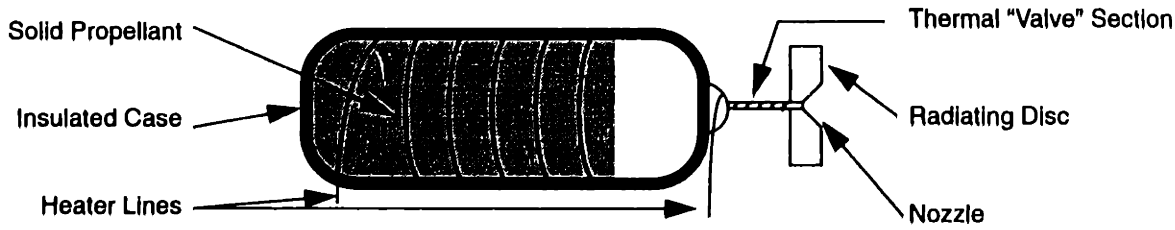

Figure 5-7: Schematic of sublimated solid propellant attitude control thruster.

The power to thrust relationship for the sublimated thrusters is 2.8W/mN. The desired thrust level, F, is 1mN and average pulse duration is 50msec. The energy needed is therefore $4x10^{-5}$W·Hr per pulse. This energy is negligible, even for the total required for the entire mission, and would therefore not impact the load on the battery and solar array. In addition, this 2.8W pulse is well within the capacity of the solar array, which has a peak capability of 5.5W. The mass of each thruster depends primarily on mission duration. Based on data from the MSTI spacecraft, an attitude control thruster fires once every 30 seconds [11] which, for an eight months mission, requires $6.9x10^5$ pulses. The total firing time, t, is therefore 34560sec. The required propellant mass, m_p, is therefore calculated as follows:

$$F \times t = m_f \times \Delta V \Rightarrow \Delta V = \frac{(1 \times 10^{-3}) \times (34560)}{3} = 11.5 \text{ m/sec total}$$

$$m_p = m_f\left(e^{\frac{\Delta V}{gI_{sp}}} - 1\right) = 3\left(e^{\frac{11.5}{9.8 \times 65}} - 1\right) = 0.055 \text{ kg}$$

where ΔV is the total required change of velocity and m_f is the final spacecraft mass.

Because of the low internal pressure, the propellant case requires very little mechanical strength for containment; this case normally amounts to about 10% of the total propellant mass. With 15% propellant contingency, the total mass amounts to 70g. Each thruster weighs less than 9g, and with a density of $1.28g/cm^3$, it occupies $7cm^3$. With such a low volume requirement and a flexibility in the dimensions, these thrusters can easily be integrated to the MCM-based structural bus. Each can be mounted on an MCM edge (which is mostly occupied by interconnects) and reside in the space between the modules.

An additional measure of control can be provided by the microthruster array (see Section 5.7.2). Since the array is curved, the outer thrusters have a vector component tangential to the main thrust

vector that does not go through the center of mass of the spacecraft. Each microthruster can be controlled independently or several can be operated at the same time to produce the desired thrust vector. This resource can be exploited, especially in the case where one of the attitude control thrusters runs out of fuel; however, because the thruster array can only compensate for failures of the bottom four thrusters, the contingency for the upper four thrusters is a bit greater.

5.7 Propulsion and Fluid Management

The primary propulsion system on the SGM is comprised of a single 0.9N monopropellant thruster, the size of a Voyager attitude control thruster, that provides a specific impulse performance of 225 seconds. A hydrazine tank pressurized with helium is connected (via a filter) to this single-valved engine. The attitude control thrusters tap on to the hydrazine via a gas generator and an accumulator. This architecture (shown in Figure 5-8), although relatively simple, still requires a considerable amount of lines and fittings (estimated at 15% of the total subsystem dry mass).

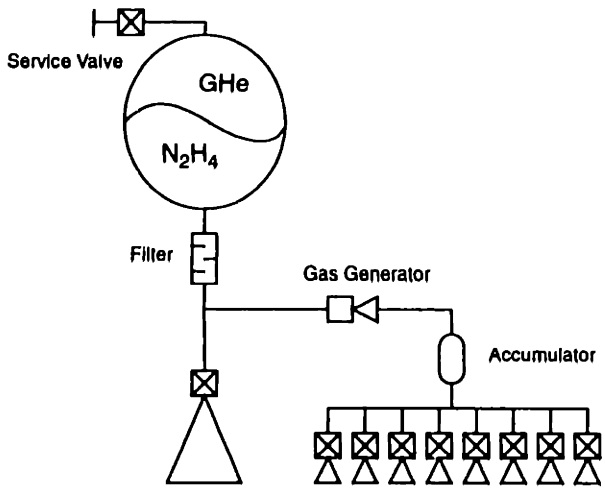

Figure 5-8: A schematic of the SGM propulsion system.

Changes to this architecture in the NGM design were driven by two primary objectives. The first is to reduce plumbing and the second is to make the entire system more compact. Reduction in plumbing was accomplished by making the reaction control system independent from the primary propulsion, as was discussed in Section 5.6.2. The attitude control thrusters are not only isolated, but they are solid-state as well thus eliminating any plumbing associated with this system. The compactness of the system was achieved by making changes to the propellant tank and to the main thrusters. The spherical tank with a diameter of 10cm was modified so that it has a diameter equivalent to the of the spacecraft bus, 13cm. To maintain a constant volume, the tank was "flattened" into an ellipsoidal container which can be manufactured just as easily as spherical tanks with fiber winding. This allows the height of the

tank to be reduced to 7.66cm. The structural integrity of this tank is not compromised by this modification and hence, its mass is not increased. More critical to the issue of compactness is the main thruster. The SGM thruster is 14.7cm long and has a maximum diameter of 3.4cm, a rather awkward extension of the tank. Replacing this single piece of hardware by an array of microthrusters made from a single substrate less than half a centimeter thick can decrease the overall length of the spacecraft, thus increasing its compactness. However, there are many outstanding issues associated with the design and performance of such microthruster array, as will be discussed below.

5.7.1 Propellant Management

Propellant storage and delivery on the NGM varies little from the SGM baseline. Hydrazine monopropellant is pressurized with helium gas and pressure fed to the thrusters. Due to the size of the thruster array and to the multitude of valves involved, a plenum is provided between the bottom of the tank and the thruster array thus only a single orifice is needed at the bottom of the tank. This plenum is constantly kept full and each of the thrusters draws fluid by controlling its own valve. Because if its smaller size, NGM requires less propellant thus the tank size is smaller. In addition, the tank configuration is modified to ellipsoidal with the larger diameter equivalent to that of the spacecraft bus which allows for an easier integration into the bus structure.

Propellant Tank Size and Mass

The required volume of the tank is determined by the amount of propellant needed. Using the rocket equation, a ΔV of 200m/s moving a 3kg (dry) spacecraft with an I_{sp} of 200sec[1] requires 322g of propellant. For hydrazine (ρ=1.008g/cm^3) this translates to 320cm^3. Assuming a blowdown ratio of 5:1 (80% fill), total tank volume is 400cm^3. An ellipsoidal tank with a 13cm wide diameter will have a height of 7.66cm. The biggest constraint on the reduction of the tank mass is manufacturing. The 400psi (2.76MPa) internal pressure can be supported by a fraction of a millimeter-thick graphite-epoxy composite ellipsoid; however, such a composite can only be manufactured with a minimum thickness of a couple of 14mils (0.036cm) [11]. The resulting stress in this shell is 180MPa, considerably less than the 1379MPa ultimate stress for graphite-epoxy; the resulting mass (ρ=1.57g/cm^3) is 40g. Since the isentropic fiber composite is rather porous, it can support the internal pressure but not contain the fluid; a liner is needed. An aluminum "foil" or some other kind of a metallic liner may be used. The liners are also limited by manufacturing. A minimum manufacturable thickness of 10mils (0.025cm) will result in a liner mass of 20g. In addition, a fitting factor of 15% (10g) is necessary to account for miscellaneous hardware such as mounting bosses, outlets, etc. The total tank mass is therefore 70g.

---

1. Performance degradation from the SGM which uses an I_{sp} of 225sec is due to the thruster array, see discussion in Section 5.7.2.

Pressurant Mass

The amount of helium required to keep the hydrazine pressurized at 400psi is determined as follows [30]:

$$m_o = \frac{P_p V_p}{R T_o} \times \frac{a\gamma}{\left(1 - \frac{P_g}{P_o}\right)}$$

where P_p is the required initial pressure of the tank (2.76MPa), V_p is the volume of the propellant (320cm^3), R is the gas constant for helium (2077J/kg·K), T_o is the initial tank temperature (273K), a is the ullage factor (1.05), γ is the specific heat ratio for helium (1.667), and the P_g/P_o is the inverse blowdown ratio (1:5 or 0.2). The required mass of helium pressurant is therefore 4g.

5.7.2 Thruster Array

One of the revolutions that the micromachining technology has enabled is in the area of fluid flow control. This area is of particular interest to biotechnologists who would like to build tiny machines that can be injected into the blood stream and release controlled quantities of drugs at the proper time and location. The development of microvalves for these applications brought about the idea of an array of microthrusters. There are several advantages to this concept. The first is compactness; a micro-thruster array can be etched onto a thin substrate. The second is low mass; such a substrate has the potential of being lighter than a single thruster system. The third is graceful degradation; the failure of one or several of the thrusters does not disable the entire propulsion system.

Array Design

The thruster array for the NGM is designed to fit at the bottom of the propellant tank which has a diameter of 13cm. Although the array can be curved to fit the form of the tank, this curvature can only be modest. For this reason the array is sized as a thin circular plate of a 10cm diameter, thus avoiding the extreme curvature at the edges. The number of thrusters that can be etched into this array is constrained by the required chamber length. Unlike other propulsion parameters, this length cannot be scaled down because a certain distance is needed to allow the chemical reaction taking place in the chamber to reach equilibrium. For hydrazine decomposition, this length is 13mm [11]. Assuming that a 3mm space is required between one thruster and the next (in all directions), 108 thrusters can be fitted in the array as is shown in Figure 5-9. Each must provide a thrust of 8mN in order to achieve a total thrust level of 0.86N which is slightly lower than that of the SGM. Since the NGM is smaller, however, g loads remain lower than a third of a g. The key to minimizing this substrate's mass is to keep the thickness small. This is achieved by positioning the chambers perpendicular to the thrust vector which is out of the plane of the array.

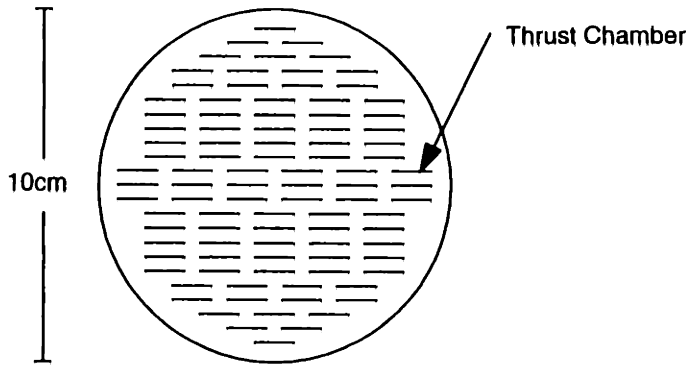

Figure 5-9: Top view of microthruster array.

Microthruster Design

Aside from the chamber length, the other design parameters of the microthruster were sized using basic propulsion equations and conservative parameters. The results of this analysis for several area ratios are shown in Table 5-4. These calculations assume a thrust of 8mN, chamber pressure of 250psi, molecular weight of 15 (average of decomposition products), gas constant of 300J/kg·K, and I_{sp} of 200sec. The I_{sp} used here is lower than traditional hydrazine systems (225sec) because a certain level of reduced efficiency might result from microfluids effects. These effects are still unknown; they are currently being studied in universities and research institutions [31].

Table 5-4: Microthruster Performance and Size Parameters

Area Ratio (A_{exit}/A_{throat})	10	25	50	100
Exit Pressure, P_e [atm.]	0.11	0.03	0.01	0.00
Thrust Coefficient, C_f	1.65	1.70	1.73	1.75
Throat Diameter, d_t [μm]	61	60	60	59
Chamber Diameter, d_c [μm]	612	602	597	593
Exit Diameter, d_e [μm]	193	301	422	593
Nozzle Length, l_n [μm]	247	449	676	996
Characteristic Velocity, c^* [m/sec]	1191	1153	1134	1121
Chamber Temperature, T_c [K]	2216	2078	2011	1964

One of the greatest concerns in this microthruster design is the thermal issue. The combustion taking place in each of the chambers produces a considerable amount of heat that can damage the array, particularly when all thrusters are operating concurrently. For this reason the highest area ratio of 100 was chosen because it resulted in the lowest chamber temperature. The resulting chamber temperature is actually lower than the 1964K shown since the decomposition of ammonia (one of the by-products of hydrazine) is endothermic. Based on knowledge of existing hydrazine thrusters, the

chamber temperature should be on the order of 1300K. The substrate supporting the thruster can be made out of a ceramic material with a high melting temperature. Silicon carbide melts at 2970K, however, the silicon that is used in the microvalve melts at 1683K. Thus a layer of insulation is needed between the chamber/nozzle array and the microvalve array located above it. Much of the thermal energy can be radiated to space through the bottom of the array. It is therefore important that the substrate has a high thermal conductivity as well. For this reason, synthetic diamond was also considered as a possible substrate material. Although it has a high melting point and thermal conductivity an order of magnitude greater than Si (five and a half times that of SiC) it is expensive and still unmanufacturable in large quantities (see previous discussion on page 49).

The choice of an area ratio dictates several key dimensions of the microthruster. These are shown in Figure 5-10. While the chamber diameter (0.6mm) and the nozzle length (1mm) are fixed, the microvalve array can be designed to accommodate any reasonable height requirements. This array was designed for a 1.5mm height (see below) for a total thruster array thickness of 3.5mm. This thickness also allows for sufficient rigidity such that substrate deflection during launch is no more than a micrometer (see discussion in Section 5.12.1). A first order mass estimate for the microthruster array assumes a solid SiC (ρ=3.2g/cm^3) circular substrate with a 10cm diameter and a 3mm thickness (3.5mm total minus the 0.5mm plenum) resulting in a total valve, thruster and nozzle array mass of 75g. The entire array, substrate and valves, can be micromachined as a single unit, layer by layer.

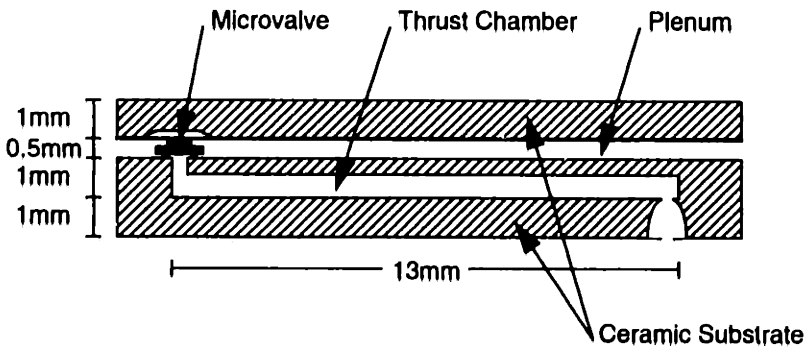

Figure 5-10: Schematic of a single microthruster in an array of microthrusters.

Microvalve Design

The most complex part of the thruster is its valve. In the case of the microthruster array, a matching microvalve array is needed to control the flow between the fully pressurized plenum and the thrust chamber which is normally at vacuum. Because of this large pressure differential and the low leakage requirement, most of the microvalves that are currently being developed by researchers for such industries as biomedicine are inadequate for space propulsion application. However, a proposed design for a pressure-balanced microvalve [32] could be implemented on the microthruster array described above.

This microvalve takes advantage of the existing plenum and uses the present fluid as a balancing force on the moving part of the valve. Thus, instead of doing work directly against the upstream tank pressure, the valve works against a preset cavity pressure already balanced by the propellant. This scheme requires far less actuation force. The actuation method chosen for this valve is electrostatics because of the ease in which it can be integrated into the fabrication sequence [32]. A schematic of this microvalve is shown in Figure 5-11 where P_{IN} is the tank/plenum pressure and P_{OUT} is the chamber pressure. Electrostatic force is generated by creating a potential difference between the plate layer which supports the plunger and the top substrate with the cavity. This applied force pushes the plate up against the cavity's internal pressure (which normally keeps the valve closed) allowing fluid to escape from underneath the circular plunger.

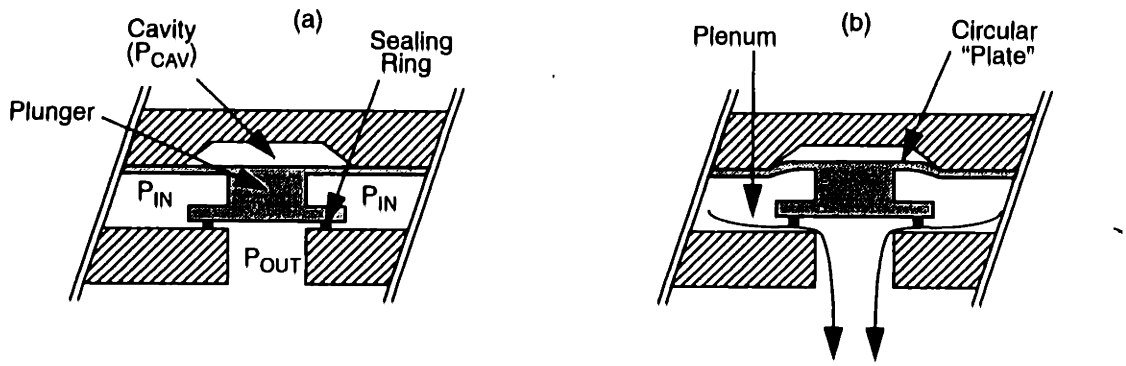

Figure 5-11: A Schematic of a pressure-balanced microvalve in the (a) closed and (b) open positions.

There are two parameters key to the design of the microvalve: the orifice diameter (d_o) and the maximum plunger deflection (w). These can be calculated from the equation for the flow rate through an orifice [32]:

$$Q = \frac{2\delta^2 D_h A_o}{\mu}(P_{IN} - P_{OUT})$$

where Q is the flow rate in ml/sec, δ is the discharge coefficient (0.157 for a sharp-edged slit orifice), D_h is the hydraulic diameter (=2w), A_o is the orifice area (=$\pi d_o w$), and μ is the viscosity of the fluid (9.7×10^{-4}Pa·sec for hydrazine). The worst-case pressure differential occurs right before combustion begins when P_{OUT} ($P_{chamber}$) is equal to zero. The pressure differential is then 400psi (2.76MPa), the pressure of the tank. From design of the propulsion system:

$$\dot{m} = \frac{F}{g I_{sp}} = 4.25 \times 10^{-6} \text{ kg/sec}$$

where F is the thrust (8.33mN) and I_{sp} is 200sec. Since the density of hydrazine is 1.008g/cm^3, the flow rate, Q, is 4.22×10^{-3}ml/sec. Incorporating these values and equations, the flow rate equation can be written in terms of d_o and w:

$$w_{max} = \sqrt{\frac{2.4 \times 10^{-12}}{d_o}}$$

The valve orifice diameter needs to be much less than the chamber length (13mm). An orifice diameter of 0.1mm results in a maximum deflection of 15.5μm which is about 75% of the thickness of the support plate (20μm).

While the valve deflections are on the order of micrometers, the total valve array height needs to be 1.5mm. The bottom substrate shown in Figure 5-11 is part of the chamber/nozzle substrate and the top substrate is required to be strong enough to withstand launch loads. The plunger height is a function of the plenum height which is arbitrarily (and conveniently) set at one-half of a millimeter. Thus, with a 1mm top substrate (which easily supports the 30μm cavities) the total microvalve array height is 1.5mm.

Outstanding Issues

The microthruster array presents a new concept for a propulsion system. Because of this and the limited resources available for this study, many outstanding issues still remain. The behavior of microfluids could significantly affect the performance of the microthruster array. The long and narrow combustion chamber will impose greater levels of interaction between the fluid and the wall which could either provide an advantage or a disadvantage. However, the large surface area to volume ratio certainly alleviates some of the thermal concerns. Since the heat flux resulting from the reaction is constant, the increased surface area reduces the amount of heat absorbed at any point along the chamber wall. On the other hand, it is still unclear whether the microvalve array can be sufficiently insulated so that the silicon components will not be damaged from the combustion heat. It is also unclear what the leakage rates are of such microvalves and whether they are acceptable. Finally, the voltage needed to operate these electrostatically-actuated valves is very high (on the order of 300V). This could pose a problem if the hardware required to upconvert the bus voltage cannot be fitted on the MCM carrying the valve drivers. Although all of these issues are serious, this concept provides many advantages and should be looked at more carefully.

The mass summary for this propulsion system design is given in Table 5-5.

5.8 Power Management

The architecture of the electrical power system used in the SGM design is shown in Figure 5-12. It is an unregulated peak power tracking system. The peak power tracker (PPT) is a DC/DC converter with an efficiency of 94% that tracks the peak power point of the solar array when energy demand exceeds peak power [33]. The solar array (S/A) is sized to fully accommodate the power load during

Table 5-5: Mass Summary for the Propulsion System

Component	Mass [g]
Propellant Tank	70
Thruster Array	75
Manual Valve	20
Filter	30
Pressurant	4
Lines/Fittings	25
Total:	224

the downlink phase which is the most power consuming. The rechargeable battery stores enough energy to accommodate maximum power load for 1.2 hours. Power "consumption" attributed to the inherent losses in the power system is 40% of the overall spacecraft power requirement. The NGM design retained this overall architecture, but it considered two additional battery architectures: a primary battery and a distributed battery system.

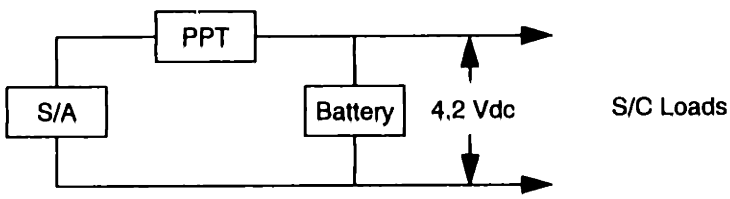

Figure 5-12: Architecture of the SGM electrical power system.

Figure 5-13 shows the power profile used in sizing the electrical power system. It is based on the power list for the RF comm option shown in Appendix A. Power consumption during full operations (prior to and post TCM and during encounter) is 2.2W for all but telecom power. During steady-state the average power is slightly lower, since functions are not all being performed at the same time (as in full operation). The most power-taxing phase, data transmission, is divided into short phases to allow for battery charging and for easier DSN scheduling. Each short transmission phase (5.5W power demand) is an hour long plus an additional fraction of an hour for data and system preparation.

5.8.1 Solar Array

The solar array is sized to provide the maximum power level required during the data transmission phase. The calculations assume a sun incidence angle of 0^{o}; any off-axis orientation will require that additional power will be supplied by the battery. No contingency is provided there since the battery can provide sufficient power for the entire transmission phase on its own. Advanced thin-film solar cell

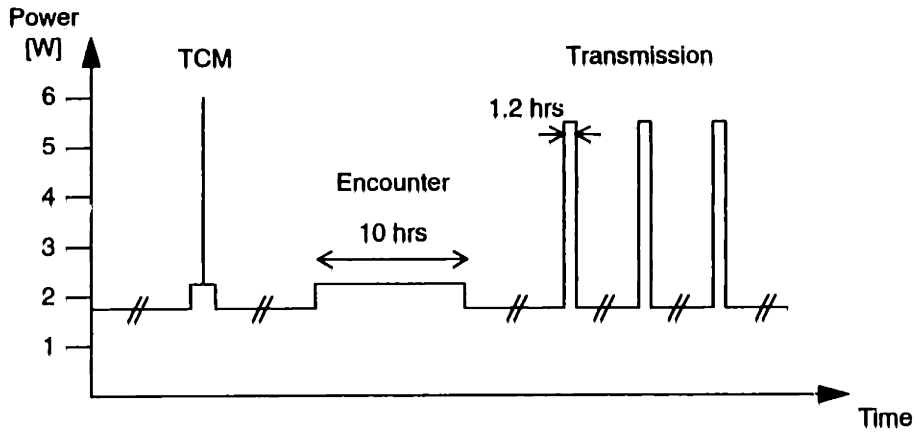

Figure 5-13: Power profile for a standard asteroid flyby mission using RF comm.

technology allows for high energy conversion efficiency as well as low mass. Cadmium Telluride (CdTe), chosen for the SGM design, has a theoretical cell efficiency of 27.5% and a practical array efficiency of 18% [34].

The solar flux, Φ_{sun}, at 1.2AU (worst-case sun range) is 943W/m^2. Assuming an overall system efficiency of 85% [35], the power produced by a CdTe array at the beginning of the mission is:

$$P_{BOL} = \Phi_{sun} \times \eta_{sys} \times \eta_{Array} \times \cos\alpha = 144.3\frac{W}{m^2} = 0.0144\frac{W}{cm^2}$$

Thus a 5.5W array (RF comm option) requires 382cm^2, and at a density of 0.144g/cm^2, the total array mass is 55g; a 4.6W array (opt comm option) requires 320cm^2 weighing 46g. The solar array is divided into three panels (each 13x10cm) that "wrap around" the spacecraft during launch and deploy into a single unit, angled at 45^o relative to the spacecraft (more specifically to the FOV), during operations.

5.8.2 Battery

Energy storage on the SGM spacecraft was achieved using a $LiTiS_2$ secondary battery, which is currently in the research stage [36]. This battery was re-sized for the NGM mission. Two additional architectures were traded against this design: a primary battery and a distributed set of secondary thin-film batteries. Although each of these has problems that cannot be resolved within the context of this study, both provide interesting architectural alternatives that should be seriously considered for future designs. The battery sizing is based on a worst-case scenario of a single data transmission phase where no energy is being drawn from the solar array.

Centralized Secondary Battery

The $LiTiS_2$ cells are 1A·hr with a 2.1V discharge capacity. Each of these "AA" cells weighs 18g. The number of cells needed is determined from the required rated battery capacity. This capacity is calculated as follows [33]:

$$C_r = \frac{P \times T}{C_d \times Vd \times \eta}$$

where C_r is the rated battery capacity, P is the required power, T is time (1.2hr), C_d is the depth of discharge (80%), V_d is discharge voltage (4.2V), and η is the transmission efficiency between battery and load (95%). For the RF comm option, where the peak power is 5.5W, the C_r is 2.07A·hr; and for the peak power in the opt comm case (4.6W), the C_r is 1.73A·hr. In both cases two $LiTiS_2$ cells are needed (the 0.07A·hr energy deficit in the RF comm option can be easily compensated for by the solar array, even in the worst case). The battery case accounts for about 50% of the cells' mass, resulting in an overall battery mass of 55g. This results in a specific energy of 120W·hr/kg, which is the low end of the projected performance for this battery technology [36].

Centralized Primary Battery

Because of the relatively short mission duration and the high projected specific energy for advanced batteries, it may be possible for a primary battery to be lighter than a rechargeable one. In addition, since the solar array is sized to provide sufficient power during all mission phases, it seems as though the battery provides a level of unnecessary redundancy. To make a proper comparison between the two, however, it is necessary to determine exactly the total energy that the battery will have to store. This depends not only on the overall power profile, but also on the exact spacecraft orientation at all times during the mission. Since this latter information is not available with great precision, the comparison might not be accurate.

A good measure of the total needed battery capacity would be the energy required to fully complete data transmission. The solar array can handle power loads during the cruise phase since it was sized to accommodate the much higher transmission loads. For the 2.2W steady-state load, the solar array can even be angled up to 66° to the sun (60° in the optical communication option) and still provide the necessary power. The total energy needed for data transmission is a direct function of the required transmission time. According to an SGM analysis [7], the total scientific data gathered during a sample mission is 106Mbits of compressed data. The calculated total energy based on this transmission capacity is shown in Table 5-6. The battery mass was then derived assuming an energy density of 400W·hr/kg, which represents an advanced primary lithium battery (Li-$SOCl_2$) [36][2].

This table reflects a battery mass that is considerably larger than the 55g required for the secondary battery, however, these calculations are made independently of any solar array power contribution. A primary battery can provide an advantage when power loads are handled by both power sources,

2. It was assumed that the reference chart from which the energy density was derived is applicable to the energy ranges for the NGM.

Table 5-6: Primary Battery Mass Derivation

	RF Comm (5.5W)	Opt Comm (4.6W)
Data Rate [bps]	60	1000
Required Xmission Time [hrs]	490.7	29.4
Total Energy Required [W·hr]	2699	135.2
Battery Mass [g]	6747.5	338.0

During cruise the spacecraft power needs can be easily fulfilled by the solar array since it is sized to handle the maximum power load during data transmission, which is twice that of the cruise. Thus, if during transmission the solar array can be maintained on sun axis as much as possible, the need for a battery can be quite minimal. This is not unreasonable since the angle of the solar array with respect to the spacecraft (or the spacecraft's FOV) can be preset to match the exact needs of any particular mission. Most of the redundancy between the solar array and the battery can be eliminated; however, since the sun-spacecraft-earth angle varies with time, the array cannot be maintain sun-pointing at all times. Figure 5-14 shows calculated primary battery masses for various *average* (over the transmission phase of the mission) off-axis sun angles. The dashed line in Figure 5-14 represents the 55g associated with the secondary battery. Thus in the case of RF comm, an off-axis angle of 7^{o} or less can result in a primary battery that is lighter than a secondary. This tolerance, however, is quite tight. In the opt comm case, average off-axis angles less than 33^{o} can provide battery mass benefits using comfortable angle tolerances.

Distributed Energy Storage

The physical architecture of the NGM is that of a bus made out of MCMs. The more functions that can be placed on these modules, the higher the level of integration on-board would be. Since each module consumes a fraction of the total power budget, it would be advantageous for each to have its own energy storage device and thus become "self sufficient." The portable electronics industry is very interested in this type of chip-level battery that can be directly integrated with the electronics [15]. It is possible that in the future, this type of battery can be fabricated as part of the MCM using the same micromachining techniques used to make electronics.

One of the primary problems with this technology is that it is immature. Current thin-film batteries can only provide a specific energy of 30W·hr/kg, although the projected performance is at the 150W·hr/kg level. Another issue is the specific energy with respect to MCM surface area. It would be inefficient to spend a large percentage of this area on a battery and power regulation electronics rather than on the electronics required to perform the specific functions for which the MCM was conceived. In addition, it is unclear how decentralizing the energy storage function will affect the rest of the power

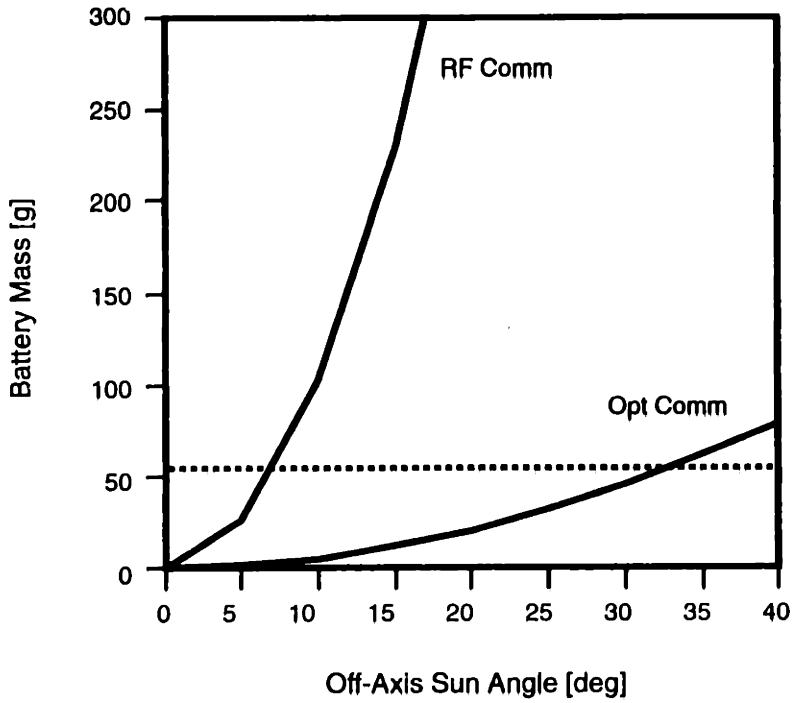

Figure 5-14: Primary battery mass as a function of average solar array orientation during the data transmission phase.

electronics, especially since all past spacecraft have used a centralized architecture. Finally, another advantage of this decentralized architecture is the reduction of power cabling, even though there is still a fair amount of cabling involved in connecting each of these batteries to the solar array. Most of these reservations are a result of technology immaturity and lack of experience with this type of architecture. Nonetheless, the advantages of this option will become clearer as the technology matures.

5.8.3 Power Electronics

There electronics controlling the power distribution and regulation functions are mounted on a single double-sided MCM. This centralized power electronics include the peak power tracker, power conversion and distribution units, and solid-state switches. Although power conditioning equipment has not followed the trend of miniaturization at the same rate as other hardware, some major advances have been made. The use of power integrated circuits (PICs) enables the packaging of all power electronics on MCMs, and chip-level regulators provide the necessary fine voltage conversion to chips directly on each MCM.

The power conditioning MCM contains the peak power tracker and the power distribution unit on one side and the solid-state power switches on the other. The solid-state switches share the MCM surface with the valve drivers. This module is placed immediately above the tank and farthest away from the optics and the sensitive communication hardware (refer to the concept schematics shown in

Figures 5-3 and 5-4) so that any interference created by the switches and valve drivers can be minimized. The masses of these MCMs are estimated based on MCM size, thickness, and average density (see Section 5.12). The mass summary for the power subsystem is shown in Table 5-7.

Table 5-7: Mass Summary for the Power Subsystem

Element	Mass [g]	
	RF Comm	Opt Comm
Solar Cells	55	45
Solar Array Support Structure	50	45
Secondary Battery	55	55
Integrated Power Electronics	250	250
Total:	410	395

5.9 Computation and Memory

The computation and data storage aspects of the NGM, much like those for navigation, are mostly software based, and are thus quite similar to the SGM design [7]. All data processing on-board is accomplished centrally by three processors: logic, math, and neural. Table 5-8 shows the specific functions accomplished by each. Processing speeds necessary to perform these functions have not yet been evaluated. Another shared resource on-board is data storage. Mass memory for raw, high-rate sensor data and data processing products was given a substantial strawman size of 1 gigabit. Read-only memory was sized at 4 gigabits. This non-volatile[3] knowledge base contains a multi-mission database (for information such as full sky maps and characteristics of bright objects) and a mission-specific database (for information such as sequencing, decision criteria, algorithms, and target ephemeris and characteristics).

Table 5-8: Processing Functions Performed By On-Board Processors

Logic/Fuzzy Logic Processor	Math Processor	Neural Processor
Timing	Attitude Determination	Star Identification
High-Level Reasoning	Attitude Control	Planet Identification
Resource Management	Navigation Analysis	Target Identification
Anomaly Recovery	TCM Control	Adaptive Target Modelling
Sequence Execution	Data Compression	Anomaly Detection
Telemetry Collection	Memory/Downlink Coding	Adaptive S/C Modelling
Downlink Formatting		Data Analysis
Downlink Rate Selection		

3. Requires no power when not reading from or writing to.

Although functionality has not changed from the SGM baseline, the NGM design includes a different chip package for the computation and memory hardware. While the SGM baselined five MCMs, all with holes in their centers to accommodate back end optics, the NGM baselined a single five-layer UHDI MCM (see Section 4.4.1). The latter design also rearranged the chip spread of the layers and made all layers two dimensional (necessary of UHDI); the SGM had several 3D stacked areas. The surface area dedicated to chips for a given function was not, however, reduced in any of the cases. In fact, the total surface area increased from 520 to 845cm^2. This is so primarily because the NGM MCMs are 13x13cm while the SGM supports 10x10cm modules. The functionality of each of the layers was arranged as follows:

1. Mass memory storage (1Gbit) and I/O
2. Logic, fuzzy logic, and math processors provide CPU, FPU, RAM, and Boot ROM
3. Neural processors
4. Knowledge base (2Gbit)
5. Knowledge base (2Gbit)

The mass memory storage and I/O are located in the top layer to allow for a simple interface to the focal plane detector directly above it. This layer also includes the focal plane temperature control.

The single five-layer UHDI MCM structurally supports itself in addition to dissipating, through its edges, all the heat generated by its chips (for thermal calculations, see Section 5.14). The thermal problem is not as severe as in the SGM since low-voltage technology reduces power consumption as well as total heat dissipation. The five-layer wafer has a thickness of less than 5mm [14]. This diminutive size allowed for a 60% reduction in the mass of the computation and memory system.

5.10 Anomaly Management

There are several ways to handle on-board anomalies. Traditional spacecraft have the capability to determine the source of the fault and execute a simple solution to the problem, such as switching on a redundant component. When the problem is more complex, ground control intervenes and, if one exists, offers a solution. In a system architecture such as those of the SGM and NGM neither of these possibilities exist. Both spacecraft are entirely single-string and neither support an uplink.

Although one of the main ideas behind having multiple small systems is to allow for the failure of several without undermining the success of the entire mission, it is preferable to give the spacecraft the ability to recover from as many anomalies as possible. This way, the success rate of the whole mission can be increased. Adaptive spacecraft modelling takes advantage of the computing power available on-board and simple internal health monitoring. Using software, the gathered telemetry allows the computer to model the spacecraft on any one of several levels: structurally, thermally, or intertially. Faults can be injected into these models and decisions can be drawn on what actions should be taken.

The neural processor is used in this adaptive modelling process and in the detection of any discrepancies between the model and the actual vehicle, while the logic processor is responsible for using this information to determine the steps needed for anomaly recovery.

It is not necessary to downlink gathered telemetry since the ground cannot act on this information. It might be useful, however, to have this data in case of a system failure, so that an understanding of malfunctions can be gained. The spacecraft can carry subroutines that command it to downlink only the information which points to the system fault. The mass of the sensors associated with telemetry data acquisition is included in the system cabling. The engineering multiplexer and the associated analog-to-digital converter (ADC), the necessary interfaces between the telemetry sensors and the computer, are situated on a single multi-chip module. This single-sided MCM also supports the IRU and weighs approximately 250g.

5.11 Telecommunication

The design of the telecommunication system is a primary driver of the vehicle's power requirements, as power consumption during transmission determines the size of the solar array and battery. In addition, an aperture is needed to perform this function which also places constraints on the overall configuration. Because of the above issues, three communication systems were traded: X-Band (8.4GHz), Ka-Band (31GHz), and optical communication (283THz).

The opt comm system provides several significant advantages. Since it is able to utilize the telescope already on-board, it is able to transmit a much higher data volume. This eliminates the need for a dedicated aperture (the antenna) for telecommunication (see discussion in Section 4.3.1). This technology, however, has two drawbacks. First, it is not as mature as RF communication; although it was proven to work in the lab as well as in flight (a Galileo experiment), the RF system has much more flight experience. Second, the infrastructure necessary to support the opt comm is still non-existent. While the DSN already provides full coverage for S-, X-, and (soon) Ka-bands, the photon-buckets necessary to receive optical signals are only present in laboratories, and are not organized in such a way as to provide full coverage around the globe. Despite these limitations, the opt comm technology shows much promise and should be seriously considered. For these reasons, both the RF and the opt comm options were carried in parallel.

5.11.1 RF Communication

The communication requirement for the SGM specified a low data rate (<100bps) system with a downlink only. Since high levels of data compression were assumed to take place on board prior to transmission, the data rate was not as critical an issue as were the mass and power. The SGM design team considered two transmission bands: X-band, the high frequency standard, and Ka-band, a higher

frequency band that is emerging as a standard. Assuming a standard system architecture, consisting of a driver, power amplifier, network distribution system, and patch array antenna, the two bands were traded. The NGM design incorporated the X-band system utilized by the SGM, and further traded two architectural design options: amplification before and amplification after network distribution.

Antenna Selection

Patch array antennas are emerging as the leading antenna design for miniature spacecraft applications. This is primarily due to their simple configuration of a thin plate, which is not only light but also comfortable and simple to integrate into a small and compact bus [37]. Their drawbacks are a narrow bandwidth, low power-handling capability, and higher losses when arrayed at higher frequencies; however, the tremendous mass-savings possible with this technology relative to traditional reflector antennas makes it very attractive. The radiating patches, only microns thick, are mounted on top of a dielectric layer (sometimes referred to as air dielectric), which can be made from a honeycomb substrate and is therefore very light. Most of the mass in these patches is nested in the substrate material upon which the air dielectric rests. This substrate also provides the conductive ground plane. Additional mass can be saved by using existing surfaces on the spacecraft bus to mount the air dielectric, thus saving most of the antenna mass. In the NGM design, where the MCMs are the bus, the air dielectric and the radiating patches are mounted on one side of an MCM dedicated to the telecommunications system. This double-sided MCM carries the antenna on one side and the solid state devices (not including the power conversion unit) on the other, making the telecom system a single "board" unit.

The patch antenna used in the NGM design is a 13x13cm patch with 25 radiating elements distributed 0.75 times the wavelength (2.7cm) apart. It is a passive array with broadside fixed beam of 15^{o} beamwidth. The insertion losses are 1.25dB and the overall efficiency is 75%. The overall thickness of the patch is on the order of 1.5mm.

X versus Ka

The results of the X- versus Ka-band trade were quite surprising. The Ka-band, the higher frequency of the two, was expected to require less DC input power and to weigh less; however, this was not the case. The X-band provides a better solution because of the one-way communication supported by the spacecraft. In two-way communication, the on-board system remodulates the uplinked frequency and sends it back down, while in the one-way case the system must generate the frequency on board. The DC power needed to drive the exciter (oscillator) scales with frequency; thus the Ka system requires more power than the X. Table 5-9 shows the mass and power breakdown for a system using both bands [35]. The power figures shown do not reflect aggressive, low power technologies (addressed later in this section). Appendix B.1 and B.2 shows the link budgets associated with the

design of both systems. In both cases, effective antenna gain (20dB), EIRP (46.5dBm), data rate (60bps), and receiving station parameters were kept constant. The transmitter power output for the X-band is 0.5W and the output power for the Ka-band is 0.53W; these numbers, however, do not reflect the difference in power consumption of the exciter.

Table 5-9: Comparison of Mass and Power for X- and Ka-Band Communication Systems

Element	X Band		Ka Band	
	Mass [g]	Power [W]	Mass [g]	Power [W]
Exciter/Modulator	200	0.8	200	1.1
SSPA	300	4.0	400	5.0
Antenna Transition	10	0.0	10	0.0
Total:	510	4.8	610	6.1

Single versus Distributed Amplification

The standard architecture for a simple, one-way communication system (see Figure 5-15) consists of a driver, a solid-state power amplifier (SSPA), a power distribution network, and a patch array antenna, connected in that order. This is the simplest architecture since it requires the fewest components. While trying to derive alternative architectures that might help reduce the DC power consumption of the system, the idea was brought about to make each of the antenna elements a "self sufficient" unit, each providing its own amplification as well as power radiation [38]. Although this system, shown in Figure 5-16, is more complex, it made it possible to reduce power consumption by 30%.

The power reduction possible with the latter architecture is due to the fact that the losses associated with the power distribution network are taken prior to amplification. Figures 5-15 and 5-16 show the method used to make the comparison. In both cases, the input power is 10.3dBm and the EIRP (output power) is 47dBm. These are the requirements dictated by the link budget for the X band system. The network distribution losses are 1.3 dB which is the case for a 20dB-gain 5x5in patch array. The DC power required to drive the distributed SSPA array is 0.9W and the single SSPA requires 1.2W. This power savings is a direct benefit of the power distribution losses. Table 5-10 shows the power reduction levels for various values of network losses.

It is important to note that although the distributed SSPA system requires less DC power (as well as allows for graceful degradation), it is more complex than the single SSPA approach and thus more expensive. The power gap can be reduced if the power distribution network can be made more efficient. One of the ways to accomplish this is to increase the gain of the antenna by increasing its dimensions and therefore its mass.

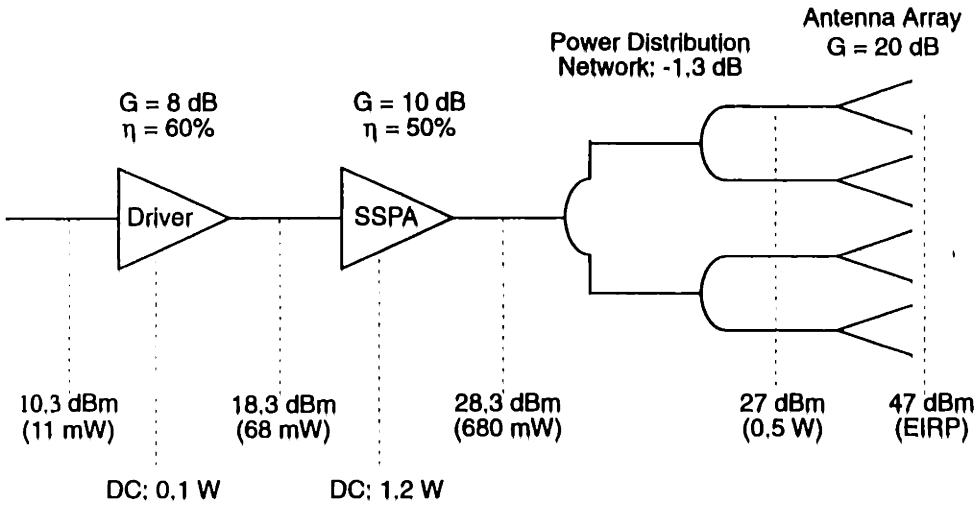

Figure 5-15: Derivation of power consumption for a single SSPA approach.

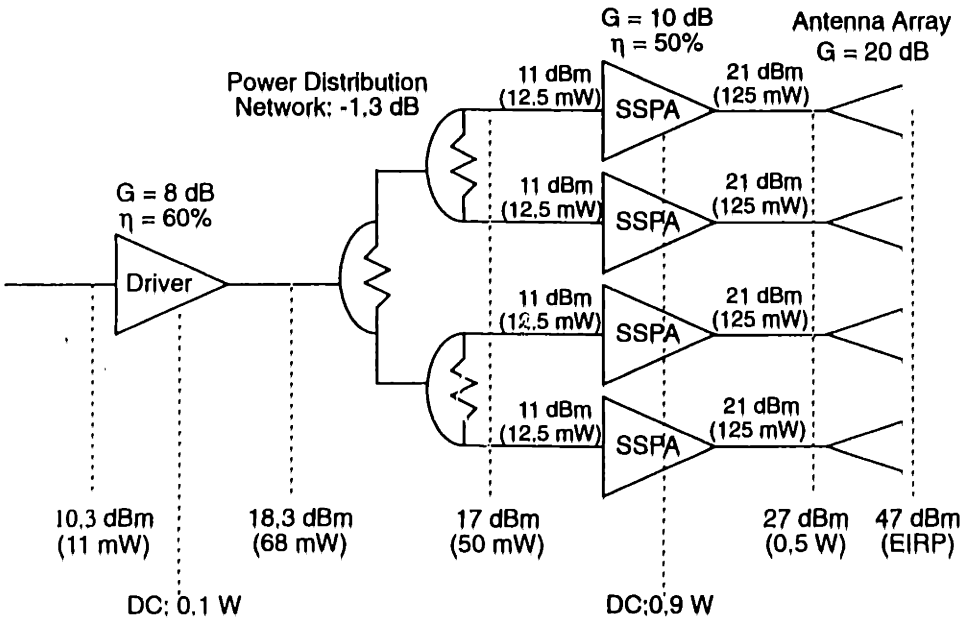

Figure 5-16: Derivation of power consumption for a distributed SSPA approach.

Table 5-10: DC Power Consumption for Various Distribution Losses

Power Distribution Losses [dB]	Single SSPA DC Power [W]	Distributed SSPAs DC Power [W]	% Reduction
0	0.97	0.97	0
1	1.2	0.99	17.5
2	1.5	1.01	32.7
3	1.9	1.04	45.3

Power Reduction

In addition to the DC power reduction possible due to a change in amplification architecture, low-voltage technology (see Section 4.5.2) can provide further benefits in that direction. The SGM baseline design included neither low-voltage logic nor low power devices. The power consumption levels shown in Table 5-11 represent SGM technologies operating on 5V logic. In the NGM design, these numbers were modified as follows:

- SSPA power consumption is reduced by 30% due to a distributed amplification architecture (see discussion above); power for each individual amplifier is independent of logic voltage
- The telemetry modulation unit (TMU) is voltage dependent and its power is reduced by 90% assuming a reduction from 5V to 1.5V logic (DC/DC conversion losses are included)
- Though the exciter is independent of operating voltage, hetero-bipolar transistor (HBT) and other low power devices (all pursued by the cellular phone industry) are projected to reduce its power by 30%.

The new power budget for this technologically aggressive system is also shown in Table 5-11.

Table 5-11: Power Consumption of an X Band System

Element	SGM Baseline [W]	NGM Design [W]
SSPA	1.0	0.7
TMU (includes modulator/encoder)	2.8	0.3
Exciter (upconverter)	1.0	0.7
Total:	4.8	1.8

Power Conversion

The telecommunication power conversion unit convert digital signals generated by the computer to analog signals in the microwave frequency band. The unit is mounted on a single-sided MCM and is separated by an EMI shield from the RF devices (the exciter, SSPA, and TMU). This is to prevent any harmful magnetic field interaction between the two modules. The underside of the power conversion MCM is used as a "ceiling" for the optical bench (refer to the spacecraft schematic in Figure 5-3).

The mass breakdown for the RF communication system is shown in Table 5-13.

5.11.2 Optical Communication

There are several key advantages to using a communication system operating at frequencies in the visible band. First, optical communication is capable of transmitting data at much higher rates without impacting the size of the system. In fact, transmission at 60bps (the data rate used in the RF communication system) requires just as much mass and power as does transmission at 1000bps. Second, an opti-

Table 5-12: Mass Summary for an RF Communication System

Element	Mass [g]
Patch Antenna	50
SSPA/TMU/Exciter MCM	200
EMI Shield	50
Power Converter MCM	180
Total:	480

cally-based system can use the existing optics on board, thus reducing both the number of elements needed and the overall complexity of the system. Third, the focal plane array can be used for tracking the earth, so no beam-scanning mirrors or optical relay elements (as is common with conventional opt comm systems) are necessary. The key drawback to this system is the immaturity of the technology involved.

There are four main elements to this system [39]:

1. A two-dimensional microchip laser array
2. A lens array matched to the laser elements in the laser array
3. A mirror coating on the tertiary mirror that is either highly reflective over a very broad spectral band except for a very narrow band (<1nm) in the 800 to 900nm wavelength range, or reflectance coating that can be made reflective or transmissive on command
4. A set of ASIC chips: laser driver/temperature controller, acquisition/tracking data processor, and data interface

This system does not degrade the quality of the optics. The only change to the optical system is the replacement of the reflective tertiary mirror with a dichroic element which enables light of a narrow frequency band generated by the laser to go through while reflecting all other radiation. Such coatings are common in optical systems. The optical configuration for the opt comm system is shown in Figure 5-17.

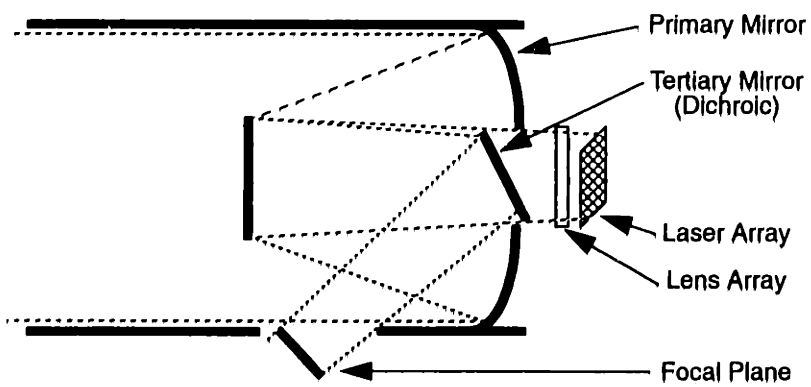

Figure 5-17: Spacecraft optical configuration including an optical communication system.

The laser array is not an array of individually packaged diode lasers, rather it is a single package with closely-spaced emitting pixels (several tens of microns inter-spacing). These types of lasers have been proven in laboratories and are expected to become commercially available within a year. The lens array uses binary optics technology, in which micromachined patterns on a flat surface cause light to be focussed behind the surface, as though it was a lens. The advantage of this technology is that it allows the creation of a large array of microlenses from a single wafer, with high optical quality due to the extreme precision of the manufacturing technique. These types of lens arrays are currently commercially available. The electronics needed to support this system (three ASIC chips) can easily be incorporated into the electronic packages used for other on-board functions. The mass breakdown for this system is shown in Table 5-13.

Table 5-13: Mass and Volume Summary for an Optical Communication System

Element	Mass [g]	Volume [cm^3]
Laser Transmitter	70	< 1
Lens Array	30	< 1
Electronics	(included in elect. packages)	
Support Structure	100	TBD
Total:	200	

The power consumption levels are presented in Table 5-14. These figures show ASIC power requirements only, as the lens array does not consume power and the laser array is powered by one of the ASICs. The focal plane array and computation power needs are not included here since they are shared resources on-board. A worst-case link analysis (daylight transmission) is presented in Appendix B.3. Note that the pointing accuracy used in this budget is 0.5mrad while that overall spacecraft pointing accuracy is only 4mrad. This increase in pointing accuracy is possible since each of the pixels in the array can be addressed individually. The laser beam can be directed at the exact pixel on the focal plane where the detector determined the earth to be, thus increasing accuracy beyond that which is provided by the spacecraft.

Table 5-14: Power Consumption of an Optical Communication System

ASIC	Power [W]
Modulated/Temp.-Controlled Laser	0.7
Acquisition/Tracking Processing	0.3
Computer Interface	0.3
Total:	1.3

5.12 Electronics Packages

All electronics on-board are integrated into five multi-chip modules (three in the case of optical communication). These modules support themselves both structurally and thermally, and their integration actually comprises the spacecraft bus. Each MCM is 13x13cm which is the size of the microstrip antenna. These dimensions were maintained even in the optical communication option primarily because the emerging standard for MCM size is 5x5in. The actual die coverage area is the central 10x10cm, while the four corners are used for structural integration and the edges are used for electrical interconnects. The thickness of the substrate for each of the modules was determined based on two constraints; the maximum allowed deflection during maximum load that would not damage surface hardware and the minimum substrate cross sectional area required to conduct all heat generated by electronics to radiators located at two opposing edges.

The chip-stacking techniques used on each of the MCMs were chosen based on the particular application of the mounted hardware. Section 4.4.1 (page 45) gives an overview of all stacking techniques considered. The following is a list of the MCM types needed for either of the two communication options:

- *Computation and memory* - 5 layer UHDI package
- *IRU/MUX/ADC* - single sided package, horizontally stacked die (back side is used for optical communication ASICs for that option)
- *Integrated Power Electronics* - double sided package, horizontally stacked die on both; peak power tracker and power regulation electronics on one side, solid-state switches and valve drivers on the other
- *RF Solid-State Devices* - single sided package, horizontally-stacked die
- *RF Power Conversion* - single sided package, unstacked die

5.12.1 Structural Rigidity

The allowed deflection of the MCM substrate during maximum load is constrained by three aspects; proximity to the next module, allowed deformation of the edges, and effect on the on-substrate interconnects. The interconnects are the most sensitive to any deformation of the substrate and thus determine the allowed deflection. The average height of die mounted on MCMs is a fraction of a millimeter and the sensitivity of the interconnects depends on the interconnect method chosen. A conservative estimate for the allowed deformation is therefore on the order of 1μm.

MCMs need to withstand a maximum load of 7.5*g*'s which occurs during the Pegasus' first stage burn-out [40]. Because this load is applied perpendicularly to the modules, they can be modelled as thin plates, simply supported on all edges and uniformly loaded. The maximum mid-point deflection of such a plate is given by $\delta_{max} = 0.004\frac{qa^4}{D}$, where the uniform load per unit area $q = 7.5mg/a^2$ [41]. Since the modules basically need to support only their own weight (die and interconnect weight is relatively

negligible and is included in contingencies), $q = 7.5t\rho g$, the edge length a = 13cm, and the flexural rigidity $D = \frac{Et^3}{12(1-\nu^2)}$. A Poisson ratio ν = 0.3 is assumed. The density ρ and Young's Modulus E depend on the choice of material (see Table 4-3 on page 49). Figure 5-18 presents the resulting mid-point deflections as a function of substrate thickness for three possible materials: Si, SiC, and AlN. A deflection of 1μm or less can be achieved with a minimum thickness of 0.4cm in all three cases. Additional rigidity can be provided, if necessary, by impregnating the substrate with fibers, turning it into a composite structure.

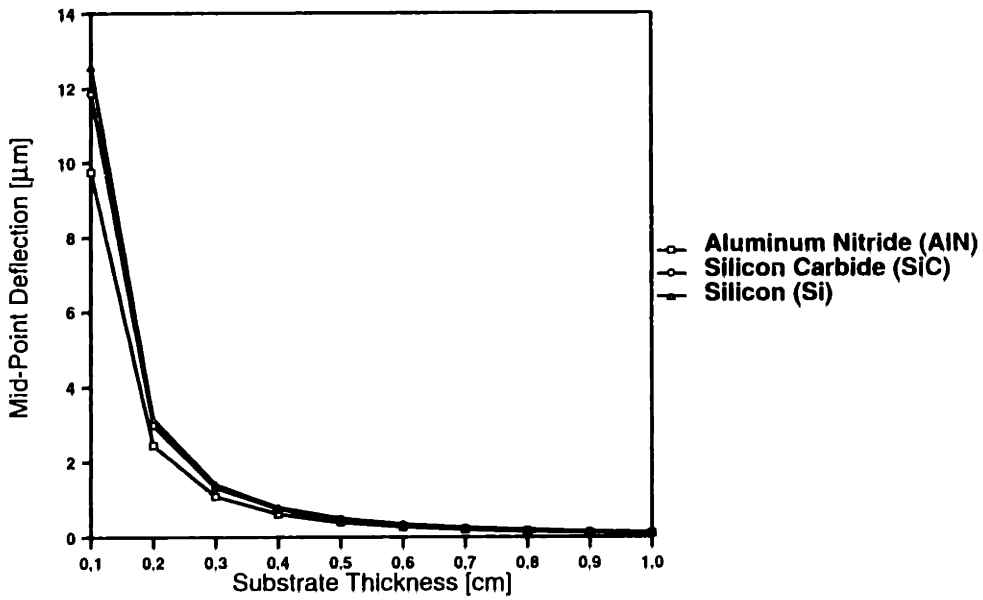

Figure 5-18: Maximum mid-point deflection of MCM substrate under a 7.5*g* load.

5.12.2 Heat Dissipation

A basic thermal model of each MCM shows that the substrate thickness necessary to support structural loads can also provide sufficient cross-sectional area to transfer all heat generated by the supported electronics. This model, shown in Figure 5-19, assumes a uniform heat distribution load across the face of the MCM. Heat can be radiated out to space through two of the 13x13cm substrate's edges. The heat conductivity is described by the equation:

$$\frac{\partial}{\partial t}T(x) = Ak\frac{\partial^2 T}{\partial x^2} + q_{in}$$

where T is the temperature, A is the cross-sectional area (13cm times the substrate thickness), and k is the conductivity of the substrate (1.08W/cm·K for Si at 100°C). In the steady-state condition, the temperature does not vary with time (i.e. $dT/dt=0$). Therefore, the temperature at any point on the substrate can be found by solving:

$$\frac{d^2T}{dx^2} = -\frac{q_{in}}{Ak}$$

The boundary conditions are $T(x=0) = 380K$ (maximum allowed junction temperature by JPL specifications [42]) and $dT/dt(x=0) = 0$ (heat at the center line can be conducted to either of the two radiators). The resulting temperature distribution is as follows:

$$T(x) = -\frac{Q}{l^3 tk}\frac{x^2}{2} + 380$$

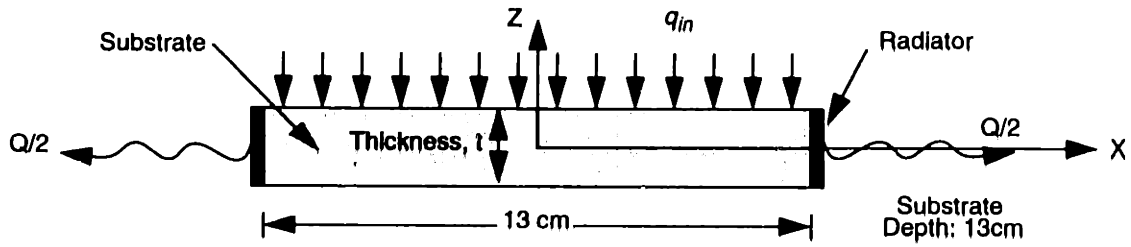

Figure 5-19: MCM model used in thermal analysis.

The factor determining the substrate thickness is the limitation on the temperature at the edge of the substrate ($x=l/2$). According to JPL quality assurance specifications [42], temperature differentials between any two points on a board should not exceed 35K. Therefore, the edge temperature should be maintained at 345K in steady state. Using l = 13cm and k = 108W/mK, the thickness can be determined by $t = Q/3931.2$, where Q is the module's total dissipated power. Table 5-15 shows the resulting thicknesses for each of the five layers of the computation and memory UHDI module as well as the other four MCMs. The efficiency value refers to the percentage of the DC input power that is dissipated as energy other than thermal. To ensure a margin of safety, it was assumed that most or all of the input power was converted into heat, thus the efficiencies shown much poorer than in actuality.

In addition to ensuring that the substrate can conduct all heat loads to its edges, it is also necessary to provide sufficient area to radiate this heat into space. The required radiator size is determined by the radiator heat flux:

$$q = \varepsilon\sigma T_r^4$$

where ε is the emissivity (0.8), σ is Boltzman's constant (5.67×10^{-12} W/cm^2·K^4) and T_r is the radiator temperature (345K, the junction temperature minus the allowed temperature differential). The available heat flux is therefore 0.067W/cm^2. The required radiator area is determined by multiplying the radiator heat flux by the dissipated power, Q. Table 5-15 shows these results as well. The required height is equivalent to the substrate thickness and is defined by the area divided by the edge length. Should the radiator height be greater than the length of the substrate, additional spacing must be added between this MCM and the next to accommodate the larger radiator surface area. Two of the five mod-

Table 5-15: Results of First Order Thermal Analysis of MCMs

Module	Computation and Memory				
Layer	Data, I/O	CPU/RAM	Neural Nets	ROM	ROM
DC Power [W]	0.2	0.2	0.1	0.0	0.0
Efficiency [%]	0	0	0	0	0
Dissipated Power, Q [W]	0.2	0.2	0.1	0.0	0.0
Req'd Substrate Thickness [cm]	0.005	0.005	0.003	0.000	0.000
Req'd Radiator Area [cm^2]	1.13	1.13	0.56	0.00	0.00
Radiator Height [cm]	0.09	0.09	0.04	0.00	0.00
Req'd MCM/MCM Spacing [cm]	0.00	0.00	0.00	0.00	0.00

Module	IRU/Eng. MUX/ADC	RF Hardware		Integrated Power Elect.	
Layer		Pwr Conv.	SS Devices	PPT/PDU	Swtchs/VD
DC Power [W]	0.3	0.7	1.8	2.4	2.4
Efficiency [%]	25	25	25	25	25
Dissipated Power, Q [W]	0.23	0.53	1.35	1.80	1.80
Req'd Substrate Thickness [cm]	0.006	0.013	0.034	0.046	0.046
Req'd Radiator Area [cm^2]	1.69	3.98	10.15	13.53	13.53
Radiator Height [cm]	0.13	0.31	0.78	1.04	1.04
Req'd MCM/MCM Spacing [cm]	0.00	0.00	0.38	0.79	0.79

ules require radiator surfaces with areas greater than the lengths of their edges. The double-sided power MCM and the RF comm module require an intermodule spacing of less than 1cm.

5.12.3 Mass Derivation

Because of the immaturity of the MCMs design and the lack of specitic circuitry and other hardware layouts, their mass estimates have a greater level of uncertainty than some of the other technologies used in the NGM design. Die densities and power consumption levels are only approximates, making the substrate thickness calculations very rough. The mass approximation includes an allocation for both the substrate and the electrical elements; all are assumed to be silicon-based. The five-layer UHDI module requires a thickness of 0.5cm to accommodate both die and interconnect layers; its mass is therefore 197g. The stacked modules can have a thickness of 0.4cm, resulting in a mass of 158g. A 70% die coverage and an average die thickness of 0.5mm present an aggressive yet realistic approximation [18]. Thus, each stacked die layer weighs about 10g.

Due to the high level of uncertainty, mass approximations were rounded up. Mass derivations for each MCM are shown in Table 5-16.

Table 5-16: Mass Summary for Electronic Packages

MCM	Mass [g]		Module Description
	Opt Comm	RF Comm	
Computation and Memory	200	200	5-layer UHDI of 0.5cm total thickness
IRU, Eng. Mux, A/D Converter	250	200	RF: 0.4cm substrate, 4 die layers Opt: 0.5cm substrate, 5 die layers
Integrated Power Electronics	250	250	0.5cm substrate, 5 die layers
RF Solid State Devices		200	0.4cm substrate,4 die layers
RF Power Conversion		180	0.4cm substrate, 2 die layers
Total:	700	1030	

5.12.4 Module Stacking Configuration

A tight stacking of modules reduces the overall length and volume of the bus. Ideally, modules would be stacked one directly on top of the other; there are a couple of elements, however, that force a certain level of spacing between each of the modules. It is necessary to have sufficient space for the stacked die as well as space above the die to allow the module above to deflect under applied loads. In addition, for heat dissipation purposes, a certain amount of radiator surface area is necessary for each of the modules. When that area exceeds the edge area, additional spacing is necessary to allow for the greater size of the radiator.

Based on the substrate heights given in Table 5-16 and the radiator area requirements derived in Table 5-15, Figure 5-20 shows the configuration for the RF comm option; in the case of the optical comm the top two modules are simply omitted. The additional layer of die required for the opt comm electronics (placed on the bottom of the IRU/MUX/ADC module) does not require additional spacing, since additional spacing is already provided for the increased radiator surface area required of the integrated power electronics module.

5.13 Structural Integration and Cabling

Since the physical architecture of the NGM is one of an integrated bus with the electronics packages comprising the primary structure, no additional frame is necessary to integrate the various elements that make up the vehicle. The stacked MCMs latch onto each other via connectors located at each of their four corners. These connectors can support all lateral loads. The optical bench, situated directly above the packages, is supported by baffling in the front and several spiders in the back. This alone is not rigid enough, especially in the RF comm option where the optical bench needs to support the RF modules, as well as the antenna. Additional corner connectors are therefore necessary to integrate the top of the DC electronics packages to the optics and to the communication hardware. The

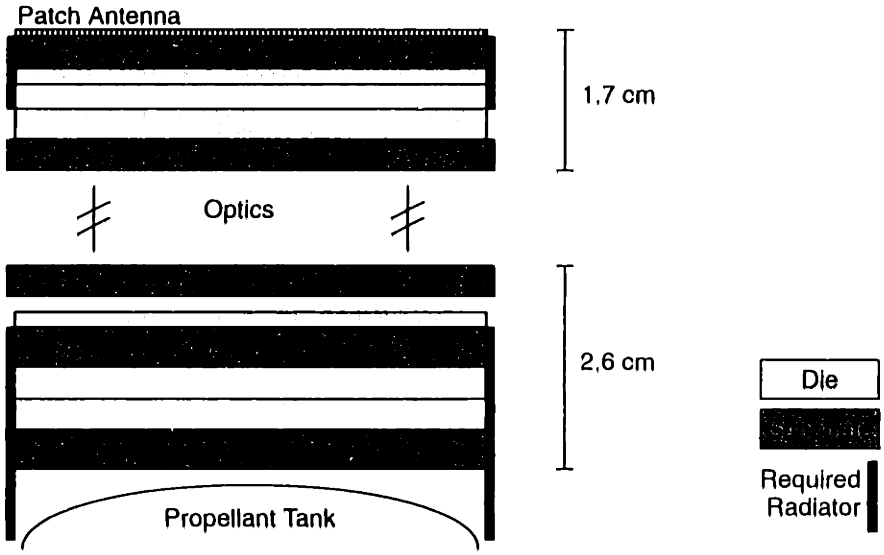

Figure 5-20: MCM configuration on the NGM bus.

mechanical integration via the corner connectors provides lateral support only; additional support structures are necessary to accommodate torsional loads. The torsional support can be provided by thin composite strips that are made out of a uni-directional fiber drawn from the composite-wound tank. This method also resolves the issue of integrating the tank into the bus. Simple cross-strapping on three sides (the fourth has the optical aperture which needs to be unobstructed) provides sufficient structural support. Figure 5-21 shows a schematic of these fibers (shown in thicker lines).

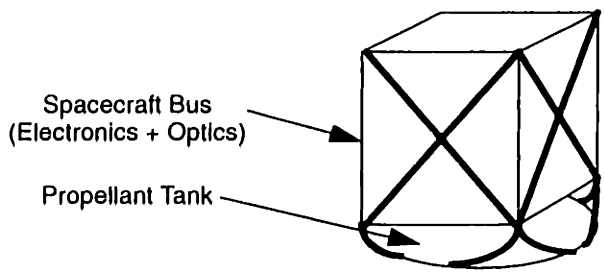

Figure 5-21: Schematic of the structural integration of the tank and the bus.

In addition to the tank, several other elements need to be integrated with the spacecraft bus. Antenna, reaction control thrusters, radiators, thruster array, and solar array are all external elements joined to the bus after the electronics packages, optics, and propellant tank are integrated. The radiating elements of the antenna (without the support substrate) are positioned directly on the reverse side of the RF electronics MCMs and the reaction control thrusters are mounted on the edges of the MCMs. These elements do not require any additional support structure. The two radiators are mounted along two opposing sides of the bus on top of the composite strips, and require only small fasteners for integration.

The thruster array, which encompasses the plenum as well as the microvalves, thrust chambers, and nozzles, is attached to the bottom of the propellant tank -- possibly through thin extensions of the ceramic array wrapped by composite fibers. The solar array has a single attachment node to the bus, on the top edge opposite the optics aperture. This single node allows the deployment of the solar array so that the angle between it and the FOV best matches the particular needs of each mission. Since the solar array is divided into three panels that "wrap around" the bus during launch, three release-and-hold mechanisms are needed: two for the deployment of the side panels to their full array configuration and one for the deployment of the array to its final, angled configuration. These deployment mechanisms can be rather simple since they only need to release and latch once; they cannot be pyrotechnic, however, because the resulting shock would damage the diminutive vehicle.

Power and data cabling, which has traditionally accounted for 8% of spacecraft dry mass, is mostly eliminated due to the compact MCM configuration. The cabling necessary to reach the RF hardware (or the laser in the opt comm option), the focal plane, and the thruster array is rather minor because of the short distances associated with these lines. The hardware necessary for the structural integration is shown in Table 5-17. Due to the immaturity of this design, the figures shown are allocations based on scaling from the SGM design where appropriate.

Table 5-17: Mass Summary of Structural Integration Hardware

Element	Mass [g]
Composite Fiber Strips	50
S/A Deploy and Hold Devices	100
Miscellaneous Fasteners	50
Cabling	50
Total:	250

5.14 Thermal Management

Thermal considerations drove many of the decisions in the development of the NGM system. This architecture features three key characteristics:

- Electronics packages are capable of conducting generated heat to their edges and bus dimension is limited to MCM size so that radiators can be mounted directly on the substrate edges;
- Optical elements and MCM substrates are constructed from SiC which provides a high thermal conductivity and a low coefficient of thermal expansion. The selection of a single material allows for an athermal design;
- Integration of the propellant tank with the spacecraft bus provides a convenient method to transfer heat from the electronics directly to the tank as required to maintain acceptable temperatures for liquid hydrazine.

The thermal control on the NGM is passive, involving radiators and multi-layer insulation (MLI) only. The radiators are optical solar reflectors (or second surface mirrors) mounted on two opposing sides. During the mission the spacecraft is oriented such that these radiating surfaces always point out of the solar plane. The lower DC power consumption levels on the NGM allow for a lower radiator surface area. Using $q = \varepsilon\sigma T^4$ where the emissivity $e = 0.8$, Boltzman's constant $\sigma = 5.67 \times 10^{-8} W/m^2 \cdot K^4$, and the radiating temperature $T = 290K$ (an average temperature for the electronics operation in steady-state), the radiation flux is $320 W/m^2$. Assuming a 0% power efficiency, the required radiator area is $172 cm^2$ for the RF option ($P_{max} = 5.5W$) and $144 cm^2$ for the opt comm option ($P_{max} = 4.6W$). With an area density of $0.125 g/cm^2$, the radiators for the RF and opt comm options weigh 22g and 18g, respectively. Although the SGM design includes louvers, the NGM omits them because the radiators are nominally perpendicular to the sun axis and the second surface mirrors already reflect incoming energy (as is the case for the SGM).

The MLI is used to insulate the spacecraft as a whole, as well as individual components internal to the vehicle. Estimated coverage area for the MLI includes the tank, the spacecraft bus, and the optical bench, including the focal plane. About $1000 cm^2$ of MLI is necessary for a complete coverage. At $0.035 g/cm^2$, this lightweight MLI has a mass 35g. Miscellaneous hardware such as sensors and small heaters account for an additional 50g.

The greatest thermal concern of this design is the performance of the thruster array. Although the ceramic substrate is capable of withstanding the high temperatures associated with combustion, the thermal shocks associated with thrusting might damage it. This can be resolved by using coatings that either provide better insulation or a better thermal path to heat sinks such as the propellant tank or deep space. Fluid from the plenum can also be used to cool the substrate. As was mentioned in Section 5.7.2, further analysis in this area is necessary.

5.15 Flight System Summary

Figures 5-22 and 5-23 show respectively the configuration of the NGM spacecraft during flight and during launch. A detailed list of components used in the NGM system design (for both communication architectures) and their associated masses is given in Table 5-18. A power list for the two power modes (comm on and comm off) is given in Table 5-19.

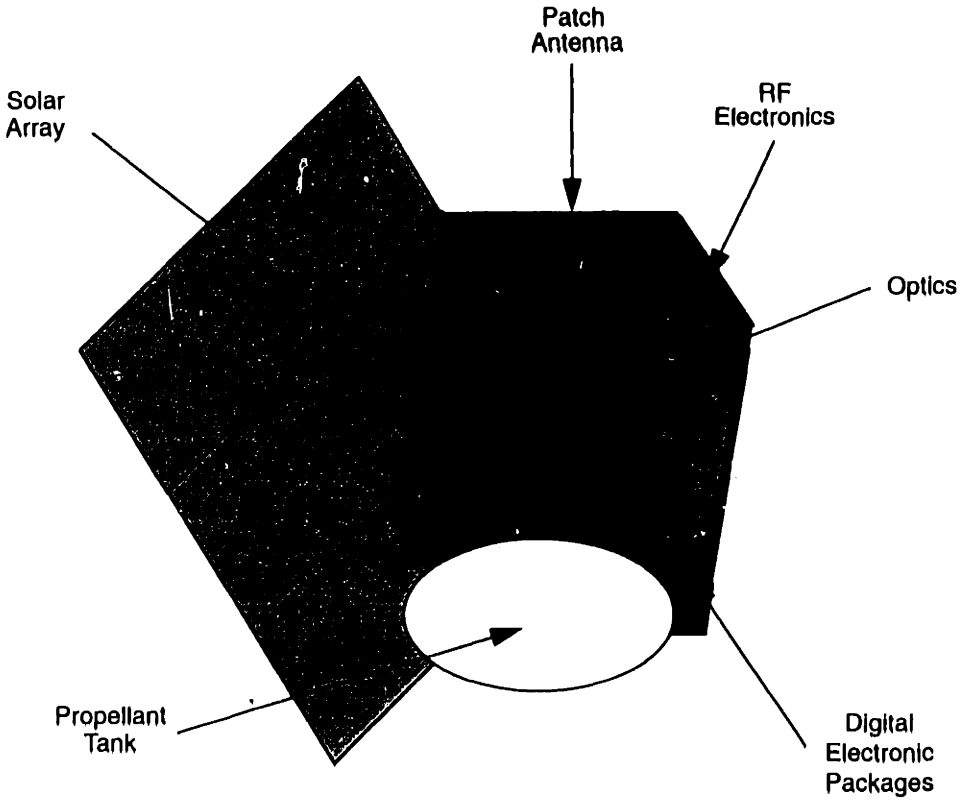

Figure 5-22: Configuration of NGM during flight.

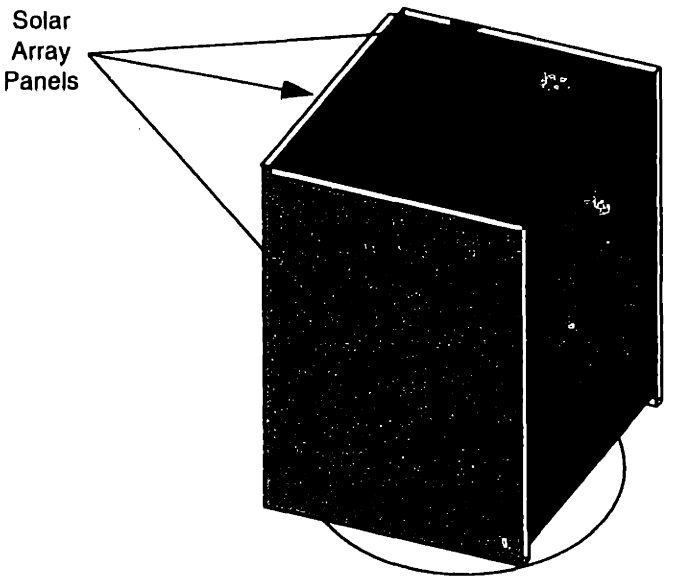

Figure 5-23: Configuration of NGM during launch.

Table 5-18: Detailed Mass Summary for the NGM

Component	Mass [g]		Comments
	RF Comm	Opt Comm	
OPTICS			All but corrector and
Optical Elements			insulation are SiC
Primary Mirror	20	20	
Secondary Mirror	4	4	
Tertiary Mirror	2	2	
Corrector	9	9	
Focal Plane	50	50	
Support Structure			
Main Tube	23	23	
Focal Plane Tube	2	2	
Spiders (3)	1	1	
Secondary Alignment	15	15	
Baffling	30	30	
Optically Insulating Surfaces	10	10	
RF HARDWARE			
Patch Antenna	50		Supported by the SSPA MCM
SSPA/Exciter/Modulator MCM	200		X-Band
EMI Shield	50		
Power Converter MCM	180		
OPT COMM HARDWARE			
Laser Transmitter		70	
Lens Array		30	
Support Structure		100	
DIGITAL ELECTRONICS			
Computation and Memory MCM	200	200	
IRU/Engineering MUX/ADC MCM	200	250	Opt Comm electronics on back
Integrated Power Electronics MCM	250	250	
SOLAR ARRAY			
Solar Cells	55	46	CdTe cells
Support Structure	50	45	
BATTERY	55	55	Secondary $LiTiS_2$

Table 5-18: Detailed Mass Summary for the NGM

Component	Mass [g]		Comments
	RF Comm	Opt Comm	
TEMPERATURE CONTROL			
Radiators	22	18	
MLI	35	35	1000cm^2 coverage
Sensors/Heaters	50	50	Allocation
STRUCTURAL INTEGRATION			
Composite Strips	50	50	
S/A Latch & Deploy Devices	100	100	Allocation/same as SGM
Misc. Fasteners	50	50	Allocation
Cabling	50	50	
PROPULSION			
Tank	70	70	Composite ellipsoid
Thruster Array	75	75	Etched SiC
Filter	30	30	Same as SGM
Manual Valve	20	20	Same as SGM
Lines/Fittings	25	25	25% of SGM allocation
Pressurant	4	4	Helium blowdown system
RCS Thrusters (8)	70	70	Independent sublimated thrusters
SUBTOTAL	2107	1859	
30% CONTINGENCY	632	558	
TOTAL (DRY) W/ CONTINGENCY	2739	2417	
PROPELLANT	294	260	I_{sp} = 200sec
TOTAL (WET)	3033	2676	

Table 5-19: Detailed Power Summary for the NGM

	Average Power [W]			
	RF Communication		Optical Communication	
	Comm Off	Comm On	Comm Off	Comm On
Telecommunication				
Solid State Power Amplifier	0.0	0.8		
Telemetry Modulation Unit	0.0	0.3		
Exciter (Upconverter)	0.0	0.7		
Modulator/Temp Controlled Laser			0.0	0.7
Acquisition/Tracking Data Processor			0.0	0.3
Data Interface Electronics			0.0	0.3
Detectors, FP Electronics, Temp. Control	0.3	0.3	0.3	0.3
Computation and Memory	0.6	0.6	0.6	0.6
IRU, Eng. Multiplexing, A/D Conversion	0.3	0.3	0.3	0.3
Power (40%)	0.5	1.2	0.05	1.0
SUBTOTAL	1.7	4.2	1.7	3.5
30% CONTINGENCY	0.5	1.3	0.5	1.1
TOTAL W/ CONTINGENCY	2.2	5.5	2.2	4.6

Chapter 6

Programmatic Issues

The prime reason for miniaturization, as was discussed in the introduction, is the reduction in the cost of an entire program which includes the development, launch, and operation phases. With the elimination of the uplink function, the ground operation costs are reduced considerably; and due to the small size and mass of each microspacecraft the launch of many on a single LV reduces launch costs for each individual mission. On the other hand, the development of the advanced technologies required to realize this type of spacecraft may be very costly. The cost of developing all needed technologies, however, might not be included in the total cost of each individual mission. A broader microtechnology base is needed to realize this class of missions. Each mission would benefit from this technology base, as well as share its costs. This chapter will discuss the impact of each of the three program phases on the total "life-cycle" cost of a microspacecraft mission.

6.1 Technology Development

There are two primary aspects that allow the miniaturization of the NGM. The first is its modified architecture, and the second is a set of advanced technologies. Of the two, the advanced technologies provide a greater limitation. Although the rate of technology development cannot be predicted, technology needs can be identified so that funding can be directed appropriately, providing the proper environment for technology growth in the areas required. This section provides a summary of all technologies needed to realize the NGM concept as well as a discussion of such related issues as readiness and risk.

6.1.1 Enabling Technologies

Table 6-1 presents a list of new systems and technologies that are required to realize the NGM as it was described in the prior chapter. This list contains only new technologies that are not already included in the SGM baseline. A full list of NGM technologies (including specific performance requirements) is presented in Appendix C. The emphasis in Table 6-1 is on the specific systems and technologies that were chosen for this design as well as their desired characteristics. The identification of these requirements will allow for the applications of technologies and solutions which are forthcoming, but which cannot be predicted at this point.

Table 6-1: Summary of Advanced Systems and Technologies Used in the NGM Design

Function	Desired Characteristics	System and/or Technologies
Telecommunication	Low Power Maturity	RF Communication: Distributed Amplification, Low Power Devices
	Low Power High Datarate	Optical Communication:[a] Laser and Microlens Array
Propulsion	Compact, Supports Graceful Degradation	Ellipsoidal Composite Tank Microthruster Array Microvalve Array
Reaction Control	Very Low Thrust Levels	Independent Sublimated Thrusters
Energy Storage	High Energy Density	Primary Battery Secondary Battery[a]
	Compact	Thin-Film Distributed Battery[a]
Electronics Packaging	High Chip Densities	Die-Stacking Techniques and Ultra High Density Integration
	Support Structural Loads Support Thermal Loads	SiC Substrates Synthetic Diamond Substrates[a]
Structural Integration	Low Mass, Less Components	Extended Tank Fibers
Heat Transfer	Low Mass	Uni-directional Composite Fibers already available for struct. integ.

a. Alternate option.

6.1.2 Risk Issues

Reliance on the availability of the advanced technologies listed above is risky. Risk is defined as the chance that a particular technology will not achieve the required maturity by the specified time; it is a result of the fact that the rate of technology development cannot be predicted. This risk may be addressed using three main parameters: The first is the current state of the technology; a low level of "readiness" indicates immaturity and a higher probability that the projected performance will not be achieved. The second is the past, present, and projected levels of funding provided for developing this technology; lack of funding indicates a lack of understanding and a driving need for this technology. The third is the breadth of interest in turning a technology concept into reality; such interest from commercial industries ensures that funding levels do not depend solely on NASA. Thus, to be able to quantify or evaluate the levels of risk associated with each technology, each of these aspects needs to be examined.

Table 6-2 lists all NGM technologies and presents their current NASA readiness level, interested organizations, and the associated levels of risk. The readiness level is based on a standard NASA scale defined as follows:

1. Basic principles observed (*i.e.*, concept only)
2. Technology concept and/or application formulated
3. Analytical and experimental critical function and/or characteristic proof-of-concept
4. Component and/or breadboard validation of laboratory environment
5. Component and/or breadboard validation in relevant environment
6. System/subsystem model or prototype demonstration in relevant environment
7. System prototype demonstration in a space environment
8. Actual system completed and "flight qualified" through test and demonstration
9. Actual system "flight proven" through successful mission operation

The readiness "ratings" shown in the table were extracted either from literature or information provided directly by the technology developers (see references in Appendix C). In most cases, the readiness levels were not specifically stated by these sources, but rather created from the available information by the author.

As stated above, the risk associated with the realization of each technology is governed by the rate of possible technology development (physical limitations) and the level of continuous funding provided ("political" limitations). Technology readiness is a good indication of the first criteria and a diversified interest (commercial and government) in the technology is an indication of the second. Since specific information on past, present, and projected levels of funding at NASA, other governmental agencies, and private industry is not readily available and nor is the current status of each technology, it is difficult to quantify risk. For these reasons, three levels of risk are used: low, medium, and high. These are loosely defined as follows:

- *Low Risk*: NASA Technology Readiness of >5 and apparent industry interest
- *Medium Risk:* NASA Technology Readiness >3 and apparent industry interest, or
  Medium Risk: NASA Technology Readiness >7 and no industry interest
- *High Risk:* NASA Technology Readiness <5 and no industry interest

These definitions are not very specific and as a result, the risk levels presented in the table are a subjective assessment made by the author. The microthruster and microvalve array are the only primary (non-alternate) technologies that are categorized as "high risk" technologies. This is essentially due to the fact that they were conceptualized for the NGM concept.

Table 6-2: Risk Associated with NGM Advanced Technologies

Technology	Developer	Readiness	Risk
Distributed Solid-State Power Amp.	Needed	2[a]	Medium
Low Power RF Devices	Cellular phone industry	4	Low
Microchip Laser Array	Several	4	Medium
Microlens Array (Binary Optics)	Several (including JPL)	4	Medium
Dichroic Coating	Several	4	Medium
Ellipsoidal Composite Tank	Metal Liner - TRW/PSI	5	Medium
	Shell - Needed	4	Medium
Microthruster Array	Needed	1	High
Microvalve Array	Needed	1	High
Sublimated Ammonia-Salt Thruster	TRW (no current interest)	5	Low
Li-$SOCl_2$ Primary Battery	Several	6	Medium
$LiTiS_2$ Secondary Battery[b]	Several	6	Medium
$LiMn_2O_4$ Thin-Film Battery[b]	Bellcore, portable electronics Indst	3	High
Die-Stacking on MCMs	Hughes, Others	5	Low
Ultra High Density Integration	Texas Instruments, Others	4	Medium
Ceramic Substrate for MCM	Several	4	Medium
Diamond Substrate for MCM[b]	Several	3	High
Drawn Tank Fibers	Needed	1	Medium[c]

a. Technology for individual SSPAs exist, however, no one is developing an array of amplifiers.
b. Alternate option.
c. This is categorized as 'medium' since capability exists, though never used for this application.

6.2 Vehicle Development, Test, and Integration

The primary costs associated with the development phase are a result of technology development work. Many trades are necessary to determine whether the cost benefit associated with the miniaturization level enabled by a particular technology is greater than the cost of its development. These are difficult trades since the development cost can be shared by each of the microspacecraft that make up a mission, and even by several missions. Aside from technology development, there are also system development costs. This particular aspect should greatly benefit from the production of a large number of microspacecraft, as prescribed by a multiple vehicle launch. The learning curve effect will reduce the average cost of developing each of these systems which have a common system architecture.

The costs associated with test and integration provide an interesting balance for microspacecraft such as SGM and NGM. Although the system is a highly integrated one which complicates the testing procedure and therefore increases cost, the facilities needed for testing and integration are much smaller. Massive, dedicated clean rooms are not necessary. The controlled, clean environment used to micromachine many of the components on board (such as the MCMs) can also be used for system integration, thus reducing costs. Finally, due to the large number of spacecraft, the launch vehicle integration is more complex, hence, higher costs. This aspect is nicely balanced, however, by lower transportations costs associated with the shipment of minute spacecraft.

Many trades are necessary to determine if the considerably smaller size of the microspacecraft will result in lower test and integration costs that can offset the tremendous costs associated with advanced miniature technology development.

6.3 Launch

The AIM spacecraft was specifically designed so that three similar vehicles can be launched simultaneously on a single Pegasus. Although the SGM design addressed upper stage issues, no specific launch strategy was developed. The NGM design offers a launch scheme that groups microspacecraft on several SGM upperstages and then groups those upperstages on a Pegasus. Four NGM vehicles can be supported by a single SGM upperstage. Thus a cluster of four microspacecraft can target a particular asteroid and observe it from different angles. This flexibility is allowed by the ΔV capability provided on-board. Each cluster, however, can target any asteroid (or a group of asteroids) in the 0.8-1.2AU range.

The SGM upper stage is a new concept which involves a bipropellant system (I_{sp} = 310sec) where the tanks provide the structural support. The length and diameter of these tanks can be traded based on the dimensions of the payload and the propellant mass required. A schematic of this concept is shown in Figure 6-1. The difficulty in applying this concept to a single NGM is due to the small size of the NGM base (13cm). This dimension would require very long and narrow tanks which would degrade overall structural integrity. Thus, utilizing a single upperstage for the propulsion of four NGM vehicles keeps the diameter-to-length ratio of the upperstage at the levels used for the SGM.

The proposed launch architecture for the NGM is shown in Figure 6-2. The required diameter of each upperstage is 30cm, allowing sufficient spacing between any two microspacecraft for solar panel (which is wrapped around each 13cm-diameter body) and for deflections during launch vibrational loads. Scaling the SGM upperstage from its 5.5kg carrying capacity to 12kg (four NGMs) and fixing the diameter at 30cm, results in a 1m-tall, 10.5kg (est.) stage. Three such stages can be placed side-by-side across the 112cm diameter of the Pegasus and seven can fit side-by-side across the payload

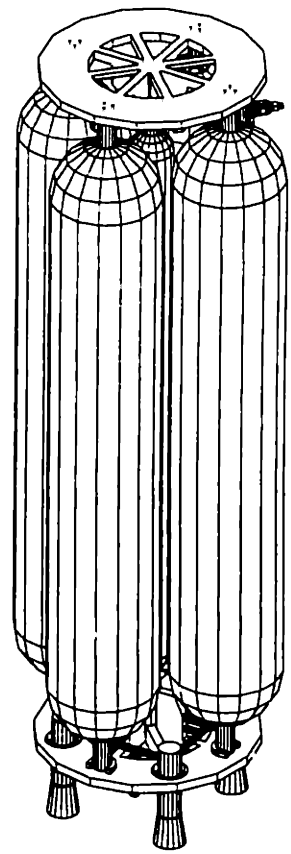

Figure 6-1: Schematic of the SGM upper stage.

shroud. The total mass for this seven-upperstage, 28-NGM configuration is 157.5kg, far below the 370kg launch capability of the standard Pegasus to 200km circular orbit [43]. The total length of the NGM-upperstage unit is 123cm which restricts the launch configuration to a single "layer" of vehicles in the 211cm-long standard Pegasus payload envelope. An additional seven-upperstage layer, however, can easily fit in the 330cm-long (137cm wide) Taurus envelope. The resulting total payload mass for this configuration is 315kg. In either of the two configuration, a rather complex adapter configuration will be required.

6.4 Ground Operation

Due to the lack of uplink capability on the spacecraft, the ground operations segment of the mission is reduced considerably. Although the sequencing aspect of ground ops is eliminated entirely, there are still costs associated with program management, planning and analysis, data capture, and data processing. Particular to the multi-spacecraft mission, additional costs will be incurred due to scheduling work necessary to ensure optimum sequencing and operation of DSN facilities. Based on a JPL mission operations cost comparison of traditional versus no-uplink asteroid flyby spacecraft [7], a 60% reduction in overall post-launch operations is possible.

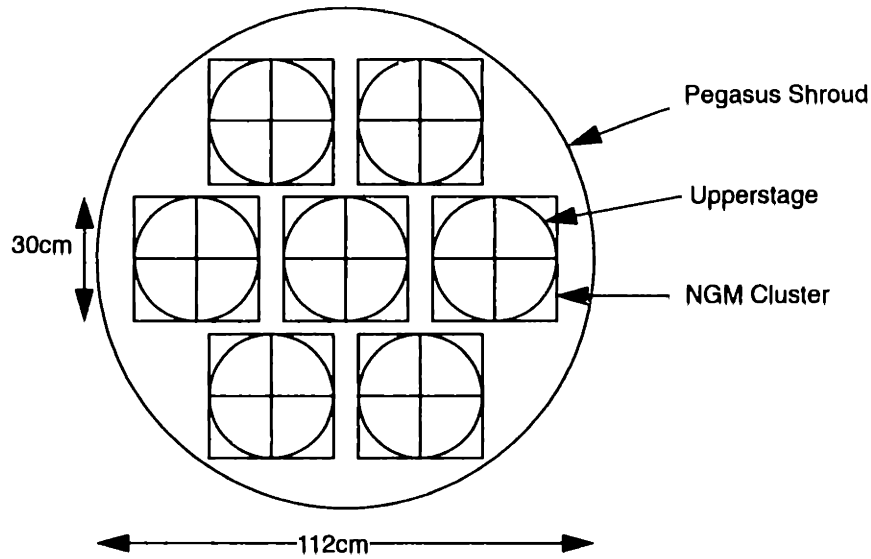

Figure 6-2: Cross-sectional schematic of the NGM within the Pegasus payload shroud.

Chapter 7

Conclusions

The objective of this research project was threefold. The first was to develop a methodology to approach the miniaturization process of small-scale spacecraft. The second was to apply this methodology via a system design for an asteroid flyby mission which would result in a certain level of miniaturization over its predecessor (JPL's "Second Generation Microspacecraft," SGM). The third was to identify a set of advanced technologies that would allow for the development of this class of microspacecraft. The outcome of each of these objectives and some final comments are given below.

7.1 Miniaturization Methodology Developed

The various miniaturization techniques used in this study are presented in Chapter 4. These methods are applied in the following chapter, Flight System Design. Based on the outcome of this design (or designs, since two concepts were developed), three approaches to miniaturization are identified as the most effective:

1. *Design through functionality* - eliminating functions obviously reduces supporting hardware and thus overall mass, however, additional reduction in hardware is possible with integration of functions which allows hardware elements to perform more than one function thus reducing the total number of elements on-board. (See Sections 4.2 and 4.3)
2. *Design for compactness* - reducing overall volume of the vehicle by creating a volume-efficient physical architecture greatly minimizes necessary support structure which consumes a considerable fraction of the spacecraft's mass. (See Section 4.4 and discussion in the next section)
3. *Design for low power consumption* - reducing operating voltage or component architecture to allow for lower levels of power consumption not only reduces battery and solar array size but also produces far less heat and thus requires less hardware to dissipate it. (See Section 4.5)

7.2 Miniaturization Level Achieved

The miniaturization techniques described in Chapter 4 and applied in Chapter 5 resulted in two spacecraft designs; one featuring an RF communication system and the other an optical communication system. The first concept's overall (wet) mass is estimated at 3.0kg while the latter is estimated at 2.7kg. Relative to the SGM, these two NGM concepts represent a 45% and 51% mass reduction, respectively. Table 7-1 shows the values of the three parameters that define spacecraft "size": mass, power, and volume. These are the factors which the term miniaturization applies to. The table also shows the percent reduction from the value of the preceding concept.

Table 7-1: Comparison of Vehicle "Size" Parameters of Asteroid Flyby Spacecraft

	Mass [kg]	% Red.	Power [W]	% Red.	Volume [m^3]	% Red.
PNEAF	77.5		66.2		0.5	
AIM	35.7	54	42.0	37	0.1	80
SGM	5.5	85	13.0	69	0.01	90
NGM (RF)	3.1	44	5.5	58	0.0038	62
NGM (Opt)	2.7	51[a]	4.6	65[a]	0.0036	64[a]

a. Relative to SGM.

Compared to the 85% mass reduction achieved by the SGM, the NGM level of miniaturization seems rather modest. Revisiting the trend in miniaturization for asteroid flyby concepts presented in the introduction (Figure 1-1 on page 19), however, shows that the progress is that of an exponential decay. Figure 7-1 presents this progress (including the NGM contribution) on a logarithmic scale. This plot shows that the NGM concept continued the miniaturization trend at a rate similar to its predecessors.

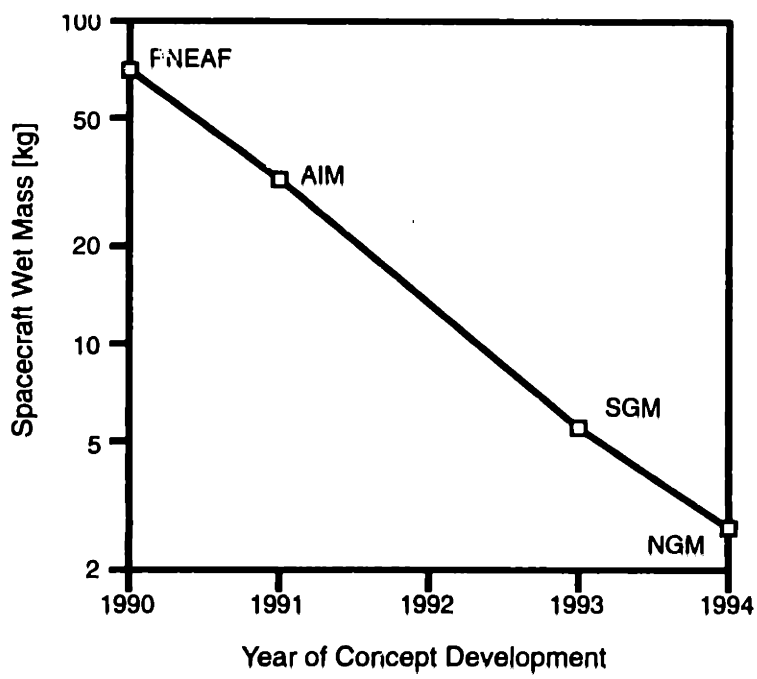

Figure 7-1: Trend in miniaturization of near-earth asteroid flyby concepts (revisited).

A derivative of the miniaturized parameters shown in Table 7-1 is the idea of spacecraft "density." The issue of compactness was raised many times throughout this thesis and was a driver in many trade-offs; in particular the modification of the propulsion architecture which is the most radical change in

the NGM design in comparison to the SGM. Figure 7-2 shows the growth in spacecraft "densities" within the asteroid flyby class. These densities are simply the mass of the spacecraft divided by the volume it occupies during launch. Note that "cavities" in the vehicle (such as the volume between the solar array and the bus in the SGM, see Figure 3-6 on page 33) are included in the total volume since they are not available for use during launch, however, such extensions as the thruster on the SGM are not. This figure shows that with respect to volume "efficiency" (i.e., efficient use of launch vehicle payload shroud), the NGM concept has taken a significant step forward.

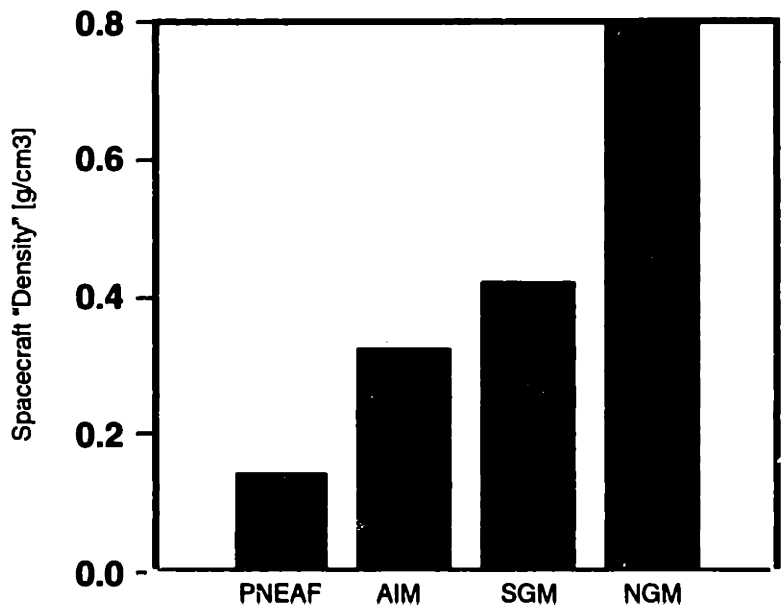

Figure 7-2: Increase in spacecraft densities for asteroid flyby concept vehicles.

7.3 Advanced Technologies Identified

Since the NGM design relies on the SGM as a baseline, many of the advanced technologies required to realize the NGM were already identified for use on the SGM. Section 6.1.1 outlined the specific technologies that are required for the NGM beyond those technologies that are required for the SGM. A full list of technologies used in the NGM design is presented in Appendix C. There are three key technologies critical to the NGM design:

1. Electronic packages capable of carrying a variety of miniature hardware (in addition to ICs) and supporting themselves structurally and thermally
2. Low voltage RF and DC devices that consume far less power and produce less heat
3. Compact propulsion system that allows for high performance and graceful degradation as well as reduction in mass

These three technologies are a direct result of each of the three primary approach to miniaturization presented in Section 7.1 above. They present the areas where these approaches have the greatest impact on the design.

7.4 Final Comments

In addition to the three objectives specified above, the point design presented in this thesis provides two additional benefits. First, it provides another example of a microspacecraft concept that increases the "visibility" of this type of spacecraft. Second, it provides another step in the miniaturization process that attempts to define the limit to miniaturization. In light of these two benefits, the question raised at this point is what should be the next step.

7.4.1 Future Outlook

Due to the shrinking NASA budget, it is quite clear that future deep-space spacecraft will need to be smaller and cheaper, yet provide a valuable scientific insight into the world around, as their predecessors d' Not only the annual program cost should be kept low, but also the total "life-cycle" cost needs to be minimized. Establishing a set of core technologies with a flexibility towards evolution will allow the design and construction of a whole class of spacecraft; the construction of which can benefit from the learning curve effect. The benefits of this effect can certainly be utilized in the case of launch of multiple spacecraft on a single LV.

Increased awareness for the potential of small-scale spacecraft demands greater research of advanced technologies that enable the miniaturization process. This demand will increase with time and interest. The development of other feasible concepts, both for asteroid flybys and beyond, should heighten the benefits of these technologies. Also, since there is a great interest in the commercial field (in such industries as portable electronics and cellular phones) for miniature technologies, many of these can be "adapted" for space application with a cost which is far less than that required for developing these technologies from the ground up. The resulting technology base should provide the proper environment for building miniature spacecraft.

Finally, this concept (as well as its predecessors) anticipate that the conceptual physical limit of miniaturization has not been reached yet. As new technologies and techniques are introduced (as they do on what seems to be a daily basis) smaller concepts can be developed. It is not unreasonable to think that within the next couple of years concepts will be developed that can fit in a "coffee can," as was projected in 1987 [2].

7.4.2 Recommended Work

Future work on microspacecraft should focus on two primary areas; expanding on existing concepts and developing additional ones. The former area involves resolving outstanding technology issues such as the microthruster array and optical communications, targeting specific architectural issues such as further reducing "dead" volume on-board (primarily applies to the optics), and continuing work on upperstages. The second area involves developing additional, smaller concepts for an asteroid flyby mission as well as developing similar concepts for other types of missions and other types of science that can be accommodated.

In addition, careful attention should be paid to advanced technologies. Technologies currently under development, expected technologies, and technology needs should be tracked, cataloged, and identified. These task is already in progress at JPL. Such resources will greatly assist in the process of system concept development.

Appendix A

Spacecraft Parameter Comparison

A.1 Mass

All Values are in kg	PNEAF	AIM	SGM	NGM	
				RF	Optical
Science/Optics	3.5	3.5	0.14	0.17	0.17
Telecommunication	6.7	4.8	0.86	0.48	0.20
Power (and Pyro, if used)	6.7	3.3	0.57	0.41	0.15
Attitude Control	4.4	0.5	0.10	0.07	0.07
Central Computing	5.7	2.2	0.52	0.40	0.45
Stucture, Cabling, Devices	21.7	5.3	0.73	0.25	0.25
Temperature Control	2.2	2.2	0.24	0.11	0.10
Prouplsion (dry)	6.5	3.0	0.72	0.22	0.22
Subtotal:	57.4	24.8	3.88	2.11	1.86
Contingency Mass (30%)	17.2	7.4	1.2	0.63	0.56
Propellant	7.0	3.4	0.48	0.29	0.26
Total Wet Mass:	81.6	35.6	5.52	3.03	2.68

A.2 Power

All values are in Watts	PNEAF	AIM		
		Cruise	Encounter	Downlink
Optics, Science, or Integrated	4.0	0.0	4.0	0.0
Telecommunication	21.4	5.0	5.0	13.6
Power (and Pyro, if used)	9.0	5.5	7.5	6.3
Attitude Control	5.6	12.0	18.5	8.5
Central Computing	8.5	2.0	2.0	2.0
Temperature Control	0.7	1.0	1.0	1.0
Prouplsion (dry)	0.2	2.0	0.0	0.0
Subtotal:	49.4	27.5	38.0	31.4
Contingency Power (30%)	14.8	8.2	11.4	9.4
Total:	64.2	35.7	49.4	40.8
Power Available from S/A	66.2	42.0	42.0	42.0
Margin	2.0	6.3	-7.4	1.2

All values are in Watts	SGM		NGM			
			RF Comm		Optical Comm	
	Telecom Off	Telecom On	Telecom Off	Telecom On	Telecom Off	Telecom On
Optics, Science, or Integrated	0.3	0.3	0.3	0.3	0.3	0.3
Telecommunication	0.0	4.8	0.0	1.8	0.0	1.3
Power (and Pyro, if used)	0.8	2.0	0.5	1.2	0.1	1.0
Attitude Control/Health	0.6	0.6	0.3	0.3	0.3	0.3
Central Computing	2.4	2.4	0.6	0.6	0.6	0.6
Temperature Control	0.0	0.0	0.0	0.0	0.0	0.0
Prouplsion (dry)	0.0	0.0	0.0	0.0	0.0	0.0
Subtotal:	4.1	10.1	1.7	4.2	1.7	3.5
Contingency Power (30%)	1.2	3.0	0.5	1.3	0.5	1.1
Total:	5.3	13.1	2.2	5.5	2.2	4.6
Power Available from S/A	13.0	13.0	5.5	5.5	4.6	4.6
Margin	7.7	-0.1	3.3	0.0	2.4	0.0

Appendix B

Link Budgets

B.1 X-Band Communication Link

The link provided below was custom created for this study by the author on January 12, 1994, with assisstance from Jack Meeker of Section 336 of JPL.

TRANSMIT VARIABLES			XMIT CALCULATIONS		
Band	X				
Frequency	8.415	GHz	Wavelength	3.57	cm
Transmitter Power Output	0.5	W	Transmitter Power Output	26.99	dBm
Transmitter Circuit Loss	-0.4	dB	Transmit Antenna		
Transmit Antenna			Effective Gain	20.00	dB
Diameter	.153	m	Peak Gain	22.60	dB
Efficiency	55	%	Beamwidth	13.51	deg
Ellipticity	3	dB	Pointing Loss	0.00	dB
Pointing Error	0.7	deg	EIRP	46.59	dBm

PATH VARIABLES			PATH CALCULATIONS		
Range	1.6	AU	Space Path Loss	-278.52	dB
Elavation	25	deg	Atmos. Attenuation @ Zenith	-0.0731	dB
Weather Quality	95	%	Atmos. Attenuation @ Elav.	-0.17	dB
			Atmos. Mean Physical Temp.	279.25	°K
			Atmos. Noise Temperature	10.90	°K
			Other Losses		dB

RECEIVE VARIABLES			RECEIVE CALCULATIONS		
Receive Antenna			Polarization Loss	-0,01	dB
Diameter	34	m	Receive Antenna		
Efficiency	85,5	%	Effective Gain	68,85	dB
Ellipticity	0,7	dB	Peak Gain	69,53	dB
Pointing Error	0,003	deg	Beamwidth	0,06	deg
			Pointing Loss	-0,02	dB
			System Noise Temparture	31,0	°K
			Noise Spectral Density (No)	-183,68	dB_m/Hz

LINK VARIABLES			LINK CALCULATIONS		
Ranging Carrier Suppression	-0,18	dB	Total Received Power	-163,32	dB
Ranging Mod Index	11,75	deg	Pr/No	20,37	
Data Rate	60	bps	Pd/No (power in data)	20,37	
Desired Bit Error Rate	1E-06		Pc/No (power in carrier)	0,00	
Telemetry Mod Index	90	deg	Eb/No	2,58	
Required Eb/No	2,29		Margin	0,29	dB

B.2 Ka-Band Communication Link

The link provided below was custom created for this study by the author on January 12, 1994, with assisstance from Jack Meeker of Section 336 of JPL.

TRANSMIT VARIABLES			XMIT CALCULATIONS		
Band	Ka				
Frequency	31	GHz	Wavelength	0.97	cm
Transmitter Power Output	0.53	W	Transmitter Power Output	27.24	dBm
Transmitter Circuit Loss	-0.4	dB	Transmit Antenna		
Transmit Antenna			Effective Gain	19.99	dB
Diameter	.042	m	Peak Gain	22.59	dB
Efficiency	55	%	Beamwidth	13.53	deg
Ellipticity	3	dB	Pointing Loss	-0.03	dB
Pointing Error	0.7	deg	EIRP	46.80	dBm

PATH VARIABLES			PATH CALCULATIONS		
Range	1.6	AU	Space Path Loss	-289.85	dB
Elavation	25	deg	Atmos. Attenuation @ Zenith	-0.0731	dB
Weather Quality	95	%	Atmos. Attenuation @ Elav.	-0.17	dB
			Atmos. Mean Physical Temp.	279.25	°K
			Atmos. Noise Temperature	10.90	°K
			Other Losses		dB

RECEIVE VARIABLES			RECEIVE CALCULATIONS		
Receive Antenna			Polarization Loss	-0.01	dB
Diameter	34	m	Receive Antenna		
Efficiency	85.5	%	Effective Gain	80.18	dB
Ellipticity	0.7	dB	Peak Gain	80.86	dB
Pointing Error	0.003	deg	Beamwidth	0.02	deg
			Pointing Loss	-0.32	dB
			System Noise Temparture	31.0	°K
			Noise Spectral Density (No)	-183.69	dBm/ Hz

LINK VARIABLES			LINK CALCULATIONS		
Ranging Carrier Suppression	-0.18	dB	Total Received Power	-163.37	dB
Ranging Mod Index	11.75	deg	Pr/No	20.32	
Data Rate	60	bps	Pd/No (power in data)	20.32	
Desired Bit Error Rate	1E-06		Pc/No (power in carrier)	0.00	
Telemetry Mod Index	90	deg	Eb/No	2.53	
Required Eb/No	2.29		Margin	0.24	dB

B.3 Optical Communication Link

The link provided below was produced by Hamid Hemmati of Section 331 of JPL on January 3, 1994 using the Optical Communciation Link Analysis Program, Version 4.00.

Transmitter Parameters:		
Tranmitter average power	.2000E-01	Watts
Wavelength of laser light	1.0600	μm
Transmitter antenna diameter	.8000E-01	m
Transmitter obscuration diameter	.3000E-01	m
Transmitter optics efficiency	.75	
Transmitter pointing bias error	.5000	μrad
Tranmitter rms pointing jitter	.5000	μrad
Modulation extinction ratio	.1000E+07	
Receiver Parameters:		
Diameter of receiver aperature	10.000	m
Obscuration diameter of receiver	3.000	m
Receiver optics efficiency	.70	
Detector Quantum Efficiency	.80	
Narrowband filter transmission factor	.50	
Filter spectral bandwidth	.1000	angstroms
Detector diameter FOV	100.00	μrad
Operational Parameters:		
Alphabet size, M =	4.000	
Data rate	1.000	kbits/s
Link distance	1.6	AU
Required link bit error rate	.1000E-05	
Atmospheric transmission factor	.30	
Dead time	2000.0	μsec
Slot width	2.000	nsec

	Input		Factor		dB	
Min required peak power	.20E+05	Watt				
Laser output power			.200E-01	Watt	13.0	dBm
Antenna diameter	.080	m				
Obscuration diameter	.030	m				
Beam width	24.662	µrad				
Transmitter antenna gain			.282E+11		104.5	
Transmitter optics efficiency			.750		-1.2	
Bias error	.500	µrad				
RMS jitter	.500	µrad				
Transmitter pointing efficiency			.989		.0	
Space loss (at 1.6 AU)			.124E-36		-369.1	
Antenna diameter	10.000	m				
Obscuration diameter	3.000	m				
Field of view	100.000	µrad				
Receiver antenna gain			.799E+15		149.0	
Receiver optics efficiency			.700		-1.5	
Bandwidth	.100	A				
Narrowband filter xmission bandwidth			.500		-3.0	
Detector quantum efficiency			.800		-1.0	
Atmospheric transmission factor			.300		-5.2	
Received background power	.236E-09	Watt				
Received signal power			.436E-14	Watt	-113.6	dBm
Photons/joule			.534E+19		157.3	dB/mJ
Detected signal PE/second			.186E+05		42.7	dBHz
Symbol time			.200E-02	sec	-27.0	dB/Hz
Detected signal PE/symbol			37.3		15.7	
Detected background PE/slot	2.01					
Required signal PE/symbol			22.0		13.4	
Margin			1.69		2.3	

Appendix C

Enabling Technologies

The table below shows all technologies selected for the NGM spacecraft. These specific technologies are not required; their preformance (quantitative or qualitative), however, is necessary to anticipate effectiveness in the NGM design. A future technology with the same performance parameters, or better, can certainly be substituted. The Technology column lists these technologies by the primary function which they support. Alternative options worth further examination are also shown. The readiness scale was defined in Chapter 6 (see page 103) and the SGM column indicates whether this technology was initally chosen for this design (thus an 'N' represents a new technology for the NGM design).

Technology	Performance Parameters	Readiness	Ref.	SGM	Comments
OPTICS					
All-SiC optical elements (excluding corrector)	Athermal, light, strong	4	[26]	Y	
Room-temp. Si detector	0.4-0.9μm	4	[44]	Y	Uses active pixel sensing (APS)
Room-temp. InGaAs detectors (spectrometers)	0.9-1.7μm 1.7-2.65μm	3 2	[44]	Y	Photodiodes up to 1.7μm proven in lab, no APS though.
ATTITUDE DETERMINATION					
IRU or IMU "on a chip"		4	[35]	Y	Draper concept.
Efficient pattern recognition technique				Y	
ATTITUDE CONTROL					
Sublimated thrusters	F = 1mN, $I_{sp} \geq 65$sec	4	[29]	N	Late 60s concept. Work discontinued.
NAVIGATION					
Algorithms for autonomous optical navigation				Y	
PROPULSION					
Microthruster array	$F_{tot} < 1$N $I_{sp} \geq 220$sec	2		N	Concept developed in this study.

Technology	Performance Parameters	Readiness	Ref.	SGM	Comments
Microvalve array	$\Delta P = 400psi$ $\dot{m} = 4.25mg/s$	3	[32]	N	Proof-of-concept achieved for a single valve.
Ellipsoidal composite tank	P = 400psi 13cm x 7.7cm	3	[11]	N	Technology exits, never used for this application
POWER					
CdTe solar cells	85% Efficient	3	[34]	Y	
Peak power tracker			[35]	Y	
High-efficiency power conversion				Y	
$LiTiS_2$ secondary battery	120W·Hr/kg	4	[35]	Y	
Li-$SOCl_2$ primary battery	400W·Hr/kg	4	[36]	N	
$LiMn_2O_4$ thin-film battery	150W·Hr/kg	3	[15]	N	Currently: 30W·Hr/kg
COMPUTATION AND MEMORY					
Low-voltage logic	1.5V	2	[20]	N	
Neural networks		3	[45]	Y	Already in use in terrestrial applications.
Mass memory (random-access)	$0.1Gbit/cm^3$	2	[14]	Y	
Non-volatile knowledge base (read-only)	$0.04Gbit/cm^2$ $0.2Gbit/cm^3$	2	[7]	Y	Vertical Bloc Line technology considered
Lossless compression algorithms	3:1	4		Y	
RF COMMUNICATION					
X-band patch antenna	20dBi, X-band	4	[37]	Y	
Array of solid-state power amp.		3	[38]	N	Single SSPA technology exists.
Low-power RF devices		3		N	Strong interest in the cellular phone industry.
OPTICAL COMMUNICATION					
Microchip laser array	20mW output	4	[39]	N	
Microlens array (binary optics)		4	[39]	N	Commercially available
Dichroic coating	<1nm transmissive band	3	[39]	N	Used in optical computing applications.
ELECTRONIC PACKAGES					
Ultra-High Density Integration		4	[14]	N	Texas Instruments concept .

Technology	Performance Parameters	Read iness	Ref.	SGM	Comments
Stacked IC chips		4	[14]	Y	
SiC substrates		2	[18]	N	
Diamond substrates		3	[17]	N	
THERMAL CONTROL					
Variable emissivity radiators				Y	

References

[1] J. D. Burke, "Micro-Spacecraft," JPL Document #715-87, 1981.

[2] R. M. Jones, "Electromagnetically Launched Microspacecraft for Space Science Missions," *Journal of Spacecraft and Rockets*, September-October 1989, pp. 338-342.

[3] D. H. Collins, "Pegasus-Launched Near-Earth Asteroid Flyby: Spacecraft System Study," JPL, 4 October 1990.

[4] *The Role of Near-Earth Asteroids in the Space Exploration Initiative*, Science Application Internation Corporation Study #1-120-232-S28, September 1990.

[5] C. G. Salvo, "Asteroid Investigation with Microspacecraft (AIM)," JPL, October 1991.

[6] C. G. Salvo, et al., "Asteroid Investigation with Microspacecraft (AIM) Conceptual Mission and Spacecraft Design Study," Microspacecraft Preliminary Design Review, JPL, 13 August 1992.

[7] D. H. Collins, et al., "Year-End Status Report -- A Second Generation Microspacecraft Vision and Conceptual Design," JPL Document #11185, 11 October 1993.

[8] Paul A. Penzo, "A Multi-Mission Flyby Strategy for the Near-Earth Asteroids," American Institute of Aeronautics and Astronautics, 1992.

[9] *Discovery: Near-Earth Asteroid Rendezvous (NEAR), Report of the Discovery Science Working Group, Excecutive Summary*, October 1991.

[10] J. Stevens, Personal communications, Geology and Planetology Section (326), JPL, 11 January 1994.

[11] D.M. Stevens, Personal communication, Propulsion and Chemical Systems Section (353), JPL, 4 April 1994.

[12] Kim Aaron, "Elastic Scaling of Small Structures," Proceedings of the 7th Annual AIAA/USU Conference on Small Satellites, 13-16 September 1993.

[13] "MCM Overview", Honeywell, Inc. presentation to JPL on 27 September 1993.

[14] L. Alkalaj, Personal communication, Robotic Systems and Advanced Computer Technology Section (347), JPL, 6 January 1994.

[15] F. K. Shokoohi, J. M. Tarascon, B. J. Wilkens, D. Guyomard, C.C. Chang, "Low Temperature $LiMn_2O_4$ Spinel Films for Secondary Lithium Batteries," *Journal of the Electrochemical Society*, July 1992.

[16] L. Alkalaj, "MESUR Network Microelectronics Study: Final Report," JPL, 24 September 1993.

[17] T. J. Moravec, R. C. Eden, D. A. Schaefer, "The Use of Diamond Substrates For Implementing 3-D MCMs," *ICEMM Proceeding*, 1993.

[18] L. Lowry and B. Tai, Personal communication, Materials Processes Laboratory, Space Material Science and Engineering Section (355), JPL, 11 January 1994.

[19] D. Gephardt, M. C. Klonower, "Destination Laptop," *Byte*, February 1991, p. 242.

[20] B. Prince, R. H. W. Salters, "ICs Going on a 3-V Diet," *IEEE Spectrum*, May 1992.

[21] M. Mehregany, "Microelectromechanical Systems," *IEEE Circuits and Devices*, July 1993.

[22] R. T. Howe, R. S. Muller, K. J. Gabriel, B. S. N. Trimmer, "Silicon Micromechanics: Sensors and Actuators on a Chip," *IEEE Spectrum*, July 1990.

[23] H. Helvajian, E. Y. Robinson (editors), "Micro- and Nanotechnology for Space Systems: An Initial Evaluation," The Aerospace Corporation Report No. ATR-93(8349)-1, March 1993.

[24] L. Muller, "Notes from the 7/16/93 Meeting on Optical Subsystem for Second Generation Microspacecraft," JPL Interoffice Memorandum (un-numbered), 27 July 1993.

[25] C. Sepalveda, Personal communication and un-numbered memos, Optical Sciences and Applications Section (385), JPL, 9 January 1994.

[26] D. Coulter, "Mass Estimates for Silicon Carbide and Beryllium Telescope," JPL IOM #383-DC93-010, 13 September 1993.

[27] J.H. Martin, "Efficient Interconnection of MCMs," *ICEMM Proceedings*, 1993.

[28] R. Bartman, "Laser-Driven Microthrusters for Spacecraft Attitude Control," A proposal for JPL's Director's Discretionary Fund for Fiscal Year 1994.

[29] I. Grossman, I.R. Jones, D.H. Lee, "Auxiliary Propulsion Survey, Part III: Survey of Secondary Proupsion and Passive Attitude Control Systems for Spacecraft," TRW Report #10063-6001-R000, 14 December 1967.

[30] G.P. Sutton, *Rocket Propulsion Elements: An Introduction to the Engineering of Rockets*, John Wiley & Sons, 1986.

[31] E.B. Arkilic, "Gaseous Flow in Micron-Sized Channels," Master's thesis, Massachusetts Institute of Technology, January 1994.

[32] M.A. Huff, M.S. Mettner, T.A. Lober, M.A. Schmidt, "A Pressure-Balanced Electrostatically-Actuated Microvalve," *IEEE Solid-State Sensor and Actuator Workshop*, Hilton Head, SC, 4-9 June, 1990.

[33] J. R. Wertz and W. J. Larson (ed.), *Space Mission Analysis and Design*, Kluwer Academic Publishers, 1991.

[34] H.S. Ullal, J.L. Stone, K. Zweibel, T. Surek, and R.L. Mitchell, "Polycrystalline Thin-Film Solar Cells and Modules," *6th International Photovoltaich Science and Engineering Conference*, New Delhi, India, 10-14 February 1992.

[35] L. Muller, "Second Generation Microspacecraft Design Team Meeting on August 10, 1993," JPL IOM #3132-93-346, 10 August 1993.

[36] G. Halpert and S. Surampudi, "Advanced Energy Storage for Space Applications," *1993 European Space Power Conference*, Graz, Austria, 23 August 1993.

[37] J. Huang, *Antenna*, JPL course.

[38] Y. Guo, "Antennas and SSPAs in a Second Generation Microspacecraft Vision and Conceptual Design," JPL IOM #3363-94-001, 6 January 1994.

[39] H. Hemmati, "Optical Communication Design and Link Analysis for Second Generation Microspacecraft - Revisited," JPL IOM, 3 January 1994.

[40] *Pegasus Payload User's Guide*, Release 2.00, Orbital Sciences Corporation, 1 May 1991.

[41] S. Timoshenko, *Theory of Plates and Shells*, Second Edition, McGraw-Hill Publishers, 1959.

[42] *Galileo Orbiter Parts, Materials, and Process Requirements*, JPL Project Document #625-211, 9 May 1978.

[43] "Launch Vehicle Summary for JPL Mission Planning," JPL Document #6936, Rev. C, February 1993.

[44] C.O. Staller, Personal communication, Infrared and Analytical Instrument Systems Section (382), 3 May 1994.

[45] C.C. Klimasauskas, "What Neural Networks Really Do," *EDN*, 14 December 1989.